Correlations in nuclear matter at low densities in an extended relativistic mean-field model

Korrelationen in Kernmaterie bei kleinen Dichten in einem erweiterten relativistischen Mittelfeldmodell

Zur Erlangung des Grades eines Doktors der Naturwissenschaften (Dr. rer. nat.)
genehmigte Dissertation von Maria Voskresenskaya, M.Sc. aus Moskau (Russland)
2013 — Darmstadt — D 17

TECHNISCHE
UNIVERSITÄT
DARMSTADT

Fachbereich Physik
GSI Theorie

Correlations in nuclear matter at low densities in an extended relativistic mean-field model
Korrelationen in Kernmaterie bei kleinen Dichten in einem erweiterten relativistischen Mittelfeldmodell

Genehmigte Dissertation von Maria Voskresenskaya, M.Sc. aus Moskau (Russland)

1. Gutachten: Prof. Dr. Karlheinz Langanke
2. Gutachten: Prof. Dr. Robert Roth

Tag der Einreichung: November 27, 2012
Tag der Prüfung: Dezember 21, 2012

Darmstadt — D 17

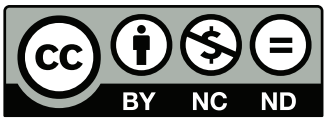

Erklärung zur Dissertation

Hiermit versichere ich, die vorliegende Dissertation ohne Hilfe Dritter nur mit den angegebenen Quellen und Hilfsmitteln angefertigt zu haben. Alle Stellen, die aus Quellen entnommen wurden, sind als solche kenntlich gemacht. Diese Arbeit hat in gleicher oder ähnlicher Form noch keiner Prüfungsbehörde vorgelegen.

Darmstadt, den März 20, 2013

(M. D. Voskresenskaya)

5

Zusammenfassung

Die Kenntnis der Zustandsgleichung stark wechselwirkender Materie wird für die Beschreibung der unterschiedlichen Kernmateriephasen in einem weiten Bereich von Dichten, Temperaturen und Protonanteilen benötigt [KBT+06, JLM+07]. Ein besonders wichtiges Problem ist die Erstellung von Zustandsgleichungen für astrophysikalische Anwendungen, z.B. bei der Untersuchung verschiedener Phasen von Kern-Kollaps-Supernova Explosionen und der Struktur von Protoneutron- und Neutronensternen [Gle00].

Für viele Jahre gab es nur eine sehr kleine Anzahl von Tabellen mit Zustandsgleichungen, die in der Simulation dynamischer astrophysikalischer Prozesse [LS91, STOS98b, STOS98a] verwendet wurden und den vollen Parameterraum abdeckten. Diese Tabellen stellen oft nicht genug Informationen zu thermodynamischen und kompositorischen Details bereit und berücksichtigten nicht alle relevanten Phasenübergänge, wenn mehrere Phasen koexistieren. In den vergangenen Jahren sind neue experimentelle Daten von Atomkernen, von Schwerionenstößen und astrophysikalische Beobachtungen erschienen. Diese Ergebnisse, der Fortschritt in der theoretischen Beschreibung von Kernmaterie und wesentliche Verbesserungen bei Supercomputern haben neue Entwicklungen zur Konstruktion von Zustandsgleichungen angestoßen. Trotzdem erlauben es die existierenden mikroskopischen Ansätze noch nicht, eine Beschreibung im gesamten Bereich von Dichten und Temperaturen bereit zu stellen. Daher sind Näherungen und Vereinfachungen zur Entwicklung praktischer Verfahren notwendig. Weiterhin werden verschiedene phänomenologische Zugänge zur Zustandsgleichung entwickelt.

In dieser Arbeit untersuchen wir die Effekte von Korrelationen auf thermodynamische Eigenschaften von Kernmaterie im Rahmen eines generalisierten relativistischen Mittelfeldmodells mit leichten Clustern als zusätzliche Freiheitsgrade über Nukleonen hinaus. Diese Korrelationen schließen Zweiteilchen-Streubeiträge und Paarungseffekte ein. Sie treten durch die kurzreichweitige Nukleon-Nukleon-Wechselwirkung bei kleinen Dichten auf und verändern die Zusammensetzung und die thermodynamischen Eigenschaften der Materie. Diese Effekte sollten in der Zustandsgleichung berücksichtigt werden, weil sie in diesem Dichtebereich die Struktur von Protoneutronsternen [SR08], die Effektivität des Wiederaufheizens der Schockwelle durch Neutrinos in Supernovasimulationen [LP04] und den zeitlichen Ablauf der Abkühlung von Neutronensternen beeinflussen.

Diese Arbeit besteht aus zwei Teilen. Im ersten Hauptteil führen wir ein verallgemeinertes relativistisches Mittelfeldmodell ein, das Cluster und Zweinukleon-Streukorrelationen in einer effektiven Weise als explizite Freiheitsgrade im thermodynamischen Potential enthält. Diese Bindungs - und Streuzustände werden durch Quasiteilchen mit dichte- und temperaturabhängige Eigenschaften repräsentiert. Alle relevanten Größen werden in thermodynamisch konsistenter Weise abgeleitet. Das Modell reproduziert die Ergebnisse des relativistischen Mittelfeldmodells in der Nähe der nuklearen Sättigungsdichte, wo sich Cluster aufgelöst haben. Das Niederdichteverhalten von Kernmaterie bei endlichen Temperaturen mit Nukleonen und leichten Kernen wird in einer Fugazitätsentwicklung des großkanonischen Potentials betrachtet und die Virialzustandsgleichung mit dem generalisierten relativistischen Mittelfeldmodell verglichen. Aus dem Vergleich der Entwicklungen werden Konsistenzbeziehungen hergeleitet, die die Quasiteilchenparameter mit den Meson-Nukleon-Kopplungen des relativistischen Mittelfeldmodells im Vakuum und den Streuphasen bzw. Parametern der effektiven Reichweit-

enentwicklung für die Nukleon-Nukleon-Streuung verbinden. Wir untersuchen verschiedene Möglichkeiten für die Wahl der Meson-Nukleon-Kopplungen und Quasiteilcheneigenschaften, die die Konsistenzbeziehungen erfüllen. Zusätzlich werden aus diesen Beziehungen relativistische Korrekturen zu der traditionellen Virialentwicklung gewonnen. Diese werden bei kleinen Dichten größer als die Effekte der Teilchenkorrelationen. Verschiedene Parametrisierungen der Abhängigkeit der Quasiteilcheneigenschaften vom Medium werden diskutiert.

Der zweite Hauptteil dieser Arbeit widmet sich der Untersuchung von Effekten der Paarkorrelationen auf die thermodynamischen Eigenschaften reiner Neutronenmaterie für Dichten bis hinauf zur Sättigungsdichte. Eine große Zahl von experimentellen Tatsachen und theoretische Ergebnisse weisen auf die Existenz der Superfluidität hin, die durch Paarkorrelationen in nuklearen Systemen bei hinreichend niedrigen Temperaturen $T \leq (0.1 - 0.3)$ MeV hervorgerufen wird. Man glaubt, dass die Neutronsuperfluidität in der Kruste von Neutronensternen eine Schlüsselrolle beim Mechanismus der Pulsar-Glitches spielt, welche als ein beobachtbarer Hinweis auf die Superfluidität in diesen Sternen angesehen werden [ST83]. Die üblichen Mittelfeldtheorien behandeln Nukleonen als unkorreliert und berücksichtigen zusätzliche Paarungseffekte nicht. Bisher vernachlässigen globale Zustandsgleichungstabellen für astrophysikalische Anwendungen Paarungseffekte. Hier erweitern wir das relativistische Mittelfeldmodell durch Berücksichtigung von Paarkorrelationen im $^1S_0$ nn Kanal. Die Rechnungen werden mit einem separablen Yamaguchi-Potential durchgeführt. Paarungsgaps werden für verschiedene Temperaturen berechnet. Die Ergebnisse für thermodynamische Größen werden mit relativistischen Fermi-Gas-Rechnungen verglichen. Ein Änderung im Druck von 10 % wird für ein gegebenes Modell beobachtet.

In dieser Arbeit haben wir den Effekt von Zweiteilchenkorrelationen auf die Zustandsgleichung von Kernmaterie gezeigt. Diese Effekte wurden selbstkonsistent in das Mittelfeldmodell eingefügt, jedoch ist unser Ansatzes nicht auf das ausgewählte generalisierte Mittelfeldmodell mit dichteabhängigen Kopplungen beschränkt. Es kann ebenso auf andere Mittelfeldmodelle angewendet werden. In der Zukunft planen wir, eine Zustandsgleichungstabelle mit Korrelationseffekten zu erstellen, die in astrophysikalischen Simulationen angewendet werden kann.

Contents

1 Introduction

1.1 Motivation and outline

Knowledge of the equation of state of strongly interacting matter is required for the description of the variety of nuclear matter phases in a wide range of densities, temperatures, and proton fractions [KBT$^+$06, JLM$^+$07]. A specifically important problem is the construction of equations of state for astrophysical applications, e.g for the investigation of various stages of core-collapse supernova explosions and the structure of proto-neutron and neutron stars [Gle00].

Thermodynamic properties of a system composed of nuclei change drastically depending on its composition, temperature and density. Various phases of the system are relevant for astrophysical applications. For instance, at low densities the matter is composed of individual nuclei and correlations and cluster formation are important. Also the properties of the system are influenced by the neutron to proton ratio, which in astrophysical environment is defined by weak interaction processes. The occurrence of "pasta" phases below a critical density and the liquid-gas phase transition below a critical temperature have to be considered as well. At higher densities uniform nuclear matter is expected, but at still larger densities a number of phase transitions may occur such as pion [Mig78, EW88] and kaon condensations [GSB99, BKPP88] and hadron-quark transition [Gle92, HPS93]. Therefore, a model is required that would globally cover the broad range in temperature, density and neutron to proton ratio needed in astrophysical applications and that would describe different compositions and transitions between different phases. Many equations of state were suggested. They are, however, restricted to a certain range in temperature, isospin asymmetry (various neutron to proton ratio) or density and often describe only particular conditions, e.g. neutron matter or isospin symmetric matter (equal number of neutrons and protons). Besides that, the construction of equation of state tables is very computationally expensive. For many years, a very small number of equation of state tables was available that have been used in simulations of dynamical astrophysical processes [LS91, STOS98b, STOS98a] covering the full parameter space needed. These equations of state have been applied in astrophysical simulations for many years, but the corresponding tables often do not supply sufficient information on the thermodynamic and compositional details and do not take into account all relevant phase transitions when multiple phases coexist. The [LS91] equation of state is motivated by Skyrme-Hartree-Fock models for nuclear matter and finite nuclei, while the [STOS98b, STOS98a] use a relativistic mean field approach. In both models heavy nuclei are represented by a single nucleus, that is described in a Wigner-Seitz cell using the Thomas-Fermi approximation. The choice of such a nucleus is made in accordance with astrophysical conditions. However, nuclear properties often alter drastically from nucleus to nucleus and such changes are not covered by these representative nuclei. Of the light clusters only α-particles are present while other light nuclei like deuteron, triton, helion are not considered. However, it has been shown that neutrino luminosities can be affected by the presence of these additional clusters [AMPO$^+$08] and therefore should be taken into account in equations of state. The change of the composition of nuclear matter can significantly affect

the supernova dynamics and influence the weak interaction processes in supernova simulations, therefore for reliable supernova simulation one needs to take into account all the compositional details when constructing an equation of state. Recent developments for the equations of state are based on a nuclear statistical equilibrium description [HSB10], [BM10] and include the full distribution of nuclei. However, these models can not describe the transition to uniform nuclear matter around saturation density and therefore need to introduce the heuristic excluded volume mechanism [BM10]. On the other hand, the quantum statistical approach [RMS82b] to nuclear matter allows to describe the medium modifications to cluster properties and their dissolution at higher densities. We will follow this approach in the following.

In recent years, new experimental data on atomic nuclei, heavy-ion collisions and from astrophysical observations appeared that need to be exploited to derive and constrain equations of state. Subsequent advances in the theoretical description of nuclear matter and significant improvements of supercomputers have triggered new developments for constructing equations of state. Nevertheless, existing microscopic approaches still do not allow the construction of a description in the whole range of densities and temperatures. Thus, approximations and simplifications are needed to develop practical schemes. Different phenomenological approaches to the equation of state continue to be developed.

We start the introduction with discussing matter at various thermodynamic conditions, densities and temperatures that may appear in nature and terrestrial experiments, see Sections 1.2 and 1.3 . The following Section 1.4 is devoted to the description of stellar matter in supernovae and neutron stars. An overview of different theoretical models and constraints for the equation of state are given in Section 1.5. A particular case of the relativistic mean-field approach used in this work is presented in Section 1.6. In Subsection 1.6.3 two-body correlations beyond the mean field considered in this work are discussed.

In this work we study the effect of two specific types of correlations on thermodynamic properties of nuclear matter within the framework of a generalized relativistic mean-field model with light clusters as additional degrees of freedom beyond nucleons. In particular, these correlations include two-body scattering contributions and pairing effects. They appear due to the short-range nucleon-nucleon interaction at low densities and modify the composition and thermodynamic properties of matter. These effects should be included in the equation of state since in this density regime they may strongly influence the structure of the proto-neutron star [SR08], the effectiveness of the neutrino re-heating of the shock wave in supernova simulations [LP04] and the cooling history of neutron stars.

This thesis is divided into two major parts. In the first major part we introduce a generalized relativistic mean-field (RMF) model that includes clusters and two-nucleon scattering correlations in an effective way as explicit degrees of freedom in the thermodynamic potential. These bound and scattering states are represented by quasiparticles with density and temperature dependent properties. All relevant quantities are derived in a thermodynamically consistent way. The model reproduces relativistic mean field results around nuclear saturation density, where clusters are dissolved. The low-density behavior of nuclear matter at finite temperatures with nucleons and light nuclei is considered within a fugacity expansion of the grand canonical potential by comparing the virial equation of state with the generalized relativistic mean field approach. From the comparison of the expansions consistency relations are derived, which connect quasiparticle parameters with the meson-nucleon couplings of the RMF model in the vacuum and the phase shifts or effective-range parameters of nucleon-nucleon scattering. We investigate different choices of the meson-nucleon couplings and quasiparticle properties set by

these consistency relations. In addition, relativistic corrections to the traditional virial equation of state are obtained from these relations. They become larger than the effects of particle correlations in the low-density limit. The medium dependence of quasiparticle properties and their parametrizations are discussed.

The second major part of this thesis is devoted to the investigation of the effect of pairing correlations on the thermodynamic properties of pure neutron matter for densities up to saturation. A large number of experimental facts and theoretical findings suggest the existence of superfluidity, due to pairing correlations in nuclear systems at sufficiently low temperatures $T \lesssim (0.1 - 3)$ MeV. The neutron superfluid in the crust of a neutron star is believed to play a key role in the pulsar glitches mechanism, which is considered to be an observational evidence of superfluidity in these stars [ST83]. Ordinary mean-field theories treat nucleons as uncorrelated quasiparticles and do not take into account additional pairing effects. Up to now, global equation of state tables for astrophysical applications neglect pairing effects. Here we extend the relativistic mean field model by including pairing correlations in the ${}^1S_0$ nn channel. Calculations are performed with a Yamaguchi separable potential. Pairing gaps are computed for various temperatures. The results for thermodynamic quantities are compared with relativistic Fermi gas calculations. An overall variation in the pressure of 10% is observed for a given model due to pairing.

The effects of two-body correlations were added self-consistently in the mean-field model, however, our approach is not limited to the chosen particular generalized relativistic mean field model with density-dependent meson-nucleon couplings. It can be applied to other mean-field approaches as well. In future we plan to build equation of state tables including correlation effects that could be applied in astrophysical simulations.

1.2 Thermodynamic conditions

We study dilute warm matter composed of strongly interacting particles, i.e. neutrons and protons. Such matter exists in nature and can be studied in the laboratory in heavy-ion collisions. The properties of the matter depend on the baryon density $n = n_n + n_p$, temperature T and proton fraction $Y_p = \frac{n_p}{n}$, where n_n and n_p are the neutron and proton number densities, respectively. Matter may exist in a variety of phases.

Cold nuclear matter can be found in atomic nuclei at baryon densities up to the nuclear saturation density $n_{sat} \simeq 0.16$ fm^{-3}. The proton fraction in medium-mass nuclei is $Y_p \approx 1/2$ and below 0.4 for the most heavy stable nuclei.

Cold neutron matter in thermodynamical equilibrium with $Y_p < 0.1$ is expected to exist in the interior of neutron stars, where the density may reach values up to $\sim 10\, n_{sat}$. These stars are born in core-collapse supernova explosions as proto-neutron stars, where dense and hot baryon matter is formed with a temperature $T \lesssim (50 - 100)$ MeV at Y_p ranging between 0.3 and 0.4.

In the laboratory, non-equilibrium dense nuclear matter is produced in heavy-ion collisions. A diversity of nuclear phases such as nuclear liquid, nuclear gas or quark-qluon plasma can be formed in such experiments. GSI and other facilities have studied the properties of such matter and contributed to the knowledge in this field. Future facilities like Facility for Antiproton and Ion Research (FAIR) at Darmstadt and Nuclotron-based Ion Collider fAcility (NICA) at Dubna open exciting possibilities to generate non-equilibrium strongly compressed baryon rich matter.

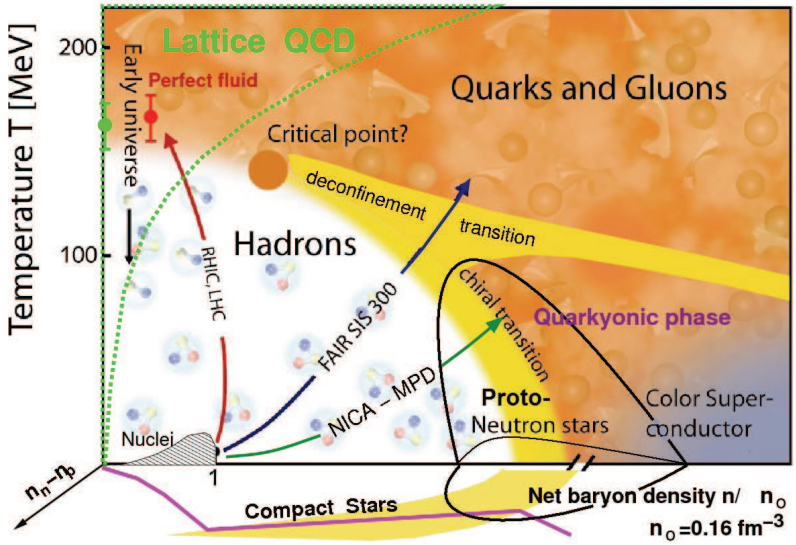

Figure 1.1.: Phase diagram of strongly interacting matter. Fig. taken from [QCD].

Different theoretical models have been developed to describe properties of dense matter at various temperatures and isospin asymmetries $\beta = 1 - 2Y_p$. These approaches can be constrained by various data from astronomical observations and terrestrial experiments. In this work we focus on matter at densities below saturation and temperatures below 20 MeV. At these conditions correlations are important, for example the formation of clusters in bound and scattering states due to the strong interaction. In this thesis we extend a relativistic mean-field model that includes light clusters, e.g deuterons and α particles, by including nucleon-nucleon scattering correlations. These contributions are constrained from the virial equation of state that is the exact model-independent low-density limit, depending only on experimentally observable quantities. In addition, the effect of pairing correlations on thermodynamic quantities is studied. Correlations modify thermodynamic properties of dilute warm matter expressed by various equations of state.

1.3 Variety of phases of dense matter

When describing strongly interacting matter in theoretical models, it is usually assumed that the particles are uncharged and there is no Coulomb interaction. Only the strong interaction is considered and will affect the properties of matter. The possible phases of dense matter and their boundaries are illustrated in Fig. 1.1 with a diagram of temperature versus net-baryon density.

Conditions similar to the low-density high temperature region of the diagram, occurred in the early Universe. At finite temperatures and densities lower than that of the atomic nuclei, α particle condensation and clustering may appear. With increasing density and at low temperatures we move to compressed nuclear matter appearing in neutron stars. At low temperatures and densities $(0.3 - 0.7)\, n_{sat}$ so-called nuclear "pasta" structures may appear. These highly inhomogeneous structures, however, can only be described when the Coulomb interaction comes into play. The competition between the long-ranged Coulomb repulsion and short-ranged nucleon-

nucleon attraction leads to the formation of these pasta phases. They do not appear in Fig. 1.1, since the Coulomb interaction is omitted in pure nuclear matter.

In Fig. 1.1 a diversity of nuclear phases such as nuclear liquid, nuclear gas, quark-gluon plasma appear. There are different types of phase transitions, for example the typical first-order liquid-gas phase transition or the hadron-quark phase transition, can be studied in heavy-ion collisions. In the high energy collisions studied at Super Proton Synchrotron (SPS), Relativistic Heavy Ion Collider (RHIC) and Large Hadron Collider (LHC), baryon-poor matter is produced. Properties of such matter are tested by lattice calculations at zero and finite baryon chemical potential $\mu \lesssim T$. These calculations predict a cross-over transition between the hadron phase and a strongly coupled quark-gluon plasma. The baryon-poor matter above the transition line at temperature $T > T_c(\mu) \approx 170$ MeV behaves as an almost perfect fluid. There is a possibility to find manifestations of the critical end point (CEP) of the hadron-quark phase transition at FAIR and NICA energies. At higher densities one deals with baryon-rich matter to the right from the CEP in the phase diagram.

A variety of new phenomena such as pion condensation, kaon condensation, quarkyonic and quark deconfined phases may occur in the dense interior of neutron stars. With the increase of density the Fermi energy of nucleons rises and correspondingly their chemical potentials. They can get very high reaching the masses of the hyperons allowing the formation of these particles. Quark matter in the dense core of neutron stars may exist in superconducting phases such as two-color-superconducting (2SC) phase, color-flavor-locking (CFL) phase, color-spin-locking phase (CSL). Ordinary nucleons in nuclei and neutron stars undergo neutron-neutron and proton-proton pairings. In some nuclei neutron-proton pairing might be possible. There may exist a broad region of densities, where matter organizes a hadron-quark pasta consisting of droplets, rods, slabs, tubes or bubbles of one phase surrounded by another phase.

In order to describe the properties of matter in such a rich phase diagram one needs to know the relations that connect different thermodynamic properties of the system in a very broad region of baryon densities and temperatures. Such relations that connect thermodynamic properties of the system like energy, pressure, free energy with natural parameters as temperature, density etc. are called equations of state (EoS). In order to construct an EoS for a broad range of densities and temperatures, it is very important to consider phenomena in different domains of (astro) nuclear physics, e.g. particle scattering, atomic nuclei, heavy-ion collisions, supernovae, proto-neutron stars, neutron stars.

Nuclear matter close to saturation can be characterized by a few parameters that can be determined experimentally. From the expansion of the binding energy per nucleon E/A around saturation density one gets

$$\frac{E}{A}(n,\beta) = a_v + \frac{K}{18}\xi^2 - \frac{K'}{162}\xi^3 + ...\beta^2\left(J + \frac{L}{3}\xi\right) + \ldots = E_0(n) + \beta^2 E_S(n) + \ldots, \qquad (1.1)$$

where $\beta = 1 - 2Y_p$ is the asymmetry parameter and $\xi = (n - n_{sat})/n_{sat}$ is the density deviation. E_0 is the binding energy in symmetric nuclear matter and E_S is the symmetry energy. The parameters a_v, K, K', etc., are experimentally determined with some uncertainty. The binding energy for symmetric matter $a_v \approx -16$ MeV and the symmetry energy $J \approx 30 - 35$ MeV can be extracted from the Bethe-Weizsäcker formula of atomic masses. The incompressibility of the symmetric matter $K \approx (210 - 250)$ MeV characterizes the resistance of the matter to compression. The skewness K' is related to surface properties of nuclei. For asymmetric nuclear matter

also the symmetry slope parameter $L \sim 60$ MeV is important. It determines the neutron skin thickness of nuclei, that is correlated to the stiffness of the neutron matter EoS [Fur02].

In this thesis we will focus on the description of hadronic matter at sufficiently low or even zero temperatures and low densities. These conditions appear in the outer regions of proto-neutron stars and the crust of neutron stars. In the next section stellar matter in supernovae and neutron stars is discussed.

1.4 Stellar matter in core-collapse supernovae and neutron stars

One of the motivations for this study is the astrophysical application of equations of state. Therefore we start with a brief discussion of phenomena in core-collapse supernova evolution, proto-neutron star formation and neutron star structure, where properties of dense matter and its composition are relevant.

1.4.1 Core-collapse supernovae

Although details of stellar evolution are not relevant in this thesis, it is worth briefly mentioning the structure of a collapsing stellar core. A star with a mass $M \approx (10-20)\ M_\odot$ terminates its existence with a gravitational collapse of the degenerate iron core. The mass of this core is estimated to be $M_{core} \sim 1.5 M_\odot > M_{\rm Ch}$, where $M_\odot$ is the solar mass and $M_{\rm Ch}$ is the Chandrasekhar mass, see [ST83, JLM$^+$07]. The in-falling matter dissociates into nucleons. Due to electron capture on protons the material gets neutron rich and neutrinos are released.

As the densities reach $n \approx 10^{-4}$ fm^{-3}, neutrinos become trapped even though they have a very small cross section. This happens because at these densities their diffusion time (due to scattering on nuclei) becomes larger than the typical timescale of the collapse. The core contraction proceeds until the central density reaches several times the saturation density. The core bounces, due to the stiffness of the nuclear matter EoS, creating a shock wave, which propagates outwards through the in-falling material. As the shock wave reaches the density region of the neutrinosphere $(10^{-4}-10^{-3})$ fm^{-3}, neutrinos start streaming freely. In realistic simulations, however, the shock wave stalls at some distance from the center, as it interacts with the in-falling matter and loses energy. This leads to the lack of the energy to trigger an explosion. Several possible scenarios of what happens next have been explored through simulations. Ref. [JR05] argues that the shock is revived by the interaction with the large neutrino flux arising from the core. Authors of [DBLO06] suggest that the free energy associated with the differential rotation converts into kinetic energy with which the explosion can be ignited. Another possibility is given in [KST06]. There the conversion of gravitational binding energy to large amplitude acoustic waves, that revive the shock due to unstable oscillations of the collapsed core, is considered.

Up to now, numerous attempts to simulate supernova explosions in spherical symmetry haven't been successful. Some of the two dimensional calculations, however, lead to the successful explosions. Nevertheless, two dimensional calculations are already computationally expensive, representing a challenge for theoretical astrophysics [BDM$^+$06, JMMS08, MJ09]. All these calculations are sensitive to the EoS used. Typical conditions in core-collapse supernova extend from zero to several (up to ten) times saturation density and cover the temperature region from 0 to (50-100) MeV.

In supernova explosions almost 99 % of energy is released in the form of neutrinos and antineutrinos. Due to the weak interaction and consequently a large mean-free path l_ν, neutrinos

are able to propagate over large distances. Therefore, it is important to include the correct description of the neutrino interaction with matter since the collapse of the supernova core and the formation of the proto-neutron star depend significantly on the weak interaction processes and neutrino transport [Lan06].

From the first several ten milliseconds to minutes after core bounce, temperatures exceed the opacity temperature $T_{\rm opac}$ inside proto-neutron stars and neutrinos are trapped. For such a temperature the mean free path of the neutrinos $l_\nu = R$, where R is the radius of the proto-neutron star . For $R \sim 10$ km the opacity temperature is of the order of MeV. Outside the proto-neutron star (at the first several ten milliseconds) neutrinos are trapped inside the neutrinosphere in the low-density region of $(10^{-4} - 10^{-3})$ fm^{-3}. Nucleons may cluster into nuclei at these densities, thus changing the transport properties for neutrinos in matter. The equations of state used in simulations so far have quite a simplistic description of the chemical composition at low densities where neutrino interaction strongly depends on the composition of the system. Therefore, it is of crucial importance to describe the low-density region, where the presence of clusters, its geometrical shape and topology might be important in supernova simulations.

Our knowledge of the properties of nuclear matter has improved in the last decades and older equations of state are not fulfilling all the constraints developed in the recent years. Therefore, one needs an improved EoS from very low to high densities for finite temperature matter. This is important for the description of the core-collapse, shock formation and its propagation [SYS$^+$05, JLM$^+$07] respecting all of the known constraints.

1.4.2 Neutron Stars

Hot compact stars with radii $R \lesssim 50$ km are formed during the first several ten milliseconds of core-collapse supernova explosions. Within tens of seconds to minutes these proto-neutron stars cool down due to the neutrino emission till the temperature reaches a few MeV. At this stage the star shrinks to the size $R \sim (10-15)$ km becoming a neutron star, one of the densest long-living objects in the Universe. Neutron star masses are typically in the range of $(1-2)\ M_\odot$ with the density in the center reaching up to $10\, n_{sat}$ for the most massive objects. Some of the neutron stars are seen as pulsars, some of them are found in binary systems. Many pulsars have very low temperatures $T \ll 0.1$ MeV because they are very old. There are different properties of neutron stars, discussed in the following, that all depend on the details of the equation of state.

Structure. The structure of a neutron star can be subdivided into the atmosphere and four internal regions: the outer crust, the inner crust, the outer core and the inner core, see Fig. 1.2.

The atmosphere is a thin plasma layer extending above the surface of the star, consisting mostly of hydrogen, with an admixture of heavy elements in some cases. This is an observationally important region, allowing to determine the surface temperature and surface magnetic field and to get information about the radius of the neutron star [PR06]. The atmosphere thickness varies from ten cm for a hot neutron star (with surface temperature $T_s \gtrsim 10^{-5}$MeV) till few mm for a cold neutron star (for $T_s \lesssim 10^{-6}$MeV). Current atmosphere models are far from being complete.

The outer crust extends from very low densities at the surface of the star till the neutron drip density $n_{ND} \approx 2.56 \cdot 10^{-4}$ fm^{-3} is reached. This is the density where under the conditions of β-equilibrium and charge neutrality neutrons drip out of the nuclei [BPS71, RHSB06]. The thickness of the outer crust is typically of some hundred meters. The EoS here is determined primarily by electrons and ions. A thin outer layer contains a non-degenerate electron gas,

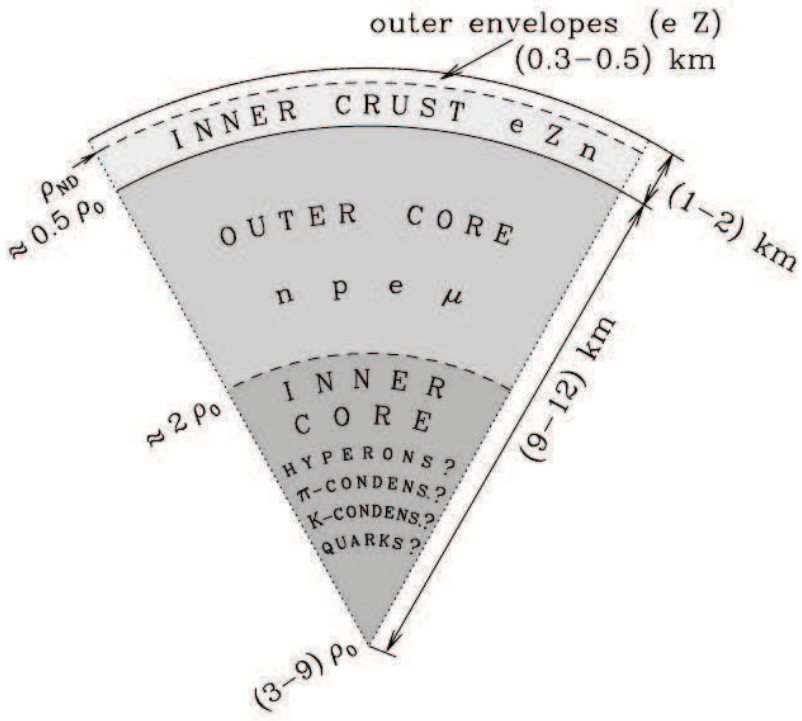

Figure 1.2.: Schematic structure of a neutron star. Here ρ_0 denotes the nuclear saturation density. Fig. taken from [HPY10].

while in deeper layers electrons become strongly degenerate. A large fraction of the outer crust is solidified with nuclei forming a lattice. As the electron Fermi energy grows with the increase of density, electrons penetrate the nuclei. This induces beta-decay processes and the neutronization of nuclei. Finally, the neutron separation energy of the nuclei goes to zero and neutrons start to drip from nuclei forming a free neutron gas. The drip line marks the point where the boundary to the inner crust is reached. The inner crust is about a few km thick [SW05, WS06]. Here matter consists of electrons, free neutrons and neutron-rich nuclei. The fraction of free neutrons grows with increasing density. They may form superfluid phases. Neutron pairing starts from the neutron drip density n_{ND} and extends to the density of about n_{sat}. Pairing occurs in the $^1S_0$ state in this density region. Some models predict the formation of nuclear pasta, various geometrical phases of inhomogeneous matter [RPW83, aHSY84, OaHY84] in the density range$(0.3-0.7)\,n_{sat}$. Pasta phases only slightly affect thermodynamic properties of the matter but may crucially influence neutrino transport properties of neutron star matter. Beyond this region, for $n \gtrsim 0.7\,n_{sat}$, the transition from the inhomogeneous crust to the homogeneous outer core occurs.

The outer core occupies the density region with $0.7\,n_{sat} \lesssim n \lesssim 2\,n_{sat}$. It contains a strongly degenerate neutron liquid with a several percent admixture of degenerate protons, relativistic electrons and in denser regions of muons. Neutrons are paired in this region most likely in the $^3P_2$ state whereas protons are paired in the $^1S_0$ state.

Deeper layers form the so-called inner core, where new degrees of freedom appear. Its structure is a question of debates due to uncertainties in our knowledge of the strong interaction at such high densities. Here new particles and phases may appear. In most models the EoS becomes softer when one adds more particle species. With the increase of the neutron Fermi

energy hyperons may be produced. Most probably first Λ and Σ^- appear. For high densities and high neutron-proton asymmetry one expects the appearance of pions or kaons. Pions undergo a strong attractive P wave πNN interaction while antikaons are subject to attractive S- and P-wave antikaon-nucleon-hyperon interaction. Pion condensates may appear due to these attractive interactions. Thus massive neutron stars may undergo first order phase transitions to states with these condensates. Even strange quark matter may be formed in dense neutron star interiors. Quarks can be paired forming various color superconducting phases, such as 2SC, CFL, CSL. The di-quark pairing gap in 2SC and CFL phases may have very large values (of the order of 100 MeV). Reviews of models including such exotic components can be found in [Gle96, RW00]. If any of the mentioned phase transitions occur, most of the equations of state become more soft, resulting in the decrease of the maximum neutron star mass.

Neutron star masses. Mass measurements are obtained from binary systems, where both objects are neutron stars or one is a neutron star and another one is a white dwarf. The lowest reliably estimated value of a neutron star mass is $1.18 \pm 0.02 M_\odot$ of the binary pulsar J1756-2251 [FKL$^+$04]. The most accurately measured value of the mass is $M = 1.4408 \pm 0.0003 M_\odot$ for the radio pulsar PSR1913+16 [TC99]. The most massive neutron star is found in PSR J1614-2230, $M = 1.97 \pm 0.04 M_\odot$ [DPR$^+$10]. The latter result sets a significant constraint on equations of state of dense matter leading to the exclusion of too soft equations of state.

Mass-radius relation. The relation between mass and the radius ($M - R$ relation) is unique for a given equation of state. It can be extracted from solving the Tolman-Oppenheimer-Volkoff equation [Tol34, OV39]. It serves as the most simple and obvious test of equations of state by comparing with existing experimental data [SLB12] and the maximum neutron star mass in particular.
The TOV equation is a first order differential equation

$$\frac{d}{dr}p(r) = -\frac{G}{r^2}[\epsilon(r) + p(r)][M(r) + 4\pi r^3 \epsilon(r)][1 - 2GM(r)/r]^{-1} \tag{1.2}$$

relating the pressure $p(r)$ and the energy density $\epsilon(r)$, depending on the radius coordinate r. G is the gravitational constant and

$$M(r) = \int_0^r 4\pi r'^2 \epsilon(r') dr' \tag{1.3}$$

is the mass $M(r)$ inside the radius r. The radius R of a star is determined when the pressure vanishes $p(R) = 0$. From these relations we see that in order to calculate the neutron star mass, we need to know the EoS $p(\epsilon)$ of the system. An analysis of recent observations of transiently accreting and bursting sources allowed the authors of [SLB12] to conclude that the radius of a neutron star with mass 1.4 $M_\odot$ should lie between 10.4 and 12.0 km. It puts additional limitations on the EoS.

Cooling. After the temperature decreases to values $T < T_{\rm opac}$, the neutron star begins to cool down by direct neutrino emission mainly from the interior region. At this stage the neutron star cooling evolution is very sensitive to the details of the core and crust structure. The value of the neutron star mass and a suggested density dependence of the nucleon-nucleon interaction strongly affect the magnitude of the neutrino emissivity. For $T < T_{cr} \lesssim (0.1 - 1)$ MeV cooling rates are significantly influenced by the values and density dependencies of the superfluid gaps.

Typically it takes several hundred years for a neutron star to cool down to temperatures $T \lesssim (0.01 - 0.1)$ MeV in their interiors. The temperature at the neutron star surface T_s is still 100-1000 times smaller than in the interior. After more than $\gtrsim 10^5$ years the neutrino emission ceases and the star continues to loose its energy due to the emission of thermal photons from the surface.

Surface temperatures are measured in soft X rays for a dozen of pulsars with a reasonable accuracy. For some others only upper limits for the surface temperatures are determined. These data points can be unified in three groups in relation to: slow coolers, intermediate coolers and rapid coolers. In order to describe all three groups of points within one consistent scenario, one needs a factor $\sim 10^3$ difference in the neutrino emissivities of these objects. Recent very accurate measurements of the time dependence of the surface temperature $T_s(t)$ [HH10] allow to put additional constraints on the neutrino cooling mechanisms. The analysis of different neutrino reactions demonstrates that the cooling via the so called direct Urca process $n \to p + e + \bar{\nu}_e$ is too rapid to explain the data. This fact produces the so called direct Urca constraint: the direct Urca process should probably not occur for stars with masses $M \lesssim 1.5 M_\odot$. Since this process occurs only in case when the proton fraction exceeds (11-14)%, it puts a restriction on the density dependence of the symmetry energy in dense matter. All data can be explained for stars with different masses by taking into account the so called medium modified Urca reactions, such as $n + n \to n + p + e + \bar{\nu}_e$, where a sufficiently strong density dependence of the NN interaction should be included in calculations.

Magnetic field and rotation. Measured magnitudes of magnetic fields vary from low values (such as $\lesssim 10^{10}$G) in LMXB (Low Mass X-ray Binaries) to $\sim 10^{13}$ G for radio pulsars such as Crab and to $\sim 10^{15}$ G for magnetars, the strongest magnets in the Universe. Some neutron stars become pulsars during their evolution. Pulsar periods vary from milliseconds, which corresponds to a rotation with velocity $\sim 10^{-2}c$, where c is the velocity of light, to very large rotation periods ($\gg$ seconds).

Concluding this section, we note that proto-neutron and neutron star physics covers a very wide range of densities (up to $10\, n_{sat}$) and temperatures (up to 50 MeV), serving as a wonderful tool to study the properties of isospin asymmetric nuclear matter. In this thesis we shall not consider the high density regime, where non-nucleonic components may appear, rather we aim at describing correlations at low baryon densities that are relevant for the description of the neutron star outer and inner crusts.

1.5 Theoretical models for the equation of state

Already in the end of fifties of the last century Nobel prize winner H. Bethe estimated that more man hours of work had been devoted to understanding the problem of nucleon-nucleon interaction than to any other scientific question in mankind's history [Bet53]. Up to now, despite the essential progress in this field and the implementation in the EoS, there are still problems to be solved.

1.5.1 Different approaches to the nuclear matter EoS

Nuclear matter at finite temperatures and low densities represents a system of strongly interacting particles, where correlations play a significant role. Such interesting and exciting phe-

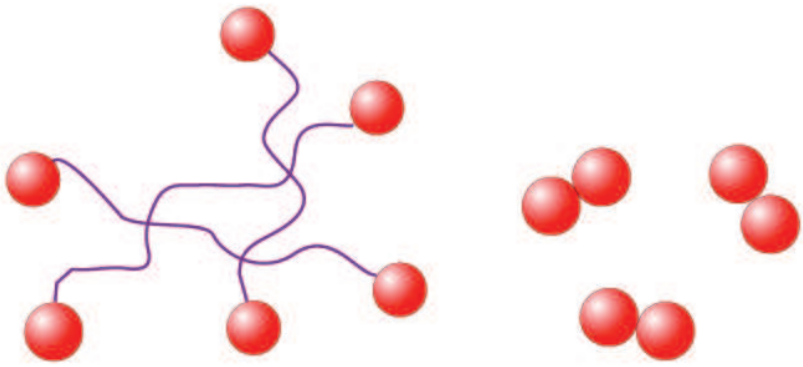

Figure 1.3.: Schematic picture of the difference between the BCS regime (left) of loosely bound fermions and the BEC regime (right) of strongly bound pairs. The picture is taken from [CH08].

nomena as clustering, formation of condensates and phase transitions occur in this region of the phase diagram. These effects influence the thermodynamic quantities of the dense matter EoS and its chemical composition. For instance, the formation of clusters at low densities has an effect on the symmetry energy [NRT$^+$10]. Its density dependence is a highly debated issue in nuclear physics. There are different types of correlations. Typical for the Fermi systems at low temperatures are the correlations of two particles with opposite spin and momentum on the Fermi surface. These are typical pairing correlations ("BCS") in momentum space. The other case is the formation of bosonic bound states like the deuteron in symmetric matter ("BEC") and these are correlations in the coordinate space. An illustration of the difference between such BCS and BEC correlations is shown in Fig. 1.3.

There are various ways to describe properties of nuclear matter, starting from microscopic many-body calculations using realistic nucleon-nucleon (NN) potentials, to simplified approaches such as non-relativistic and relativistic mean-field models. The results are sensitive to the chosen NN interaction. Realistic two-body nucleon-nucleon forces are determined from the partial-wave analysis of elastic NN scattering. An example is the Argonne v_{18} potential [WSS95] fitted to all of the nucleon-nucleon scattering data in the Nijmegen database. Other widely used realistic forces fitted to NN data are the Nijmegen [SKTdS94], the Paris [LLR$^+$80] and the CD Bonn potentials [MSS96]. All these interactions typically contain a repulsive part which accounts for NN repulsive correlations at short inter-nucleon distances, an intermediate attraction and a one-pion exchange potential as long range part. Two-nucleon forces prove to be insufficient to properly describe nucleon binding and nuclear matter properties at saturation density and three-body forces are required in realistic calculations.

One can include nucleon-nucleon correlations in theoretical methods in several ways. Some of these techniques use correlated many-body wave functions beyond the Slater determinant approximation. These methods include the Brueckner hole-line expansion [Bru55, Bet71, JLM76], the coupled cluster or exponential S-matrix approach [KLZ78, Bis98], the self-consistent evaluation of Greens functions [DM92], variational approaches using correlated basis functions [WFF88, AP97, FF98] and recent developments employing quantum Monte-Carlo techniques [SC92, Cep95].

We discuss two approaches in more detail. A review of the Brueckner-Hartree-Fock approach is presented in [Bal99]. Its relativistic counterpart, the Dirac-Brueckner-Hartree-Fock (DBHF)

theory [Mac89,LMB92,KS06,vDFF05b,vDFF04,vDFF05a,vDFF07,Fuc04,GBFF99] allows to take care of causality. Recent results of these approaches can be found in the papers [BBB97, HP00, LCK08, vDFF07, WFF88]. The resulting EoS predicts a maximum neutron star mass $\simeq 2.3 M_\odot$ exceeding the experimental value $1.97 \pm 0.04 M_\odot$. A disadvantage of DBHF calculations is the linear density dependence of the symmetry energy that results in a low threshold mass value for the occurence of the direct Urca process. Thus hadronic models based on the DBHF EoS have problems with the description of the neutron star cooling data.

An example of a variational approach is the model of Akmal, Pandharipande and Ravenhall [APR98].The corresponding EoS is too soft in the high density regime, giving a small maximum mass of a neutron star, see [LL09,APR98]. Therefore in Ref. [APR98] a three-nucleon interaction (TNI) is additionally incorporated in the model. The improved EoS describes matter up to densities $\sim 4 n_{sat}$. However, since it uses a non-relativistic potential the causality condition is violated at larger density. In order to solve this problem the model includes relativistic boost corrections. The resulting maximum mass $\simeq 2.2 M_\odot$ exceeds the experimental value $1.97 \pm 0.04 M_\odot$ of the most massive pulsar known so far.

Another way to include correlations is by introducing quasiparticles with self-energies. These mean-field models yield an energy-density functional. In full analogy with the Kohn-Sham approach [KS65] to the density functional theory [DG90], the ground state energy and the density of the system can be obtained from the minimization of the energy functional. Non-relativistic functionals can be derived from non-relativistic potentials like Skyrme [Sky59, BHR03] and Gogny [DG80].

Relativistic mean-field (RMF) theories start with a relativistic Lagrangian density for baryon and (sigma-omega-rho) meson fields, being later approximated on the mean field level. Due to the Lorentz covariance, the models have no problems with causality. In standard RMF models, see Section 1.6, NN scattering data are not used as a constraint. The parameters of the interaction are fitted to the properties of bulk nuclear matter at saturation density and properties of finite nuclei. The first widely known RMF model, the so called Walecka model [Wal74], included only two parameters fitted to reproduce the value of the binding energy at saturation density and the value of the saturation density itself. Various modified Walecka models additionally include non-linear meson self-interactions [BB77], e.g. the σ potential with two extra parameters for a better description of finite nuclei properties. Additionally the isovector ρ-meson term can be included, which allows to fit the symmetry energy at the saturation density. The parameters can now be adjusted to the values of the nuclear saturation density, the binding energy per nucleon and the nuclear symmetry energy E_s, and also to values selected for such roughly known quantities as the nuclear compression modulus K, and the nucleon effective mass M. The values of all mentioned quantities are extracted from the analysis of numerous nuclear experiments. These yield masses, radii and excitation spectra of medium-mass nuclei. Additional information is obtained from heavy-ion collisions and neutron star data.

Different equations of state, which are constructed to describe nuclear properties at saturation, might differ significantly at higher densities leading to a vast uncertainty in the energy density and symmetry energy. An example of such behavior is shown in Fig. 1.4 for various models described below in Subsection 1.6.2. Considering such uncertainties in the EoS, one would like to have at hand additional constraints from experiments. Some of them can be extracted from the precise measurement of the neutron skin of heavy nuclei [HPSM01, HP01a] and from the analysis of heavy-ion collisions [DLL02].

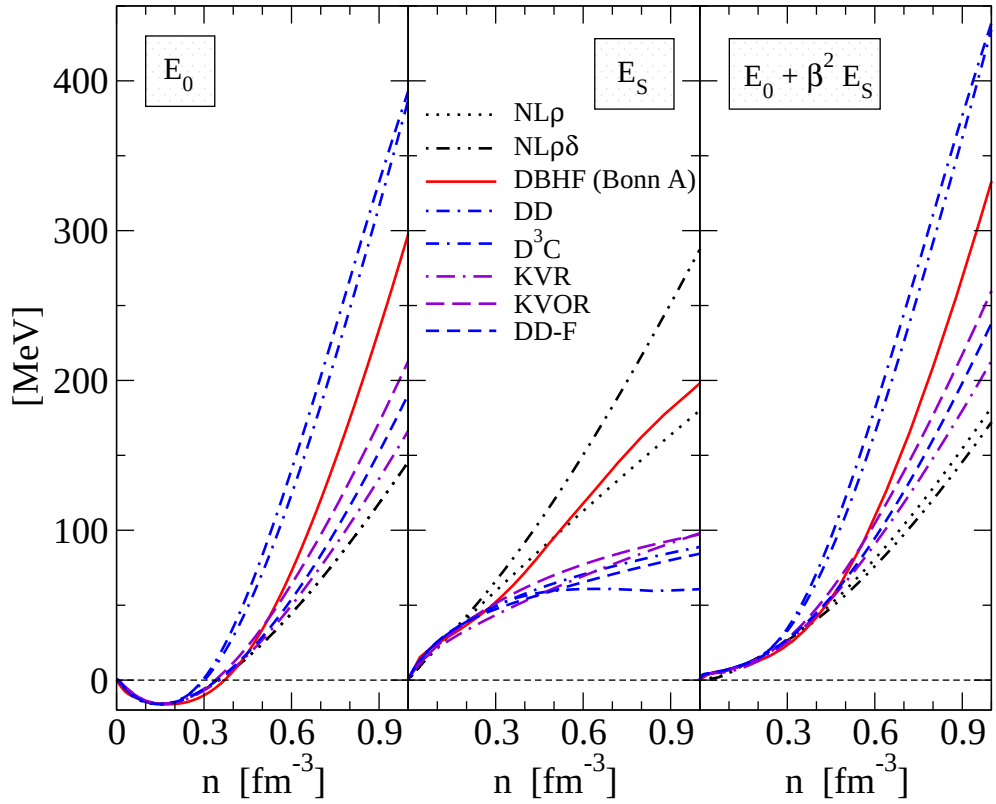

Figure 1.4.: The energy per nucleon of isospin symmetric nuclear matter E_0 (left), the symmetry energy E_s (middle), the neutron star matter energy per nucleon $E_0 + \beta^2 E_s$ (right), where $\beta = 1-2Y_p$ is the parameter of isospin asymmetry in beta-equilibrated matter, for various equations of state (labels of the curves). The Fig. is from [KBT+06].

Equations of state appropriate for astrophysical applications are required to cover a vast range of densities, temperatures and proton fractions. The temperature dependence required to describe excited nuclear matter is easily incorporated in the density functional on the mean field level with the help of the thermal fermion distribution functions.

The first models used in supernova simulations have used density functionals with parameters obtained from parameters of the liquid drop model [LLPR78]. An extension of this model that includes α-particle gas has led to the widely used Lattimer-Swesty EoS [LS91]. Another well-known EoS was developed by Shen, Toki, et al. [STOS98b], [STOS98a], which is based on a RMF model with non-linear meson self-couplings and with the use of the Thomas-Fermi approximation to describe a representative heavy nucleus in a spherical Wigner-Seitz cell. This model includes α-particles as separate species, while other light clusters are neglected. At the moment these are the most frequently used equations of state in astrophysical applications. They, however, do not take into account all the compositional details at low densities and fail to reproduce the virial limit, as will be shown in Subsection 2.5.2. In this work we try to improve the low-density description of nuclear matter by taking into account the formation and dissolution of light clusters and scattering correlations consistent with the virial limit.

1.5.2 Constraints on the EoS

Experimental data are of significant importance for constraining the EoS of dense matter. Such constraints and several equations of state are discussed in the review [KBT$^+$06]. There, a testing scheme was proposed, which takes into account information on different data from nuclear physics and astronomy. The description of the models used is given in Section 1.6.2. Below we will discuss some of the most relevant observables. We will discuss several constraints in Section 1.6.2, namely nuclear matter parameters extracted at saturation density. Additionally, equations of state should describe the properties of finite nuclei, such as binding energies, spin-orbit splittings, charge radii, diffraction radii and surface thicknesses. Another observational constraint, which can be tested in terrestrial experiments, arises from the analysis of flow data of heavy-ion collisions [DLL02] at high densities. The analysis of these data allow to indicate a certain allowed band in the pressure-density diagram. An additional constraint on the symmetric matter EoS originates from the analysis of sub-threshold kaon production [Fuc06]. Other sources of observational data are compact stars, where over a vast density range, rather cold isospin-asymmetric matter can be investigated.

A particular interest is contained in the mass-radius relationship of the neutron star, see 1.4.2 which is largely undetermined, due to the current impossibility of a simultaneous measurement of mass and radius. Equations of state of neutron stars are usually characterized as being "soft" or "stiff", depending on the slope of pressure as a function of the energy density. A stiffer EoS produces a larger maximum mass M_{max} of a neutron star. The precise measurement of a maximum mass of a neutron star has been recently performed by observation of the Shapiro delay of the radio signal from the pulsar $J1614-2230$ [DPR$^+$10]. This leads to the value of 1.97 ± 0.04 $M_\odot$, putting a rather strong constraint on the EoS of neutron star matter, since only a rather stiff EoS can reproduce such a neutron star mass. Phase transitions like pion condensation, kaon condensation, transition to quark matter etc., which may occur at supranuclear densities, result in the softening of the EoS leading to the reduction of a M_{max}. This is due to the liberation of new degrees of freedom that contribute more to the energy than to the pressure. However, recent works, which take into account corrections due to quark-quark correlations and superconductivity are consistent with a rather stiff EoS [ABPR05]. The radius of a star is sensitive to the equation of state in the vicinity of nuclear density [LP01] and to the density dependence of the symmetry energy.

Additionally, the behavior of the symmetry energy affects neutron star cooling. If the proton fraction $Y_p = n_p/(n_p + n_n)$ exceeds a critical value Y_{DU} the direct Urca process $n \rightarrow p + e^- + \bar{\nu}_e$ becomes dominating leading to a very fast cooling of a neutron star. Such a fast cooling does not allow to appropriately explain within a hadronic scenario the whole set of the soft X ray data on surface temperatures of pulsars. From the charge neutrality condition $n_p = n_e + n_\mu$ one can extract the corresponding DU-threshold value Y_{DU}

$$Y_{DU} = \frac{1}{1 + (1 + x_e^{1/3})^3}, \tag{1.4}$$

where $x_e = n_e/(n_e + n_\mu)$ is the leptonic electron fraction [KBT$^+$06]. Then the critical star mass M_{DU} (the direct Urca process occurs for $M > M_{DU}$ in an interior region of a star) can be estimated for every model. This and other constraints are presented in Table 1.1, where the successfulness of given equations of state is shown, depending on the amount of fulfilled conditions (the last column).

The measurements of rotation rates, estimates of temperature and age might also shed some light on the neutron star inner structure. Constraints on the EoS can be as well extracted from the theory. Recently additional constraints, which set a band of validity for every EoS, were introduced [HLPS10]. They were estimated based on the chiral effective field theory and many-body theory. Another constraint arises from the virial expansion at low-densities [HS06b], which allows to obtain the EoS of nuclear matter with the inclusion of α-particles [HS06a] and additionally tritons and helions [OGH$^+$07].

In Section 2.2 we will discuss nuclear matter at low densities in the virial limit which serves as an additional constraint to improve the RMF EoS.

Model	$M_{\max} \geq 1.9\ M_\odot$	$M_{\max} \geq 1.6\ M_\odot$	$M_{DU} \geq 1.5\ M_\odot$	$M_{DU} \geq 1.35\ M_\odot$	4U 1636-536 (u)	4U 1636-536 (l)	RX J1856 (A)	RX J1856 (B)	J0737 (no loss)	J0737 (loss 1% $M_\odot$)	SIS+AGS flow constr.	SIS flow+ K^+ constr.	No. of passed tests	(out of 6)
NLρ	−	+	−	−	−	−	−	−	−	−	+	+	1	2
NL$\rho\delta$	−	+	−	−	−	−	−	−	−	−	+	+	1	2
DBHF	+	+	−	−	+	+	−	+	−	+	−	+	2	5
DD	+	+	+	+	+	+	−	+	−	−	−	−	3	4
D^{3}C	+	+	+	+	+	+	−	+	−	−	−	−	3	4
KVR	∘	+	+	+	−	∘	−	−	−	+	+	+	3	5
KVOR	+	+	+	+	−	+	−	−	−	∘	+	+	3	5
DD-F	+	+	+	+	−	+	−	−	−	+	+	+	3	5

Table 1.1.: Summary of the fulfilled constraints for every model. The table is taken from [KBT$^+$06]. Non separated columns show the results for a strict (left) and weakened (right) interpretation of the corresponding constraint.

1.6 Basic features of the RMF approach

There are several reasons why RMF models are widely used in calculations of baryon matter EoS and why they have become a successful tool for the description of properties of finite-nuclei and neutron stars. Being phenomenological models, which originate from a hadronic field theory, RMF models contain several parameters, which can be tuned and adjusted to the properties of nuclear matter at saturation density. Thus one may get an EoS similar to the one that follows from more involved microscopic calculations, like that of the Urbana-Argonne group (APR EoS) [APR98]. Non-relativistic mean-field approaches are based on effective nucleon potentials. With the help of many-body techniques like Hartree-Fock, it is possible to derive the nuclear EoS, an example is the Skyrme-Hartree-Fock approach. The Skyrme force is a low-momentum expansion of the NN potential. It is expected to fail at high densities. A relativistic description is preferable over the non-relativistic one. Within the RMF approach one has no problem with causality at large densities, which arises if one uses non-relativistic potentials.

The relativistic approach allows to distinguish between scalar and vector densities, as well as Lorentz scalar and vector fields, describing essential properties of nuclear systems like the spin-orbit force. This is important for the calculation of nuclear structure, such as anomalous isotope shifts in Pb nuclei [SLR93].

Modern RMF models are extensions of the original Walecka (σ, ω) model [Wal74], where nucleons interact through the exchange of scalar (σ) and vector (ω) mesons with certain masses and coupling constants. A description of extended Walecka models and their application to the study of properties of nuclear matter can be found in [SW86]. The attractive intermediate range of the nuclear interaction is described by the scalar σ-meson, while the vector ω-meson is responsible for the short-range repulsion. With these degrees of freedom, one gets a reasonable description of saturation properties of nuclear matter. In order to consider the case of isospin-asymmetric matter one has to include the isovector ρ meson, which provides the isospin dependence of the nuclear force. The Coulomb interaction is taken into account by the inclusion of the electro-magnetic potential, which enters in the equations.

Boguta and Bodmer [BB77] extended the RMF model by introducing a nonlinear scalar self-coupling of the form $U = b\sigma^3 + c\sigma^4$ leading to a better treatment of the bulk properties of finite nuclei and the surface properties such as nuclear deformations [PRB87]. This is a standard form of the non-linear potential. In some sense this non-linear potential can be considered as a scalar density dependent σ-meson mass. Correspondingly, in many other RMF models the non-linear self-interactions of the σ meson were introduced [BB77, ST94, Bog81, RRM$^+$86, Rei88, Gmu91, Gmu92b, Gmu92a, SNR93, LKR97, LMVGZ04]. Additional non-linear interaction terms in isoscalar and isovector channels were included in [Bod91, SFM00, HP01b] in order to get a better description of finite nuclei. There have also been extensions of the RMF models, the so-called point-coupling (PC) models, obtained by expanding the energy density functional in powers of the σ, ω, ρ meson fields and their derivatives up to a given order. A number of parameterizations [SW97, ST94, FST97, DECVP01, GB04] of such RMF models have been considered.

Since RMF model parameters are determined by fitting to empirical properties of bulk nuclear matter at saturation density and properties of nuclei, one may expect that the model describes the EoS rather appropriately in the vicinity of the saturation density. However no free parameters remain to control the pressure and the symmetry energy at high and low densities. The solution of this problem might be in the introduction of density dependent meson couplings [BT92, FLW95, NVFR02, LMVGZ04] and [FLW95, TW99, HKL01, NVFR02, LNVR05]. This is a successful method to modify the density dependence of the nuclear interaction in the medium in an explicit form, leading to a flexibility in the adjustment of parameters to various properties of nuclear matter. In this work we use a RMF model with density dependent couplings and extend it to include 2-body correlations in the continuum at low densities in addition to light clusters.

1.6.1 RMF model with density-dependent couplings

In this work we extend a RMF model [Typ05] with a parameter set adjusted to the properties of finite nuclei. First we will consider the simple case with only neutrons and protons as basic constituents, represented by Dirac spinors ψ_i. We will study all cases from symmetric nuclear matter (SNM, equal number of neutrons and protons) to pure neutron matter (PNM, without the contribution of protons). Within the phenomenological approach, one tries to include as

few mesons as possible to reduce the number of fitting parameters. Our model includes σ, ω_μ, $\vec{\rho}_\mu = (\rho_\mu^1, \rho_\mu^2, \rho_\mu^3)$ meson fields, with the quantities Γ_σ, Γ_ω, Γ_ρ representing the nucleon-meson couplings. In some models, an additional vector $\vec{\delta}$ meson with couplings Γ_δ is taken into account. In general, these couplings are functionals of field operators ψ_i. The electromagnetic field is represented by A^μ with coupling constant $\Gamma_{i\gamma} = q_i\sqrt{4\pi}e$, where q_i is the charge number of nucleon i.

The Lagrangian density then assumes the form

$$\mathcal{L} = \sum_{i=n,p} \bar{\psi}_i \left(\gamma_\mu i D_i^\mu - M_i\right) \psi_i + \mathcal{L}_m\,, \tag{1.5}$$

where $\mathcal{L}_m$ is the Lagrangian density of free mesons with masses m_σ, m_ω, m_ρ, m_δ:

$$\begin{aligned}\mathcal{L}_m =& \frac{1}{2}\Big(\partial^\mu\sigma\,\partial_\mu\sigma - m_\sigma^2\,\sigma^2 + \partial^\mu\vec{\delta}\cdot\partial_\mu\vec{\delta} - m_\delta^2\,\vec{\delta}\cdot\vec{\delta} + m_\omega^2\,\omega^\mu\omega_\mu \\ & -\frac{1}{2}G^{\mu\nu}G_{\mu\nu} - \frac{1}{2}\vec{H}^{\mu\nu}\cdot\vec{H}_{\mu\nu} + m_\rho^2\,\vec{\rho}^{\,\mu}\cdot\vec{\rho}_\mu - \frac{1}{2}F^{\mu\nu}F_{\mu\nu}\Big)\end{aligned} \tag{1.6}$$

with the field tensors

$$G_{\mu\nu} = \partial_\mu\omega_\nu - \partial_\nu\omega_\mu, \quad \vec{H}_{\mu\nu} = \partial_\mu\vec{\rho}_\nu - \partial_\nu\vec{\rho}_\mu, \quad F_{\mu\nu} = \partial_\mu A_\nu - \partial_\nu A_\mu,$$

and the covariant derivative

$$iD_i^\mu = i\partial^\mu - \Gamma_{i\gamma}A^\mu - \Gamma_\omega\,\omega^\mu - \Gamma_\rho\,\vec{\tau}\cdot\vec{\rho}^{\,\mu}, \tag{1.7}$$

$\vec{\tau}$ is the isospin Pauli matrix. The effective nucleon mass M depends on the nucleon rest mass m_i and strength of the σ and δ fields:

$$M_i = m_i - \Gamma_\sigma\sigma - \Gamma_\delta\vec{\tau}\cdot\vec{\delta}\,. \tag{1.8}$$

Here and below we omit contribution of higher mass baryons and of antinucleons since their contribution is negligibly small at temperatures and densities of our interest.

Minimizing the action $\delta\int\mathcal{L}d^3xdt = 0$, one obtains the Euler-Lagrange equations

$$\frac{\partial}{\partial x^\mu}\left(\frac{\partial\mathcal{L}}{\partial(\partial\phi_i/\partial x^\mu)}\right) - \frac{\partial\mathcal{L}}{\partial\phi_i} = 0, \tag{1.9}$$

with the generalized coordinates ϕ_i being the fields. This leads to the equations of motion for the nucleons, meson and photon fields, which are then solved self-consistently. Under these conditions one obtains field equations for the meson fields

$$\begin{aligned}\partial_\mu\partial^\mu\sigma + m_\sigma^2\sigma &= \sum_{i=n,p}\Gamma_\sigma\bar{\psi}_i\psi_i \\ \partial_\mu\partial^\mu\vec{\delta} + m_\delta^2\vec{\delta} &= \sum_{i=n,p}\Gamma_\delta\bar{\psi}_i\vec{\tau}\psi_i \\ \partial_\mu G^{\mu\nu} + m_\omega^2\omega^\nu &= \sum_{i=n,p}\Gamma_\omega\bar{\psi}_i\gamma^\nu\psi_i \\ \partial_\mu\vec{H}^{\mu\nu} + m_\rho^2\vec{\rho^\nu} &= \sum_{i=n,p}\Gamma_\rho\bar{\psi}_i\vec{\tau}\gamma^\nu\psi_i.\end{aligned} \tag{1.10}$$

For the photon field one has

$$\partial_\mu F^{\mu\nu} = \Gamma_{i\gamma}\bar{\psi}_i\gamma^\nu\psi_i. \tag{1.11}$$

Fermions $i = n, p$ obey Dirac equations

$$\left[\gamma^\mu(i\partial^\mu - \Sigma_i^\mu) - (m_i - \Sigma_i)\right]\psi_i = 0. \tag{1.12}$$

The scalar self-energy Σ_i and the vector self-energy Σ_i^μ have the form

$$\begin{aligned}
\Sigma_i &= \Gamma_\sigma\sigma + \Gamma_\delta\vec{\tau}\cdot\vec{\delta}, && (1.13)\\
\Sigma_i^\mu &= \Gamma_\omega\omega^\mu + \Gamma_\rho\vec{\tau}\cdot\vec{\rho^\mu} + \Gamma_{i\gamma}A^\mu + \Sigma_R^\mu, && (1.14)\\
\Sigma_R^\mu &= \frac{j^\mu}{\rho}\left(\Gamma'_\omega\omega_\nu j^\nu + \Gamma'_\rho\vec{\rho_\nu}\cdot\vec{j^\nu} - \Gamma'_\sigma\sigma n^s - \Gamma'_\delta\vec{\delta}\cdot\vec{n^s}\right), && (1.15)
\end{aligned}$$

where the "rearrangement" contribution Σ_R^μ appears only for nucleons. The couplings Γ_m depend on the vector density $\rho = \sqrt{j_\mu j^\mu}$, where $j_\mu = \sum_{i=n,p}\bar{\psi}_i\gamma_\mu\psi_i$ is the vector current and $\Gamma'_m = \frac{d\Gamma_m}{d\rho}$ are the derivatives of the meson-nucleon couplings.

The system of coupled field equations has to be solved self-consistently, which is impossible to do for quantum fields. Therefore several approximations are applied. The field operators of the mesons and the photon are replaced by their expectation values in the mean-field approximation , e.g. $\sigma \to \langle\sigma\rangle$, and are treated as classical fields. In the following the symbol σ represents the expectation value. The same applies to the other meson fields. The source terms have also to be replaced as $\bar{\psi}_i\psi_i \to \langle\bar{\psi}_i\psi_i\rangle$. Then one has

$$\begin{aligned}
\sum_{i=n,p}\bar{\psi}_i\psi_i &\to \sum_{i=n,p}\langle\bar{\psi}_i\psi_i\rangle = n^s, & \sum_{i=n,p}\bar{\psi}_i\vec{\tau}\psi_i &\to \sum_{i=n,p}\langle\bar{\psi}_i\vec{\tau}\psi_i\rangle = \vec{n^s},\\
\sum_{i=n,p}\bar{\psi}_i\gamma^\nu\psi_i &\to \sum_{i=n,p}\langle\bar{\psi}_i\gamma^\nu\psi_i\rangle = j^\nu, & \sum_{i=n,p}\bar{\psi}_i\vec{\tau}\gamma^\nu\psi_i &\to \sum_{i=n,p}\langle\bar{\psi}_i\vec{\tau}\gamma^\nu\psi_i\rangle = \vec{j^\nu},
\end{aligned}$$

with the scalar source densities n^s, $\vec{n^s}$ and source currents j^ν and $\vec{j^\nu}$ For stationary systems of our interest only zero-components of the 4-vectors remain ($\omega^0, \vec{\rho^0}, A^0$, $n_i = j_i^0 = \langle\bar{\psi}_i\gamma^0\psi_i\rangle$). For infinite homogeneous matter also the Coulomb interaction is neglected $A^0 = 0$. These simplifications allow us to easily solve the field equations. In the mean-field approximation the vector density ρ is replaced by the ground state expectation value, hence couplings become functions of the total baryon density n. In the following we will denote nucleon densities as n_i, with the total baryon density $n = \sum_i n_i$.

Scalar and vector nucleon densities are then calculated by integrating over all momenta with the correct distribution functions

$$\begin{aligned}
n_i &= \frac{g_i}{(2\pi)^3}\int d^3k f_i(k), && (1.16)\\
n_i^s &= \frac{g_i}{(2\pi)^3}\int d^3k \frac{m_i - \Sigma_i}{e_i(k)} f_i(k) && (1.17)
\end{aligned}$$

where $g_i = 2$ and the energy

$$e_i(k) = \sqrt{k^2 + (m_i - \Sigma_i)^2}. \tag{1.18}$$

Fermi-Dirac distributions are given by

$$f_i = \left(\exp\left[\frac{(E_i - \mu_i)}{T} \right] + 1 \right)^{-1} \tag{1.19}$$

with $E_i(k) = \Sigma_{i0} + e_i(k)$ being the quasiparticle energy and μ_i is the chemical potential.

The thermodynamic quantities of the system can be calculated from the energy-momentum tensor

$$T^{\mu\nu} = \sum_i \frac{\partial \mathcal{L}}{\partial(\partial_\mu \phi_i)} \partial^\nu \phi_i - g^{\mu\nu}\mathcal{L} \tag{1.20}$$

with the ϕ_i components of the contributing fields. Then, the free energy density and the pressure are given by

$$\begin{aligned} f &= \langle T^{00} \rangle = \sum_{i=n,p} g_i \int \frac{d^3k}{(2\pi)^3} f_i e_i(k) \\ &+ \Gamma_\omega \omega_0 n_\omega + \Gamma_\rho \rho_0 n_\rho + \frac{1}{2}[m_\sigma^2 \sigma^2 + m_\delta^2 \delta^2 - m_\omega^2 \omega_0^2 - m_\rho^2 \rho_0^2], \end{aligned} \tag{1.21}$$

with $n_\omega = n_n + n_p$, $n_\rho = n_n - n_p$, $n_\sigma = n_n^s + n_p^s$ and $n_\delta = n_n^s - n_p^s$. The pressure is given by

$$\begin{aligned} p &= \frac{1}{3}\sum_{m=1}^{3} \langle T^{mm} \rangle = \frac{1}{3} \sum_{i=n,p} g_i \int \frac{d^3k}{(2\pi)^3} f_i \frac{k^2}{e_i(k)} \\ &+ (n_n + n_p)(\Gamma'_\omega \omega_0 n_\omega + \Gamma'_\rho \rho_0 n_\rho - \Gamma'_\sigma \sigma n_\sigma - \Gamma'_\delta \delta n_\delta) \\ &- \frac{1}{2}[m_\sigma^2 \sigma^2 + m_\delta^2 \delta^2 - m_\omega^2 \omega_0^2 - m_\rho^2 \rho_0^2], \end{aligned} \tag{1.22}$$

where nucleon-meson couplings and their density derivatives enter. In the thermodynamical description we calculate the pressure as the derivative of the free energy

$$p = n^2 \frac{\partial f/n}{\partial n}. \tag{1.23}$$

The calculations via the thermodynamical relation and equations 1.21-1.22 are thermodynamically consistent.

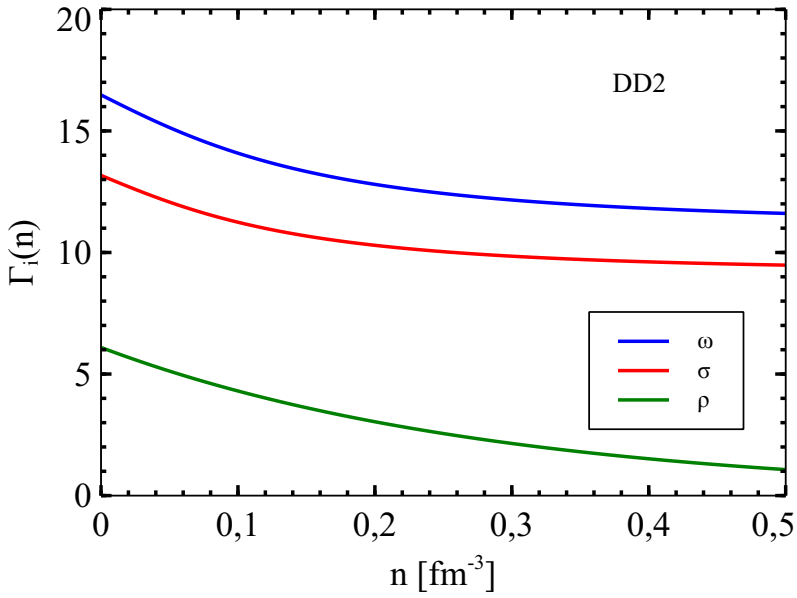

Figure 1.5.: Density dependence of coupling functions for the DD2 parametrization [TRK+10]

1.6.2 Parameters of the RMF model

In RMF models in general, the parameters of the model include the meson masses. The sigma meson mass cannot exactly be determined in experiment, whereas the masses of the other mesons are fixed from experiment: $m_\rho = 763$ MeV and $m_\omega = 783$ MeV. The sigma meson mass typically lies in the range (500-550) MeV. The other model parameters are the saturation density n_{sat} and the density dependent meson-nucleon couplings $\Gamma_i(n)$, expressed through coupling functions, which are taken in the form

$$\Gamma_i(n) = \Gamma_i(n_{\rm sat})\, F_i(x), \quad x = \frac{n}{n_{\rm sat}}, \tag{1.24}$$

with the baryon density $n = n_n + n_p$, saturation density n_{sat} and the following functions $F_i(x)$:

$$F_i(x) = a_i \frac{1 + b_i(x + d_i)^2}{1 + c_i(x + d_i)^2}, \quad \text{for the} \quad i = \sigma,\, \omega \quad \text{mesons}, \tag{1.25}$$

$$F_\rho(x) = \exp\left[-a_\rho(x - 1)\right], \quad \text{for the} \quad \rho \quad \text{meson}. \tag{1.26}$$

They depend on several parameters a_i, b_i, c_i, d_i, which are given in Table 1.2. These parameters are not independent due to constraints as discussed in [TW99].

These free parameters are usually fitted by a least-squared fit to reproduce the nuclear matter properties at saturation density and the properties of finite nuclei. Fig. 1.5 illustrates the density dependence of coupling functions of σ, ω and ρ mesons in DD2 parametrization [TRK+10], that we will further use in our calculations.

Different RMF models use different observables for the fitting of the parameters. There are non-linear RMF models, for example parametrizations NL1 [RRM+86], NL-SH [SNR93] and NL 3 [LKR97], that take into account data such as charge-radii, binding energies and neutron radii

Table 1.2.: Parameters of the couplings in the relativistic mean-field model from [TRK+10].

meson i	$\Gamma_i(n_{\text{sat}})$	a_i	b_i	c_i	d_i
ω	13.342362	1.369718	0.496475	0.817753	0.638452
σ	10.686681	1.357630	0.634442	1.005358	0.575810
ρ	3.626940	0.518903			

of spherical nuclei. These models show an almost linear rise in the symmetry energy E_s versus density, while for more modern RMF parametrizations (TW99 [TW99], DD-ME1 [NVFR02], DD2 [Typ05], D^3C [Typ05] and DD2 [TRK+10]) the symmetry energy is much softer, increasing less strongly with the density. This difference influences the results of the neutron skin thickness of ^{208}Pb. Such a correlation was shown in [Bro00] for non-relativistic Skyrme-Hartree-Fock calculations and in [TB01] for RMF models. In Table 1.3 nuclear matter properties at saturation density are given for the density dependent model parametrization (DD2) and other parameter sets. These include the NLρ model with non-linear self-interaction of the σ meson, where the isovector part of the interaction is described by the ρ meson. Additionally the scalar isovector δ meson can be included as well (NL$\rho\delta$). The other is the DBHF approach with the relativistic Bonn potential [vDFF05b, vDFF05a, GBFF99, dJL98]. The so-called KVR (and slightly modified parameter set KVOR) model includes couplings and meson masses depending on the σ field and the parameters are adjusted to describe the low-density part of the EoS from the Urbana-Argone group [APR98]. D^3C and DD-F are extensions of the model with density dependent coupling functions (DD), described in [TvCW03, KBT+06], respectively. Another RMF effective interaction with non-linear meson couplings called FSUGold [SHO11] is also presented in the table. This model is adjusted to be consistent with the universal behavior of a dilute neutron gas with large scattering length.

There is a good agreement on the value of n_{sat} and the binding energy a_v, while for other parameters we see significant deviations between the models, especially in the values of the incompressibility K and the derivative L of the symmetry energy. Taking recent constraints of these parameters into account, some of the parametrizations can be excluded, in particular with respect to the isovector parameters [LL12]. One of the observational data that might help to constrain the slope of the symmetry energy could be the measurement of a neutron star radius [LS06]. The density dependence of the symmetry energy can be probed by the precise measurement of the neutron skin thickness in ^{208}Pb [Bro00]. Experimental data of the neutron skin thickness were obtained from parity violating electron scattering in the PREX experiment [HAJ+12]. An overview of the experimental results concerning $E_s(n)$ is given in [TZD+09].

In Section 2.3 we will extend the RMF model description formulated here by including light clusters as quasiparticles [TRK+10] and scattering correlations explicitly [VT12], which will affect the low-density part of the EoS.

1.6.3 Correlations

In an interacting many-body system the properties of a constituent particle are included in the spectral function with a complicated structure. It is approximated in mean-field models by a δ function, representing a quasiparticle with a certain self-energy. In this way correlations

Model	n_{sat} [fm^{-3}]	a_V [MeV]	K [MeV]	K' [MeV]	J [MeV]	L [MeV]
NLρ	0.1459	−16.062	203.3	576.5	30.8	83.1
NL$\rho\delta$	0.1459	−16.062	203.3	576.5	31.0	92.3
DBHF	0.1810	−16.150	230.0	507.9	34.4	69.4
DD2	0.149	−16.02	242.7	−134.6	32.7	57.9
D^{3}C	0.1510	−15.981	232.5	−716.8	31.9	59.3
KVR	0.1600	−15.800	250.0	528.8	28.8	55.8
KVOR	0.1600	−16.000	275.0	422.8	32.9	73.6
DD-F	0.1469	−16.024	223.1	757.8	31.6	56.0
FSUGold	0.1482	−16.27	229.5	−523.9	32.56	60.43

Table 1.3.: Parameters of NM at saturation for various EsoS (see text).

are approximately taken into account. In contrast to that, correlations can be expressed by complicated many-body wave functions, as used in [Bru55, WFF88] and others.

In the framework of RMF models, the effect of the interaction is represented by scalar and vector self-energies. An example of such a model is the generalized RMF model (gRMF) with density dependent couplings [TRK$^+$10]. It has been recently extended where in addition to the nucleons, light clusters were included as quasiparticles with mean-field self energies. The properties of bound states are modified due to the medium and the Mott effect is taken into account, resulting in the dissolution of light clusters at higher densities. This effect originates from Pauli blocking and leads to the fact that the formation of bound states is strongly suppressed at larger densities. Thus, with increasing density the bound states will merge with the continuum and will dissolve. In order to describe such a transition, a medium dependent shift in the binding energies has been introduced, derived from the QS model [RMS82a], which allows to account for medium effects on cluster properties. In this work we concentrate on thermodynamic aspects of correlations.

Correlations modify the thermodynamic properties of matter and the EoS. One of the thermodynamically focused approaches is the generalized Beth-Uhlenbeck approach [SGS90], where an EoS is derived using the technique of thermodynamic Green's functions. The correlated nucleons form bound and scattering states. The total nucleon density then is given by:

$$n = n_{free} + n_{corr}, \quad n_{corr} = 2n_2 + 3n_3 + \ldots, \tag{1.27}$$

where n_{free} is the contribution of free nucleons and n_2 and n_3 represent the two and three-particle correlations, respectively. The aim of this thesis is to extend the gRMF model by including two-body correlations in the continuum, which become more relevant with increasing temperatures. These scattering correlations are introduced in the gRMF model as new degrees of freedom and are characterized by medium-dependent effective resonance energies with temperature dependent effective degeneracy factors. This contribution gives an impact for the low-density, finite temperature region. The consistency with the VEoS is required, where the second virial coefficient is derived from the NN phase shifts. A further extension to heavier clusters with medium-dependent binding energies is also possible and corresponding work is in progress.

The other type of two-body correlations under consideration is pairing, which is an essential feature of low temperature nuclear systems. This leads to several interesting consequences like superfluidity in the crust of neutron stars. It also affects the neutrino emission. Such pairing correlations are related to the nucleon-nucleon interaction. Similarly to the extended gRMF model, the interaction that we use is fitted to the phase shifts or scattering length and effective range. In this thesis we consider $^1S_0$ nn pairing, which contributes to the equation of state for temperatures below $T_c \approx 1.4$ MeV and densities below n_{sat}. The quasiparticle energy and thus the nucleon density will be modified by the medium dependent pairing gap $\Delta(n)$. We include pairing in the RMF density functional and perform calculations with pairing gaps derived from a separable Yamaguchi interaction. Mean-field effects lead to the reduction of the pairing gap as compared to the relativistic Fermi gas result. We show the influence of two-body pairing correlations on thermodynamic quantities of the EoS similar as with the two-body scattering correlations.

2 Constraining the nuclear matter EoS at low densities from the virial expansion

2.1 Motivation

In this chapter we describe an improved EoS, based on the relativistic mean field model (RMF), where at low densities and finite temperatures additionally to the light clusters two-body scattering correlations are taken into account. This model is called the generalized relativistic mean-field model (gRMF). Such an EoS might be relevant for the calculation of neutron star properties and in supernova simulations. In Section 2.1 we formulate the motivation for this research and discuss various approaches for the low-density nuclear matter EoS. We present a general formulation of the virial equation of state (VEoS) in Section 2.2 which is a model-independent approach that serves as a constraint for the low-density EoS in the extended RMF model. Basic quantities are defined and the notation is established. We show that correlations in continuum states can be represented effectively by temperature dependent resonances. Analytic expressions for the second virial coefficients are found from the effective-range expansion for the s-wave phase shifts. Different models like the nuclear statistical equilibrium (NSE) and the generalized Beth-Uhlenbeck approach are discussed in Subsections 2.2.3, 2.2.4 and their connection to the VEoS is established. Modifications of the conventional VEoS due to medium effects, similar to the ones in the generalized Beth-Uhlenbeck approach, are considered. The gRMF model with density-dependent meson-nucleon couplings is introduced in Section 2.3 and a series expansion of the grand canonical potential Ω in powers of fugacities is derived for low densities. The power series for the grand canonical thermodynamical potential Ω in the VEoS and gRMF are compared up to second-order leading to consistency relations between the models that are studied in various limits. An extension of the gRMF model is required in order to satisfy these consistency relations. In Section 2.4 we introduce temperature dependent resonance energies of the scattering states and modified degeneracy factors that allow to make a smooth interpolation between the VEoS and the gRMF model. These relations show that relativistic corrections to the standard VEoS are important already in the first order of the expansion. Separately we consider the case of pure neutron matter in Section 2.5 and symmetric nuclear matter in Section 2.6. The transition from low to high densities and the occurring problems are discussed in the following section. Concluding remarks and an outlook are given in Section 4. The comparison of our notations with the ones given in Ref. [HS06a] can be found in Appendix A. An expansion of the energy per particle in neutron matter at zero temperature in powers of the Fermi momentum is considered in Appendix B. This chapter is based on article [VT12] with addition of some extended discussions. Throughout this work we use natural units such that $\hbar = c = 1$.

Low-densities

As it was already stated in Chapter 1, this thesis is particularly devoted to the thermodynamic properties and the composition of nuclear matter at low densities. This region exhibits several interesting features, like two-, three-, ... many-body correlations due to the short-range nucleon-nucleon interaction. One has to take such effects into account for constructing a reliable EoS of nuclear matter. At low-densities the formation of light clusters occurs. They dissolve with increasing density due to the action of the Pauli principle and uniform neutron-proton matter emerges. A transition from inhomogeneous to homogeneous matter and the actual composition of low-density matter is important for the description of core-collapse supernovae, in particular the effectiveness of the neutrino reheating of the shock wave. There are two major paths to build an EoS of warm and dense nuclear matter for practical applications. One method starts with an ideal mixture of nucleons and nuclei leading to a nuclear statistical equilibrium (NSE) description [HSB10]. The effect of interactions between all constituents can be incorporated with the help of virial corrections. At present, however, only nucleons and light nuclei are considered in practice in such a virial equation of state (VEoS) [HS06c, HS06a, OGH$^+$07], which provides the correct finite-temperature EoS in the limit of very low densities. The results depend only on experimentally determined data, i.e. binding energies of nuclei and scattering phase shifts, and thus are model independent. Unfortunately, the application of this approach is limited to rather low densities. The dissolution of nuclei and the transition to uniform neutron-proton matter with increasing density cannot be described properly. In order to simulate such an effect, the heuristic excluded volume mechanism was employed frequently [HSB10]. Another class of EoS models for astrophysical applications is based on self-consistent mean-field methods with neutrons and protons as fundamental constituents. They are considered as quasiparticles with self-energies that contain the information on the interaction. Such an interaction is usually modeled in an effective way and not taken from a realistic nucleon-nucleon (NN) interaction fitted to phase-shift data. These mean-field models, both non-relativistic and relativistic, can be very successful in describing finite nuclei and nuclear matter around saturation density [GRT90, SW86, BHR03, KV05]. However, at low densities $n \ll n_{\mathrm{sat}}$ they do not include correlations properly. These correlations give rise to inhomogeneities and the formation of many-body bound states, i.e. nuclei. There were attempts to modify the low-density behavior of mean-field models guided by microscopic calculations, see, e.g., Ref. [MvDF07] for the zero temperature case. However, it is still challenging to include the formation of clusters properly. The deficiencies of the various models lead to the strategy of patching up or merging different approaches providing a uniform description of warm dense matter.

In this thesis we use the gRMF model which includes, besides nucleons, light nuclei as hadronic degrees of freedom in the Lagrangian. The dissolution of these light clusters is modeled by a medium-dependent shift of their binding energies originating mainly from the action of the Pauli principle. All hadronic constituents of the model are assumed to be quasiparticles that interact via the exchange of effective mesons. Such a concept of the gRMF model allows to bridge the two views on nuclear matter, i.e. a mixture of nucleons and nuclei at low densities and nucleons as quasiparticles moving in mean fields at high densities. Even though the model contains the same relevant particles at low densities as the VEoS, it does not reproduce exactly the thermodynamic properties of the VEoS as will be shown below. In fact, all presently employed EoS for astrophysical applications that are based on mean-field concepts

fail to reproduce the VEoS in the low-density limit. Thus the question arises, how the models can be modified in order to approach the correct low-density limit. Is a modification of the effective interaction sufficient to meet this aim or are there more severe changes of the models required? We will propose a solution to this problem in the framework of the gRMF model with density-dependent couplings, that could be applied to other mean-field approaches as well.

2.2 Equation of state in the virial limit

2.2.1 General formalism

Thermodynamic properties of low-density matter at finite temperatures T can be described by a model-independent approach, namely a virial equation of state. In the non-relativistic limit, which is usually considered, it describes a system of interacting particles $i, j, \ldots$ with non-relativistic chemical potentials μ_i in a volume V, provided the fugacities $z_i = \exp(\mu_i/T)$ are small ($z_i \ll 1$). The range of densities where the virial expansion is valid can be estimated by the relation $z_i \approx n_i \lambda_i^3 \ll 1$, where n_i is the number density of particle i with mass m_i and $\lambda_i = \sqrt{2\pi/(m_i T)}$ is the thermal wavelength. The following presentation gives a generalized and more symmetric formulation of the virial approach as compared to [HS06c, HS06a, OGH$^+$07]. The S-matrix formulation by Ref. [DMB69] that was recently applied to nuclear matter in Ref. [MDSS08] gives essentially identical results. Under the presupposed conditions the grand canonical partition function $\mathcal{Q}$ can be expanded in powers of fugacities as

$$\mathcal{Q}(T, V, \mu_i) = 1 + \sum_i Q_i z_i + \frac{1}{2}\sum_{ij} Q_{ij} z_i z_j + \frac{1}{6}\sum_{ijk} Q_{ijk} z_i z_j z_k + \ldots \tag{2.1}$$

with one-, two-, three-, ... many-body canonical partition functions $Q_i, Q_{ij}, Q_{ijk}, \ldots$. In classical non-relativistic mechanics, the single-particle canonical partition function is

$$Q_i = \frac{g_i}{(2\pi)^3} \int d^3 r_i \int d^3 p_i \, \exp\left(-\beta H_i\right) = \frac{g_i}{\lambda_i^3} V \tag{2.2}$$

with the spin degeneracy factor g_i (= 2 for each nucleon), $\beta = 1/T$ and the single-particle Hamiltonian $H_i = p_i^2/(2m_i)$ that only contains a kinetic contribution with momentum p_i. For the two-body canonical partition function we have

$$Q_{ij} = \frac{g_i g_j}{(2\pi)^6} \int d^3 r_i \int d^3 p_i \int d^3 r_j \int d^3 p_j \, \exp\left(-\beta H_{ij}\right) \tag{2.3}$$

with the two-body Hamiltonian $H_{ij} = p_i^2/(2m_i) + p_j^2/(2m_j) + V_{ij}$ that includes a two-body potential V_{ij} responsible for the correlations. Then, the grand canonical potential

$$\Omega(T, V, \mu_i) = -T \ln \mathcal{Q}(T, V, \mu_i) = -pV \, , \tag{2.4}$$

that is directly related to the pressure p, can be written in the form

$$\Omega(T,V,\mu_i) = -TV\left(\sum_i \frac{b_i}{\lambda_i^3} z_i + \sum_{ij} \frac{b_{ij}}{\lambda_i^{3/2}\lambda_j^{3/2}} z_i z_j + \sum_{ijk} \frac{b_{ijk}}{\lambda_i\lambda_j\lambda_k} z_i z_j z_k + \ldots\right) \tag{2.5}$$

with the (symmetrized) dimensionless cluster (or virial) coefficients

$$b_i(T) = \frac{\lambda_i^3}{V} Q_i = g_i\,, \tag{2.6}$$

$$b_{ij}(T) = \frac{\lambda_i^{3/2}\lambda_j^{3/2}}{2V}\left(Q_{ij} - Q_i Q_j\right)\,, \tag{2.7}$$

$$b_{ijk}(T) = \frac{\lambda_i\lambda_j\lambda_k}{6V}\left(Q_{ijk} - Q_i Q_{jk} - Q_j Q_{ik} - Q_k Q_{ij} + 2Q_i Q_j Q_k\right) \tag{2.8}$$

that depend on the temperature. Without interaction, the two-, three-, ... many-body partition functions factorize, e.g. $Q_{ij} = Q_i Q_j$, and the second, third, ... cluster coefficients b_{ij}, b_{ijk}, ... vanish.

Individual particle number densities are found from the relation

$$n_i = -\frac{1}{V}\left.\frac{\partial\Omega}{\partial\mu_i}\right|_{T,V,\mu_{j\neq i}} = b_i\frac{z_i}{\lambda_i^3} + 2\sum_j b_{ij}\frac{z_i z_j}{\lambda_i^{3/2}\lambda_j^{3/2}} + 3\sum_{jk} b_{ijk}\frac{z_i z_j z_k}{\lambda_i\lambda_j\lambda_k} + \ldots \tag{2.9}$$

with contributions from free particles (first term in the second equation) and correlated pairs, triples, etc. The entropy is

$$\begin{aligned} S &= -\left.\frac{\partial\Omega}{\partial T}\right|_{V,\mu_i} \qquad (2.10)\\ &= -\frac{5\Omega}{2T} + V\left(\sum_i \frac{c_i}{\lambda_i^3} z_i + \sum_{ij} \frac{c_{ij}}{\lambda_i^{3/2}\lambda_j^{3/2}} z_i z_j + \sum_{ijk} \frac{c_{ijk}}{\lambda_i\lambda_j\lambda_k} z_i z_j z_k + \ldots\right) \end{aligned}$$

with coefficients

$$c_i = T\frac{db_i}{dT} - \frac{\mu_i}{T}\,, \tag{2.11}$$

$$c_{ij} = T\frac{db_{ij}}{dT} - \frac{\mu_i+\mu_j}{T}\,, \tag{2.12}$$

$$c_{ijk} = T\frac{db_{ijk}}{dT} - \frac{\mu_i+\mu_j+\mu_k}{T}\,. \tag{2.13}$$

Other relevant thermodynamical quantities such as the free energy

$$F = \Omega + V\sum_i \mu_i n_i \tag{2.14}$$

and the internal energy

$$E = F + TS \tag{2.15}$$

can be obtained immediately.

The formulas given above can be generalized to include four-, five-, ... many-body correlations, but already contributions of the three-body term are hardly ever considered in practice. For a given temperature, two-body correlations will always dominate higher-order correlations when the density decreases. Hence, in the following, we will truncate the expansion at second order in the fugacities of the basic constituents.

In classical mechanics the second virial coefficient

$$b_{ij} = \frac{1}{2}\frac{g_{ij}}{\lambda_i^{3/2}\lambda_j^{3/2}} \int d^3 r_{ij} \left(\exp\left[-\frac{V_{ij}(r_{ij})}{T} \right] - 1 \right) \tag{2.16}$$

depends on the degeneracy factor g_{ij} and the two-body interaction potential V_{ij} depends on the distance r_{ij}. The quantum mechanical generalization of the virial expansion up to second order was given by Beth and Uhlenbeck [BU36, BU37]. In classical mechanics as we see from eq.(2.16) the interaction potential between the particles is the relevant quantity that appears in the calculation of the virial coefficients. In quantum mechanics, the Schrödinger equation has to be solved with this potential and the obtained eigenstates comprise bound and scattering states. Integrations over phase space are replaced by sums over all eigenstates of the one- and two-body system and it is obvious that the density of states becomes the relevant quantity. The result for the first virial coefficient b_i is identical to the classical value (2.6) in the continuum approximation, corresponding to the replacement of the sum over discrete momentum states by an integral. The second virial coefficient can be expressed as an integral over center-of-mass energies E

$$b_{ij}(T) = \frac{1+\delta_{ij}}{2}\frac{\lambda_i^{3/2}\lambda_j^{3/2}}{\lambda_{ij}^3} \int dE \, \exp\left(-\beta E\right) D_{ij}(E) \pm \delta_{ij} g_i 2^{-5/2} \tag{2.17}$$

with $\lambda_{ij} = \sqrt{2\pi/[(m_i+m_j)T]}$ and the quantity

$$D_{ij}(E) = \sum_k g_k^{(ij)} \delta(E - E_k^{(ij)}) + \sum_l \frac{g_l^{(ij)}}{\pi}\frac{d\delta_l^{(ij)}}{dE} \tag{2.18}$$

that measures the difference between the density of states of an interacting and free two-particle system. The last term in equation (2.17) is a quantum statistical correction with the positive (negative) sign if $i = j$ are identical bosons (fermions).

The first contribution to D_{ij} is a sum over all two-body bound states k of the system ij with degeneracy factors $g_k^{(ij)}$ and energies $E_k^{(ij)} < 0$. The second term takes into account continuum correlations in the two-particle system in all channels l with degeneracy factors $g_l^{(ij)}$ via the energy-dependent scattering phase shifts $\delta_l^{(ij)}$. In general, the index l stands for the total and angular orbital momenta of a particular channel. If the phase shift is dominated by a narrow resonance, it jumps by π in a very small energy interval around the resonance energy and the contribution to the virial coefficient resembles that of a bound state. With experimentally determined bound state energies and nucleon-nucleon phase shifts, the second virial coefficient b_{ij} and thus the low-density EoS can be established in a model-independent way.

The quantum mechanical generalization of the third virial coefficient was discussed in Ref. [PU59] but actual calculations turn out to be difficult in practice and, thus, they are not considered here. The derivation of the classical VEoS is based on non-relativistic kinematics. In order to include relativistic effects, at least the relativistic dispersion relation of the particles has to be used. The resulting modifications of the virial coefficients will be discussed when the VEoS is compared to the gRMF approach in Subsection 2.3.4.

2.2.2 Application to nuclear matter with arbitrary neutron to proton ratio

Neutrons and protons are the relevant degrees of freedom in low-density nuclear matter at not too high temperatures. Therefore, the grand canonical potential up to second order in the fugacities becomes

$$\begin{aligned}\Omega(T,V,\mu_n,\mu_p) \\ = \; -TV\left(\frac{b_n}{\lambda_n^3}z_n+\frac{b_p}{\lambda_p^3}z_p+\frac{b_{nn}}{\lambda_n^3}z_n^2+\frac{b_{pp}}{\lambda_p^3}z_p^2+2\frac{b_{np}}{\lambda_n^{3/2}\lambda_p^{3/2}}z_nz_p\right)\end{aligned} \tag{2.19}$$

where the symmetry $b_{np}=b_{pn}$ is used. The Coulomb interaction is usually neglected in the VEoS and b_{pp} is replaced by b_{nn} in (2.19), c.f. Ref. [HS06a]. The second virial coefficient b_{nn} receives contributions only from scattering states. It is convenient to split $b_{np}=b_{np0}+b_{np1}$ into two contributions with total isospin $\mathcal{T}=0$ and $\mathcal{T}=1$. The only bound two-body state in the two-nucleon system, the deuteron, appears in the isospin zero channel with $g_d=3$ and $E_d^{(np)}=-B_d=-2.225$ MeV [AWT02]. According to this notations we can write

$$b_{nn}(T) = \frac{\lambda_n^3}{\lambda_{nn}^3}\sum_l g_l^{(nn)}I_l^{(nn)}-g_n2^{-5/2}, \tag{2.20}$$

$$b_{pp}(T) = \frac{\lambda_p^3}{\lambda_{pp}^3}\sum_l g_l^{(pp)}I_l^{(pp)}-g_p2^{-5/2}, \tag{2.21}$$

$$b_{np1}(T) = \frac{1}{2}\frac{\lambda_n^{3/2}\lambda_p^{3/2}}{\lambda_{np}^3}\sum_l g_l^{(np1)}I_l^{(np1)}, \tag{2.22}$$

$$b_{np0}(T) = \frac{1}{2}\frac{\lambda_n^{3/2}\lambda_p^{3/2}}{\lambda_{np}^3}\left[g_d\exp\left(\frac{B_d}{T}\right)+\sum_l g_l^{(np0)}I_l^{(np0)}\right] \tag{2.23}$$

with the virial integrals

$$I_l^{(ij)}(T)=\int_0^\infty\frac{dE}{\pi}\frac{d\delta_l^{(ij)}}{dE}\exp\left(-\frac{E}{T}\right) \tag{2.24}$$

depending on the phase shifts δ_l^{ij}.

Formally, we can write the sum of the scattering contributions in equations (2.20)-(2.23) in the form of a single bound state contribution

$$\sum_l g_l^{(ij)}I_l^{(ij)}=\int_0^\infty\frac{dE}{\pi}\frac{d\delta_{ij}}{dE}\exp\left(-\frac{E}{T}\right)=\hat{g}_{ij}\exp\left[-\frac{E_{ij}(T)}{T}\right] \tag{2.25}$$

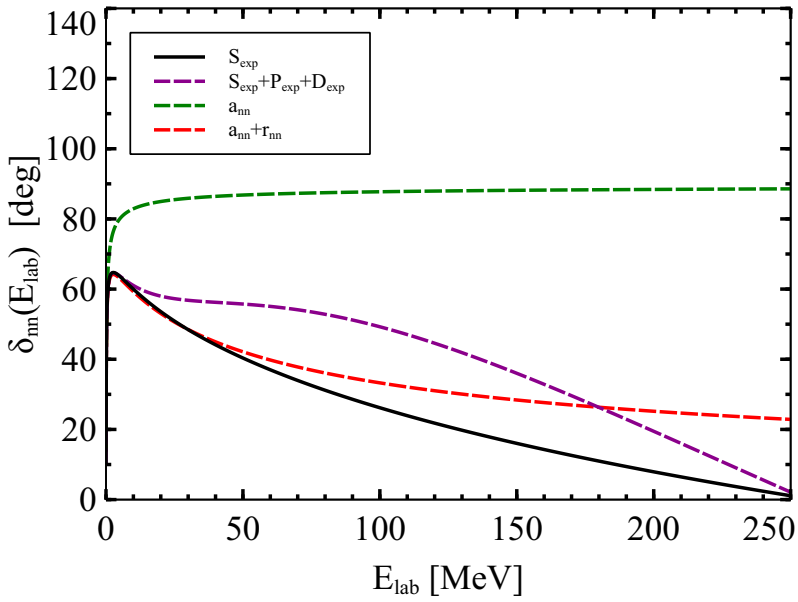

Figure 2.1.: Effective phase shift $\delta_{nn}(E_{\rm lab})$ for neutron-neutron scattering versus laboratory energy $E_{\rm lab} = 2E$. Results are shown using experimental data (including s, p and d-waves or s waves only) and the effective-range approximation with and without the contribution depending on the effective range parameter, respectively.

with a temperature dependent effective resonance energy $E_{ij}(T)$ in each ij channel by summing the contributions of all partial waves in an effective total phase shift

$$\delta_{ij}(E) = \sum_l g_l^{(ij)} \delta_l^{(ij)} \,. \tag{2.26}$$

The effective degeneracy factor $\hat{g}_{ij} = \pm g_0^{(ij)}$ is chosen such that it is identical to the degeneracy factor in the s-wave. The sign is determined by that of the integral.

In the following neutron-neutron scattering is considered in order to illustrate the behavior of the phase shifts and effective resonance energies. In this example, due to the Pauli principle only certain partial waves with total angular momentum J and orbital angular momenta l contribute to the sum of the experimental phase shifts. Taking into account all possible partial waves with $l = 0$, 1 and 2, i.e. the channels ${}^1S_0$, ${}^3P_0$, ${}^3P_1$, ${}^3P_2$ and ${}^1D_2$ in spectroscopic notation ${}^{2S+1}L_J$, one has

$$\delta_{nn}(E) = \delta_{00}^{(nn)} + \delta_{01}^{(nn)} + 3\delta_{11}^{(nn)} + 5\delta_{21}^{(nn)} + 3\delta_{12}^{(nn)} \tag{2.27}$$

using double indices Jl in $\delta_{Jl}^{(ij)}$ to indicate the partial wave. In Fig. 2.1 we show the effective phase shift for the sum of partial waves with $l \leq 2$ (dashed purple line). Higher contributions are negligible for the temperatures of interest. The results are compared with the pure s-wave contribution (black line). Note, that the laboratory energy $E_{\rm lab} = 2E$ of a neutron scattered on the target at rest is used as the argument. Since, there is no experimental data on the nn phase shifts, we use the ${}^1S_0$ np data taken from the Nijmegen partial wave analysis [SKRdS93]. At very low energies, all curves are rapidly rising. At energies above $\approx$ 10 MeV, contributions of higher partial waves become important.

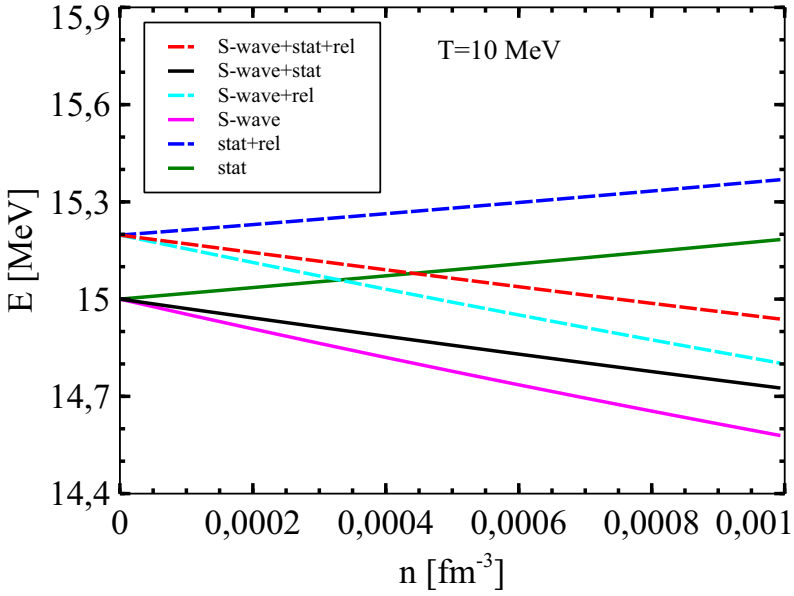

Figure 2.2.: Energy per particle calculated in the virial expansion as a function of the density in pure neutron matter including different effects.

In Fig. 2.2 we show the calculation of the energy per particle in the virial limit with only the $^1S_0$ nn contribution. The influence of different effects is shown. The ideal gas calculation for $T = 10$ MeV corresponds to $E = 3T/2 = 15$ MeV. When the statistic effects are added (green line) the energy per particle grows with increasing density. Further inclusion of scattering states reduces the energy (black line). Finally relativistic effects lead to a shift to higher energies (dashed red line), which will be discussed in Section 2.3.4. We see that these corrections are important and should be taken into account for the correct description of low-density matter.

At low temperatures, the virial integral is dominated by the low-energy phase shifts $\delta_l^{(ij)}$ and only the s-wave contributes substantially due to the large derivative with respect to the energy. The effective-range approximation [Bru96] for the s-wave phase shift

$$k \cot \delta_0^{(ij)} = -\frac{1}{a_{ij}} + \frac{1}{2} r_{ij} k^2 \tag{2.28}$$

with momentum $k = \sqrt{2\mu_{ij}E}$ and effective mass $\mu_{ij} = m_i m_j/(m_i + m_j)$ can be used to specify the energy dependence of $\delta_0^{(ij)}$ with help of the scattering length a_{ij} and the effective range r_{ij}.

Fig. 2.1 shows the result for the s-wave phase shift using only the scattering length (dashed green line) or both the scattering length and the effective range parameter (dashed red line). The experimental phase shift is nicely reproduced by the effective range expansion at very low energies. The effective range r_{ij} contribution with the k^2 term is essential to obtain a decrease of the s-wave phase shift at higher energies. In this case, the result follows more closely the experimental data, however, differences with respect to the total effective phase shift $\delta_{nn}(E)$ remain.

The effective resonance energy E_{nn} for nn scattering derived from the phase shifts in Eq. (2.25) is compared for different approximations in Fig. 2.3. In general, E_{nn} rises smoothly with increasing temperature indicating that it is not dominated by a particular resonance. Contri-

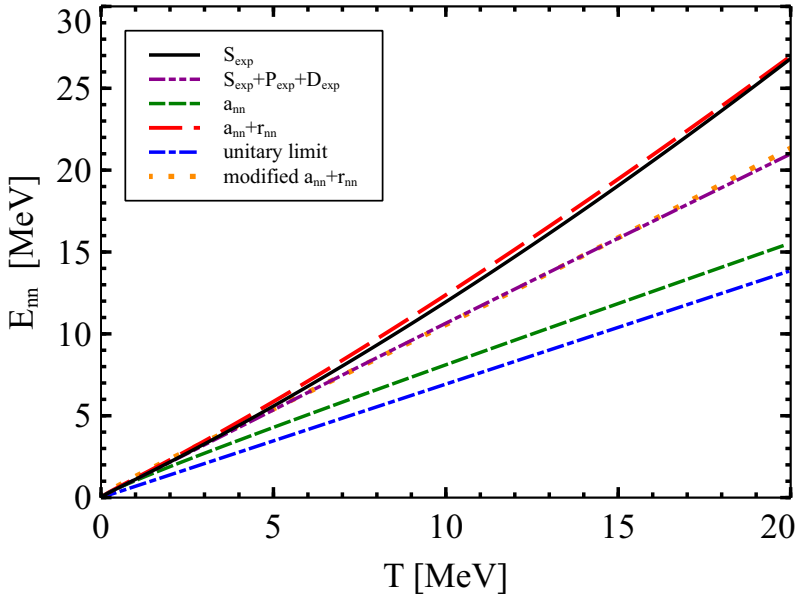

Figure 2.3.: Temperature dependence of the effective resonance energy E_{nn} for neutron-neutron scattering in different approximations. See caption of Fig. 2.1 and text for details.

butions of higher partial waves reduce the effective resonance energy as compared to the pure s-wave result.

The s-wave virial integral can be obtained analytically in the effective-range approximation as

$$I_0^{(ij)}(T) = -\frac{1}{2}\sum_{\eta=\pm1}\frac{B_{ij}^{(\eta)}}{\sqrt{A_{ij}^{(\eta)}}}\exp\left[\frac{1}{2\mu_{ij}TA_{ij}^{(\eta)}}\right]\operatorname{erfc}\left[\frac{1}{\sqrt{2\mu_{ij}TA_{ij}^{(\eta)}}}\right] \tag{2.29}$$

for $2r_{ij}/a_{ij} \leq 1$. It depends on the coefficients

$$A_{ij}^{(\eta)} = \frac{a_{ij}^2}{2}\left(1 - \frac{r_{ij}}{a_{ij}} + \eta\sqrt{1 - 2\frac{r_{ij}}{a_{ij}}}\right) \tag{2.30}$$

and

$$B_{ij}^{(\eta)} = \frac{a_{ij}}{2}\left(1 + \eta\sqrt{1 - 2\frac{r_{ij}}{a_{ij}}}\right). \tag{2.31}$$

For $r_{ij} = 0$ the integral reduces to

$$I_0^{(ij)}(T) = -\frac{a_{ij}}{2|a_{ij}|}\exp\left(\frac{1}{2\mu_{ij}Ta_{ij}^2}\right)\operatorname{erfc}\left(\frac{1}{\sqrt{2\mu_{ij}Ta_{ij}^2}}\right). \tag{2.32}$$

Using these results, the effective resonance energy can be expressed explicitly as a function of the temperature and the effective-range parameters. We use $a_{nn} = -18.818$ fm and $r_{nn} = 2.834$ fm from Ref. [WSS95]. From Fig. 2.3, we see that E_{nn} in the effective range

approximation rises more strongly with temperature when the contribution of the r_{nn} term is taken into account. At high temperatures a difference to the exact result that takes higher partial waves into account remains. However, by a readjustment of the scattering length to $a_{nn} = -11.31$ fm and the effective range to $r_{nn} = 1.06$ fm, the correct effective resonance energy obtained with all partial waves is very well reproduced for the relevant temperatures with the modified parameters (denoted by modified $a_{nn} + r_{nn}$ in Fig. 2.3). Of course, these modified values for a_{nn} and r_{nn} are not physical and do not describe the scattering in a particular partial wave. They only represent an effective way to describe the temperature dependence of the effective resonance energy.

There are several interesting limits for the virial integral. For low temperatures $T \ll A_{ij}^{(\eta)}/(2\mu_{ij})$ one finds

$$I_0^{(ij)}(T) \to -a_{ij}\sqrt{\frac{\mu_{ij}T}{2\pi}} + \dots \tag{2.33}$$

(independent of the effective range r_{ij}). In the unitary limit $a_{ij} \to -\infty$ and $r_{ij} = 0$, which describes the situation where a bound state/resonance is just at the continuum threshold, $I_0^{(ij)}(T) = 1/2$ and the effective resonance energy is given by $E_{ij} = T \ln 2$. This result is also depicted in Fig. 2.3. For positive scattering length a_{ij}, e.g. in the deuteron channel, the integral is negative and compensates part of the correlation strength that is located in the bound state of the same channel.

In Ref. [HS06a] also the α-particle was considered as a fundamental constituent in the VEoS and the additional virial coefficients b_α, $b_{n\alpha}$, $b_{p\alpha}$ and $b_{\alpha\alpha}$ appeared in the formalism. (For a comparison of the virial coefficients in the two formulations see Appendix A.) In our approach, the corresponding contributions to Ω represent four-, five- and eight-body correlations that will become irrelevant in the low-density limit as compared to two-nucleon correlations. Since chemical equilibrium requires $\mu_\alpha = 2\mu_n + 2\mu_p + B_\alpha$ with the α-particle binding energy $B_\alpha = 28.296$ MeV [AWT02], the α-particle fugacity $z_\alpha = \exp(\mu_\alpha/T)$ is not independent of the neutron and proton fugacities. The VEoS with neutrons, protons and α-particles was further extended in Ref. [OGH$^+$07] to include ^{3}H and ^{3}He as constituent particles corresponding to three-body correlations. Care has to be taken in order to avoid a double counting of states since, e.g., the α-particle states can be obtained in the ^{3}H-p and ^{3}He-n channels (or the neglected ^{2}H-^{2}H channels) that all represent four-body correlations when nucleons are assumed to be the only fundamental particles.

2.2.3 Relation to the nuclear statistical equilibrium approach

One could extend the virial expansion to include more many-body correlations. The second, third, ...virial coefficients will contain bound state contributions that correspond to ground and excited states of heavy nuclei. Neglecting the many-body continuum correlations, the grand canonical potential becomes a sum

$$\Omega = -TV \sum_{(A,Z)} \frac{g_{A,Z}}{\lambda_{A,Z}^3} \exp\left(\frac{\mu_{A,Z}}{T}\right) \tag{2.34}$$

over all nuclei with mass number A, charge number Z, chemical potential $\mu_{A,Z} = (A-Z)\mu_n + Z\mu_p + B_{A,Z}$, depending on binding energy $B_{A,Z}$, degeneracy factors $g_{A,Z}$ and thermal wavelength $\lambda_{A,Z} = \sqrt{2\pi/(m_{A,Z}T)}$. The effective degeneracy factor

$$g_{A,Z}(T) = g_{A,Z}^{(0)} + \sum_k g_{A,Z}^{(k)} \exp\left(-\frac{E_k}{T}\right) \tag{2.35}$$

is a sum over the ground state 0 and all excited states k of the nucleus ^{A}Z with excitation energies E_k, total angular momenta J_k and $g_{A,Z}^{(k)} = (2J_k + 1)$. The summation over individual states is often replaced by an integral over energy with an appropriate level density, see, e.g. Ref. [HSB10]. The temperature dependence of the degeneracy factor is a simple and efficient means to include excited states of nuclei. It will be used below in the formulation of the gRMF approach. In case of an ideal mixture of neutrons, protons and deuterons, the density of the system is the sum $n = n_n + n_p + 2n_d$, where n_d is the particle density of the deuteron with binding energy $B_d = 2.225$ MeV. In such a system the deuteron fraction grows with increasing density, no dissolution is observed, thus the system becomes pure deuteron matter.

2.2.4 Generalized Beth-Uhlenbeck approach

In the conventional VEoS one can describe matter only in the region of rather low densities. The approach, however, can be generalized in order to reach higher densities and to include the effects of dissolution of composite particles, i.e. the Mott effect. Such modifications are taken into account in the generalized Beth-Uhlenbeck (gBU) approach, based on a quantum statistical description with thermodynamic Green's functions. For details see Ref. [SGS90]. The grand canonical potential Ω in the gBU approach assumes a similar form as in the VEoS. The constituents are considered as quasiparticles with the correct statistics (Fermi-Dirac or Bose-Einstein) and with self-energies that contain already some effect of the mutual interaction. The remaining two-body correlations (between quasiparticles!) are contained in a modified second virial coefficient that is given by

$$b_{ij}(T) = \frac{1+\delta_{ij}}{2}\lambda_i^{3/2}\lambda_j^{3/2}\int dE\, f_{ij}(E+E_{\rm cont})F_{ij}(E) \tag{2.36}$$

with the correct distribution function $f_{ij}(E)$ of the composite system, i.e. Bose-Einstein for the two-nucleon-states, and the quantity

$$\begin{aligned} F_{ij}(E) &= \sum_k g_k^{(ij)} \int_{P>P_{\rm Mott}} \frac{d^3P}{(2\pi)^3}\,\delta(E - E_k^{(ij)}) \\ &\quad + \sum_l \frac{g_l^{(ij)}}{\pi}\int \frac{d^3P}{(2\pi)^3}\,2\sin^2\delta_l^{(ij)}\frac{d\delta_l^{(ij)}}{dE} \end{aligned} \tag{2.37}$$

that is related to the in-medium density of states. Similarly to the second virial coefficient in the VEoS, contributions of bound and scattering states enter. The main differences as compared to Eqs. (2.17) and (2.18) are caused by medium effects. The properties of a two-body system

ij depend on the total c.m. momentum $\vec{P}$ of the state with respect to the medium. Hence, there is an additional summation (integration) over $\vec{P}$. Bound states only appear for P larger than the Mott momentum P_{Mott} because at lower total momenta their formation is suppressed by the action of the Pauli principle. The phase shifts $\delta_l^{(ij)}(P,T,\mu_i,\mu_j)$ are determined by the in-medium T-matrix describing the scattering of two quasiparticles. Similarly $E_k^{(ij)}(P,T,\mu_i,\mu_j)$ is the medium-dependent energy of a bound state. Energies in Eq. (2.37) are measured with respect to the continuum edge E_{cont} that corresponds to the energy in the frame of the medium with zero relative momentum. The statistic is described by Bose-Einstein distribution functions f_{ij}. The $2\sin^2\delta_l^{(ij)}$ factor leads to a reduction of explicit scattering correlations, due to the fact that a part of interaction effects is already contained in the self-energies of the quasiparticles. The second term in Eq. (2.37) is related to the number of correlated quasiparticles that is different to the number of correlated particles as calculated by the usual Beth-Uhlenbeck approach in Eq. (2.18). With realistic nucleon-nucleon interactions and nucleon self-energies from mean-field models, one can determine the medium-dependent binding energy shifts. These are later used in a parametrized form in the extended RMF model, described in Section 2.3.

2.3 Generalized relativistic mean-field model

2.3.1 General formalism

An extension of the RMF model with density-dependent meson-nucleon couplings described in Subsection 1.6.1 was introduced in Ref. [TRK+10], where light clusters (bound states of ^{2}H, ^{3}H, ^{3}He, ^{4}He) were included as additional degrees of freedom with medium dependent binding energies obtained from quantum statistical model calculations. The strength of the cluster coupling to the meson fields was assumed to be a multiple of the nucleon coupling strength. Scattering states were not considered in the RMF model in Ref. [TRK+10]. The approach can easily be extended when more than the above mentioned nuclei need to be included. Such a model with nuclei as explicit degrees of freedom is called the gRMF model.

The grand canonical potential of the model is derived from the Lagrangian and can be formulated as a function $\Omega(T,V,\tilde{\mu}_i,\omega,\rho,\sigma,\delta)$ depending on the temperature T, volume V, relativistic chemical potentials $\tilde{\mu}_i = m_i + \mu_i$ of the particles and the spatially constant meson fields ω, ρ, σ and δ under consideration. Here, all four mesons are included to cover the four possible combinations of scalars and vectors in Lorentz and isospin space. As already stated in Subsection 1.6.1, in the following we neglect antiparticles because they give sizable contributions only at temperatures much higher than those relevant in the considered astrophysical applications. In the general case of inhomogeneous matter, not discussed here, Ω becomes a functional of the spatially varying meson fields and their gradients.

For uniform nuclear matter, the grand canonical potential can be written as

$$\begin{aligned}\Omega &= \sum_i \Omega_i - V\left[\frac{1}{2}\left(m_\omega^2\omega_0^2 + m_\rho^2\rho_0^2 - m_\sigma^2\sigma^2 - m_\delta^2\delta^2\right)\right. \\ &\left. + \left(\Gamma'_\omega\omega_0 n_\omega + \Gamma'_\rho\rho_0 n_\rho - \Gamma'_\sigma\sigma n_\sigma - \Gamma'_\delta\delta n_\delta\right)\left(n_n + n_p\right),\right]\end{aligned} \tag{2.38}$$

where Γ_i' are the derivatives of the density dependent couplings which determine the nucleon-meson coupling strength. Contributions from individual particles (nucleons and clusters) are

$$\Omega_i = \mp g_i V T \int \frac{d^3k}{(2\pi)^3} \ln\left[1 \pm \exp\left(-\frac{E_i - \tilde{\mu}_i}{T}\right)\right] \tag{2.39}$$

where the upper (lower) signs refer to fermions (bosons). In the case of Maxwell-Boltzmann statistics, Eq. (2.39) reduces to

$$\Omega_i = g_i V T \int \frac{d^3k}{(2\pi)^3} \exp\left(-\frac{E_i - \tilde{\mu}_i}{T}\right). \tag{2.40}$$

We assume that the degeneracy factors g_i can depend in general on the temperature as in the case of NSE models, cf. Subsection 2.2.3. The densities n_ω, n_ρ, n_σ and n_δ appearing in (2.38) are themselves functions of the temperature, chemical potentials and meson fields (see below).

The mass of a cluster $i = d, t, h, \alpha, \ldots$ with N_i neutrons and Z_i protons is written as

$$m_i = N_i m_n + Z_i m_p - (1 - \delta_{in})(1 - \delta_{ip}) B_i^{(\mathrm{vac})} \tag{2.41}$$

with neutron and proton rest masses m_n and m_p, respectively, and the vacuum binding energy $B_i^{(\mathrm{vac})} > 0$ for composite particles. For neutrons and protons the binding energy does not appear. Chemical equilibrium leads to the constraint

$$\tilde{\mu}_i = N_i \tilde{\mu}_n + Z_i \tilde{\mu}_p \tag{2.42}$$

for the relativistic chemical potentials of the clusters. With every particle $i = n, p, d, t, h, \alpha, \ldots$ of momentum $\vec{k}$, an energy

$$E_i(\vec{k}) = V_i + \sqrt{k^2 + (m_i - S_i)^2} \tag{2.43}$$

is associated that contains the vector and scalar self-energies V_i and S_i, respectively. These potentials are given by

$$V_i = \Gamma_{i\omega}\omega_0 + \Gamma_{i\rho}\rho_0 + (\delta_{in} + \delta_{ip})V^{(r)}, \tag{2.44}$$

$$S_i = \Gamma_{i\sigma}\sigma + \Gamma_{i\delta}\delta - (1 - \delta_{in})(1 - \delta_{ip})\Delta B_i \tag{2.45}$$

where Γ_{im} are the couplings of meson fields $m = \omega, \rho, \sigma, \delta$ to the particle i and the contribution of the medium-dependent binding energy shifts ΔB_i appears. We assume that the coupling strength of the clusters is a multiple of that of the nucleons, i.e.

$$\Gamma_{im} = g_{im}\Gamma_m(n) \tag{2.46}$$

with

$$g_{i\omega} = g_{i\sigma} = N_i + Z_i, \tag{2.47}$$

$$g_{i\rho} = g_{i\delta} = N_i - Z_i. \tag{2.48}$$

Other choices are possible and should be explored in the future. The meson-nucleon couplings $\Gamma_m(n)$ depend on the total nucleon density $n = n_n + n_p$ only. The functional form and the parameters of the density dependent couplings $\Gamma_m(n)$ used in the gRMF model were chosen in such a way to describe the properties of finite nuclei and nuclear matter parameters at saturation density. The parametrization DD2 used in further calculations was described in Subsection 1.6.1. The vector self-energy contains the rearrangement term

$$V^{(r)} = \Gamma'_\omega n_\omega \omega_0 + \Gamma'_\rho n_\rho \rho_0 - \Gamma'_\sigma n_\sigma \sigma - \Gamma'_\delta n_\delta \delta \tag{2.49}$$

that is only relevant for nucleons. In the medium, the actual binding energy of a cluster $B_i = B_i^{(\mathrm{vac})} - \Delta B_i$ will be shifted with respect to the vacuum value $B_i^{(\mathrm{vac})}$ by a binding energy shift ΔB_i. This quantity ΔB_i for composite particles is parametrized as a function of temperature and the Lorentz vector meson fields ω_0 and ρ_0, see, e.g. Ref. [TRK$^+$10]. The specific form of these shifts is not important in the present discussion of the low-density behavior of the EoS but it affects the transition to high densities, see Subsection 2.6.3.

The source densities in Eqs. (2.38) and (2.49)

$$n_\omega = \sum_i g_{i\omega} n_i \,, \quad n_\rho = \sum_i g_{i\rho} n_i \,, \tag{2.50}$$

$$n_\sigma = \sum_i g_{i\sigma} n_i^{(s)} \,, \quad n_\delta = \sum_i g_{i\delta} n_i^{(s)} \tag{2.51}$$

depend on the vector and scalar particle number densities n_i and $n_i^{(s)}$, respectively, that are defined as

$$n_i = -\left.\frac{\partial \Omega}{\partial \tilde{\mu}_i}\right|_{T,V,\tilde{\mu}_{j\neq i}} = g_i \int \frac{d^3k}{(2\pi)^3} f_i \,, \tag{2.52}$$

$$n_i^{(s)} = g_i \int \frac{d^3k}{(2\pi)^3} f_i \frac{m_i - S_i}{\sqrt{k^2 - (m_i - S_i)^2}} \tag{2.53}$$

with the Fermi-Dirac (Bose-Einstein) distribution function

$$f_i(\vec{k}) = \left[\exp\left(\frac{E_i - \tilde{\mu}_i}{T} \right) \pm 1 \right]^{-1} \tag{2.54}$$

or the Maxwell-Boltzmann distribution function

$$f_i(\vec{k}) = \exp\left(-\frac{E_i - \tilde{\mu}_i}{T} \right) \tag{2.55}$$

depending on the particle statistics.

The field equations for the mesons are derived from the functional Ω with the help of the Euler-Lagrange equations. They have the form

$$m_\omega^2 \omega = \Gamma_\omega n_\omega + \sum_i (1 - \delta_{in})(1 - \delta_{ip}) n_i^{(s)} \frac{\partial \Delta B_i}{\partial \omega_0} \,, \tag{2.56}$$

$$m_\rho^2 \rho = \Gamma_\rho n_\rho + \sum_i (1 - \delta_{in})(1 - \delta_{ip}) n_i^{(s)} \frac{\partial \Delta B_i}{\partial \rho_0} \,, \tag{2.57}$$

$$m_\sigma^2 \sigma = \Gamma_\sigma n_\sigma \,, \tag{2.58}$$

$$m_\delta^2 \delta = \Gamma_\delta n_\delta \tag{2.59}$$

with additional contributions to the source terms due to the dependence of the binding energies B_i on the vector meson fields. The field equations of the mesons have to be solved self-consistently for given total baryon density, asymmetry and temperature. The densities depend themselves on the meson fields through the scalar and vector potentials. All thermodynamical quantities can then be derived from Ω and its derivatives. For example, we obtain the entropy as

$$\begin{aligned} S &= -V\sum_i g_i \int \frac{d^3k}{(2\pi)^3}\left[f_i \ln f_i \pm \left(1\mp f_i\right)\ln\left(1\mp f_i\right)\right] \\ &\quad -V\sum_i \left(1-\delta_{in}\right)\left(1-\delta_{ip}\right) n_i^{(s)} \frac{\partial \Delta B_i}{\partial T} - \sum_i \frac{\Omega_i}{g_i}\frac{dg_i}{dT} \end{aligned} \tag{2.60}$$

with the usual single-particle contribution, a term due to the temperature dependence of the cluster binding energy shifts ΔB_i and a contribution caused by internal excitations of the clusters, i.e. the introduction of the temperature dependence of the degeneracy factors, described in Section 2.4, similar to the NSE model. In case of the Maxwell-Boltzmann statistics for a particle i, the integrand contains only the term $f_i \ln f_i$. In order to reproduce the model-independent low-density results of the VEoS within the gRMF model, we will derive consistency relations from the comparison of the fugacity expansions, described below, for both these models.

2.3.2 Scheme of the fugacity expansion

Introducing the modified fugacity

$$\tilde{z}_i = \exp\left(\frac{\tilde{\mu}_i - m_i + S_i - V_i}{T}\right) = \exp\left(\frac{S_i - V_i}{T}\right) z_i \tag{2.61}$$

we write the distribution function as

$$f_i = \left[\tilde{z}_i^{-1}\exp\left(\frac{e_i}{T}\right) \pm 1\right]^{-1} = \frac{\tilde{z}_i \exp\left(-\frac{e_i}{T}\right)}{1 \pm \tilde{z}_i \exp\left(-\frac{e_i}{T}\right)} \tag{2.62}$$

with the kinetic energy $e_i(k) = \sqrt{k^2 + (m_i - S_i)^2} - (m_i - S_i) \geq 0$. For $\tilde{z}_i \ll 1$ the distribution function can be expanded in a power series in $\tilde{z}_i \exp\left(-e_i/T\right)$. The appearing momentum space integrals can be evaluated explicitly [JEL96] with the integral representation of the modified Bessel functions $K_\nu(x)$ [AS65]. For the contributions (2.39) of the individual particles to the grand canonical potential we find

$$\begin{aligned} \Omega_i = -VT\frac{g_i}{\lambda_i^3}\left(\frac{m_i - S_i}{m_i}\right)^{3/2} \\ \times \sum_{n=0}^{\infty} \frac{(\mp 1)^n}{(n+1)^{5/2}} k_2\left[(n+1)\frac{m_i - S_i}{T}\right] \exp\left[(n+1)\frac{S_i - V_i}{T}\right] z_i^{n+1} \end{aligned} \tag{2.63}$$

with the nonrelativistic fugacity z_i and the functions

$$k_\nu(x) = \sqrt{\frac{2x}{\pi}}\exp(x) K_\nu(x)\,. \tag{2.64}$$

Similarly, the vector density is obtained as

$$n_i = \frac{g_i}{\lambda_i^3}\left(\frac{m_i - S_i}{m_i}\right)^{3/2} \times \sum_{n=0}^{\infty} \frac{(\mp 1)^n}{(n+1)^{3/2}} k_2\left[(n+1)\frac{m_i - S_i}{T}\right] \exp\left[(n+1)\frac{S_i - V_i}{T}\right] z_i^{n+1} . \tag{2.65}$$

For the scalar density $n_i^{(s)}$, k_2 has to be replaced with k_1. In case of Maxwell-Boltzmann statistics, only the $n = 0$ term remains. Without interaction, i.e. $S_i = V_i = 0$, the results for a relativistic Fermi or Bose gas are recovered. For $T \to 0$, i.e. $x = (n+1)(m_i - S_i)/T \to \infty$, one finds from the asymptotic expansion [AS65]

$$k_\nu(x) = 1 + \frac{\mu - 1}{8x} + \frac{(\mu-1)(\mu-9)}{2!(8x)^2} + \frac{(\mu-1)(\mu-9)(\mu-25)}{3!(8x)^3} + \ldots \tag{2.66}$$

with $\mu = 4\nu^2$ the common expressions

$$\Omega_i = -VT\frac{g_i}{\lambda_i^3}\sum_{m=0}^{\infty}\frac{(\mp 1)^m}{(m+1)^{5/2}} z_i^{m+1} , \tag{2.67}$$

and

$$n_i = \frac{g_i}{\lambda_i^3}\sum_{m=0}^{\infty}\frac{(\mp 1)^m}{(m+1)^{3/2}} z_i^{m+1} \tag{2.68}$$

for non-relativistic particles. In this limit, $n_i^{(s)} = n_i$, because the scalar density differs from the baryon density only in the relativistic description. Since the scalar and vector self-energies are themselves functions of the densities, a second expansion of the series (2.63) and (2.65) is required.

2.3.3 Fugacity expansion of the grand canonical potential up to second order

We want to compare the true series expansion of the grand canonical potential Ω of the gRMF model with the form (2.19) in the VEoS approach at low densities. In order to do that we expand (2.38) up to second order in the fugacities of neutrons and protons. In the following we will only consider neutrons, protons and deuterons in the density expansion. Since we only consider nucleons as basic constituents, nuclei with mass numbers $A \geq 3$ do not contribute in second order of the expansion. The two-nucleon cluster, the deuteron ground state, appears in the two-nucleon correlation term with

$$z_d = z_n z_p \exp\left(\frac{B_d}{T}\right) . \tag{2.69}$$

For sufficiently low nucleon densities, the self-energies of the nucleons are approximately linear in the nucleon densities. Hence, the contribution of the individual nucleon eq.(2.63) can be approximated as

$$\Omega_i \approx -VT\frac{g_i}{\lambda_i^3}\left\{k_2\left(\frac{m_i}{T}\right)\left[1 + \frac{S_i}{T}\left(1 - \frac{k_2'\left(\frac{m_i}{T}\right)}{k_2\left(\frac{m_i}{T}\right)} - \frac{3}{2}\frac{T}{m_i}\right) - \frac{V_i}{T}\right] z_i - \frac{1}{2^{5/2}} k_2\left(2\frac{m_i}{T}\right) z_i^2\right\} . \tag{2.70}$$

Applying the recursion relation

$$k_\nu'(x) = \left(1 - \frac{2\nu - 1}{2x}\right) k_\nu(x) - k_{\nu-1}(x)\,, \tag{2.71}$$

the expression (2.70) for the nucleons reduces to

$$\Omega_i \approx -VT\left[\left(1 - \frac{V_i}{T}\right) x_i + \frac{S_i}{T} y_i - \frac{g_i}{2^{5/2}\lambda_i^3} k_2\left(2\frac{m_i}{T}\right) z_i^2\right], \tag{2.72}$$

with the abbreviations

$$x_i = \frac{g_i}{\lambda_i^3} k_2\left(\frac{m_i}{T}\right) z_i\,, \tag{2.73}$$

$$y_i = \frac{g_i}{\lambda_i^3} k_1\left(\frac{m_i}{T}\right) z_i\,. \tag{2.74}$$

For the deuteron contribution we have

$$\Omega_d = -VT\frac{g_d}{\lambda_d^3} k_2\left(\frac{m_d}{T}\right) z_n z_p \exp\left(\frac{B_d}{T}\right) \tag{2.75}$$

without self-energy terms, which contribute only in higher order of the fugacities. Contrary the nucleon self-energies contribute already in the lowest order of the fugacities

$$V_n \approx C_\omega(x_n + x_p) + C_\rho(x_n - x_p), \tag{2.76}$$

$$V_p \approx C_\omega(x_n + x_p) - C_\rho(x_n - x_p), \tag{2.77}$$

$$S_n \approx C_\sigma(y_n + y_p) + C_\delta(y_n - y_p), \tag{2.78}$$

$$S_p \approx C_\sigma(y_n + y_p) - C_\delta(y_n - y_p), \tag{2.79}$$

with coefficients

$$C_m = \frac{\Gamma_m^2(0)}{m_m^2} \tag{2.80}$$

for $m = \omega, \rho, \sigma, \delta$ that depend on the density dependent meson couplings $\Gamma_m(n)$ taken in the limit $n \to 0$. The rearrangement term in the vector self-energy does not contribute at this level because it is at least quadratic in the densities. With the help of the field equations (2.56)-(2.59), the mesonic contributions in (2.38) can be expressed as quadratic forms of the nucleon

densities. Finally, after performing all necessary expansions up to second order in the nucleon fugacities, we obtain the resulting grand canonical potential

$$
\begin{aligned}
&\Omega(T,V,\mu_n,\mu_p) = \\
&\quad -TV\frac{g_n}{\lambda_n^3}\left[k_2\left(\frac{m_n}{T}\right)z_n - \frac{1}{2^{5/2}}k_2^2\left(2\frac{m_n}{T}\right)z_n^2\right] \\
&\quad -TV\frac{g_p}{\lambda_p^3}\left[k_2\left(\frac{m_p}{T}\right)z_p - \frac{1}{2^{5/2}}k_2^2\left(2\frac{m_p}{T}\right)z_p^2\right] \\
&\quad -TV\frac{g_d}{\lambda_d^3}k_2\left(\frac{m_d}{T}\right)\exp\left(\frac{B_d}{T}\right)z_n z_p \\
&\quad +\frac{V}{2}\frac{g_n^2}{\lambda_n^6}\left[\left(C_\omega + C_\rho\right)k_2^2\left(\frac{m_n}{T}\right) - \left(C_\sigma + C_\delta\right)k_1^2\left(\frac{m_n}{T}\right)\right]z_n^2 \\
&\quad +\frac{V}{2}\frac{g_p^2}{\lambda_p^6}\left[\left(C_\omega + C_\rho\right)k_2^2\left(\frac{m_p}{T}\right) - \left(C_\sigma + C_\delta\right)k_1^2\left(\frac{m_p}{T}\right)\right]z_p^2 \\
&\quad +V\frac{g_n g_p}{\lambda_n^3\lambda_p^3}\left[\left(C_\omega - C_\rho\right)k_2\left(\frac{m_n}{T}\right)k_2\left(\frac{m_p}{T}\right)\right. \\
&\quad \left. -\left(C_\sigma - C_\delta\right)k_1\left(\frac{m_n}{T}\right)k_1\left(\frac{m_p}{T}\right)\right]z_n z_p,
\end{aligned}
\tag{2.81}
$$

with contributions from free nucleons and their correlation due to statistics, the deuteron bound state and the interaction.

2.3.4 Comparison of fugacity expansions

From the comparison of equation (2.19) with the corresponding expansion (2.81) we can extract the virial coefficients b_n, b_p, b_{nn}, b_{pp} and b_{np} of the gRMF model. The first order coefficients (2.6) receive a relativistic correction with

$$b_n = g_n k_2\left(\frac{m_n}{T}\right), \tag{2.82}$$

$$b_p = g_p k_2\left(\frac{m_p}{T}\right). \tag{2.83}$$

They depend on the temperature now. In the non-relativistic limit $T/m_i \to 0$ the correction will vanish due to the asymptotic expansion of the function k_2, c.f. eq. (2.66). These corrections are important and should be taken into account for an improved description of low-density nuclear matter as will be shown below. Similarly, there is a relativistic modification to the statistical corrections in b_{nn} and b_{pp}, i.e. eqs. (2.20) and (2.21), respectively, and to the deuteron con-

tribution to (2.23). From the comparison of (2.19) and (2.81), three independent relations for the channels nn, pp and np remain

$$-\frac{T}{\lambda_n^3}\left[b_{nn}+\frac{g_n}{2^{5/2}}k_2\left(2\frac{m_n}{T}\right)\right]=-\frac{T}{\lambda_{nn}^3}k_2\left(\frac{2m_n}{T}\right)\sum_l g_l^{(nn)}I_l^{(nn)} \tag{2.84}$$

$$=\frac{1}{2}\frac{g_n^2}{\lambda_n^6}\left[\left(C_\omega+C_\rho\right)k_2^2\left(\frac{m_n}{T}\right)-\left(C_\sigma+C_\delta\right)k_1^2\left(\frac{m_n}{T}\right)\right],$$

$$-\frac{T}{\lambda_p^3}\left[b_{pp}+\frac{g_p}{2^{5/2}}k_2\left(2\frac{m_p}{T}\right)\right]=-\frac{T}{\lambda_{pp}^3}k_2\left(\frac{2m_p}{T}\right)\sum_l g_l^{(pp)}I_l^{(pp)} \tag{2.85}$$

$$=\frac{1}{2}\frac{g_p^2}{\lambda_p^6}\left[\left(C_\omega+C_\rho\right)k_2^2\left(\frac{m_p}{T}\right)-\left(C_\sigma+C_\delta\right)k_1^2\left(\frac{m_p}{T}\right)\right],$$

$$-T\left[2\frac{b_{np}}{\lambda_n^{3/2}\lambda_p^{3/2}}-\frac{g_d}{\lambda_d^3}k_2\left(\frac{m_d}{T}\right)\exp\left(\frac{B_d}{T}\right)\right] \tag{2.86}$$

$$=-\frac{T}{\lambda_{np}^3}k_2\left(\frac{m_n+m_p}{T}\right)\sum_l\left[g_l^{(np1)}I_l^{(np1)}+g_l^{(np0)}I_l^{(np0)}\right]$$

$$=\frac{g_ng_p}{\lambda_n^3\lambda_p^3}\left[\left(C_\omega-C_\rho\right)k_2\left(\frac{m_n}{T}\right)k_2\left(\frac{m_p}{T}\right)\right.$$

$$\left.-\left(C_\sigma-C_\delta\right)k_1\left(\frac{m_n}{T}\right)k_1\left(\frac{m_p}{T}\right)\right],$$

that connect the virial integrals with the strengths C_m of the zero-density meson-nucleon couplings $\Gamma_m(0)$ of the gRMF model. The expected correction factors $k_2(m_i/T)$ due to the relativistic effects were added to the VEoS part (expressed through virial integrals I_l^{ij}) of relations (2.84) to (2.86). In the following we investigate several possibilities how one can satisfy these consistency relations.

2.3.5 Temperature independent limit of consistency conditions

From a comparison of the two fugacity expansions, valid in the virial limit, we have obtained the consistency relations (2.84) to (2.86). These conditions arise from the contributions in the fugacity expansion that are quadratic in the fugacities. We perform an expansion of Eqs. (2.84) to (2.86) in powers of small T/m_i and keep the lowest order terms which are independent of T. This is equivalent of taking the limit $T\to 0$ in (2.84) to (2.86). There are no relativistic corrections in this limit, only s-wave contributions are relevant and the limit (2.33) of the integral with the scattering lengths can be used. In the gRMF model the nucleon-nucleon interaction is identical in the nn and pp systems. Thus, the first two equations, (2.84) and (2.85) cannot be considered independent but should be combined. Denoting the scattering lengths in the s-wave channels explicitly with $a_{^1S_0}^{(nn)}$, $a_{^1S_0}^{(pp)}$, $a_{^1S_0}^{(np)}$ and $a_{^3S_1}^{(np)}$ and considering the degeneracy factors $g_n=g_p=2$, $g_{^1S_0}^{(nn)}=g_{^1S_0}^{(pp)}=g_{^1S_0}^{(np)}=1$ and $g_{^3S_1}^{(np)}=3$, the two consistency conditions

$$C_\omega-C_\sigma=\pi\left\{\frac{1}{2}\left[\frac{a_{^1S_0}^{(nn)}}{m_n}+\frac{a_{^1S_0}^{(pp)}}{m_p}\right]+\frac{m_n+m_p}{m_nm_p}\frac{a_{^1S_0}^{(np)}+3a_{^3S_1}^{(np)}}{4}\right\} \tag{2.87}$$

Table 2.1.: Coupling coefficients (2.80) in the DD2 parametrization of the gRMF model [TRK$^+$10] and the DD-MEδ parametrization of Ref. [RMVC$^+$11].

model	DD2	DD-MEδ
meson m	C_m [fm^2]	C_m [fm^2]
ω	17.250448	14.539639
σ	22.639364	19.443381
ρ	2.483932	6.017331
δ	–	3.462716

and

$$C_\rho - C_\delta = \pi \left\{ \frac{1}{2} \left[\frac{a_{^1S_0}^{(nn)}}{m_n} + \frac{a_{^1S_0}^{(pp)}}{m_p} \right] - \frac{m_n + m_p}{m_n m_p} \frac{a_{^1S_0}^{(np)} + 3a_{^3S_1}^{(np)}}{4} \right\} \tag{2.88}$$

for the isovector and isoscalar meson couplings are obtained. The left side of equations (2.87) and (2.88) corresponds to the gRMF expansion, expressed in terms of couplings at zero density while the right side represents the virial expansion in the effective-range approximation.

Coupling coefficients C_m can be calculated for different RMF models with the given coupling constants at zero density $\Gamma_m(0)$ and the meson masses m_m. In table 2.1 the results are shown for the gRMF model with parametrization DD2 without δ meson following Ref. [TRK$^+$10] and for a new density dependent RMF parametrization DD-MEδ from [RMVC$^+$11] fitted to ab-initio calculations in nuclear matter including a Lorentz scalar isovector δ meson. In the DD2 parametrization the differences of the coupling coefficients are $C_\omega - C_\sigma = -5.39$ fm^2 and $C_\rho - C_\delta = 2.48$ fm^2. In contrast, the calculation with the scattering lengths from Ref. [WSS95] gives $C_\omega - C_\sigma = -14.15$ fm^2 and $C_\rho - C_\delta = -9.61$ fm^2. It is obvious that the coupling coefficients of the gRMF model do not obey the consistency relations to guarantee the agreement with the VEoS at low densities.

For the recently developed parametrization DD-MEδ [RMVC$^+$11], the differences of the coupling coefficients turn out to be $C_\omega - C_\sigma = -4.90$ fm^2 and $C_\rho - C_\delta = 2.55$ fm^2. These numbers are close to those of the DD2 parametrization. There are still differences to the values required by the consistency conditions (2.87) and (2.88) and a more drastic modification of the low-density couplings seems to be necessary. Even the inclusion of the δ meson in the RMF model with DD-MEδ parametrization does not lead to a negative $C_\rho - C_\delta$ sign as required from the consistency relation (2.88).

A particular form of the density dependence of the coupling functions $\Gamma_m(n)$ in the gRMF model was assumed. The choice was motivated by results from Dirac-Brueckner calculations of nuclear matter [TW99]. However, only near the saturation density of symmetric nuclear matter couplings are well determined from model fits to the properties of atomic nuclei. Values at zero density are found from a not well constrained extrapolation to small densities. Thus, in general, one could modify the density dependence of $\Gamma_m(n)$ for all mesons m at low densities in order to satisfy the constraints (2.87) and (2.88). Since $C_\rho - C_\delta$ has to be negative, it is clear that the standard ω, σ and ρ mesons are not sufficient and a δ meson is needed in this case.

Two additional constraints are required to fix all couplings unambiguously, since only two relations for four coupling coefficients C_m are given by equations (2.87) and (2.88), obtained from the consistency with the virial expansion. Therefore, in addition to the virial constraints, we tried to fit the vacuum couplings coefficients $\Gamma_m(0)$ by describing low-energy nucleon-nucleon scattering, i.e. experimentally determined NN phase shifts [SKRdS93], simultaneously satisfying equations (2.87) and (2.88). The corresponding Schrödinger equation in coordinate space was solved using σ, ω, ρ and δ mesons with a one-boson exchange potential [EW88] in order to fit the coupling constants of the nucleon-meson interaction and to describe the experimentally known phase shifts and effective range parameters given in [WSS95, HCC$^+$98]. The gradient terms in the potential lead to unphysical singularities at $r \to 0$, thus to avoid these singularities a cutoff was introduced as in [BS69]. Coupling constants derived in this way would serve as an additional constraint at zero densities, improving the density dependence of the coupling functions $\Gamma_m(n)$. However, even when the contribution of the pion was included, that does not contribute in the mean-field approximation, it was impossible to find a reasonable parametrization. Quite drastic modifications of the low-density meson-nucleon couplings and meson masses were required. This failure is not very surprising because the number of meson fields in the RMF model is much smaller than that in realistic NN potentials resulting in a smaller number of degrees of freedom. In addition, the meson fields in the RMF model do not represent real physical mesons and their masses, which are used as adjustable parameters, e.g. in case of the σ meson, are not identical to the true meson masses. The zero-temperature limit also leads to the shrinking of the density range applicable for the comparison with the VEoS. Therefore, we do not follow this approach but extend the gRMF model further to include temperature dependent resonance states that would lead to the correct limit.

2.4 Extension of the gRMF approach

We have found that the gRMF model fails to simultaneously describe the virial limit at low densities and the NN scattering in vacuum. Therefore a further extension of the approach is required. In addition to the bound state two-body correlation, the deuteron, we introduce additional degrees of freedom in the grand canonical potential that represent the possible two-nucleon states, nn, pp and np, in the continuum. In the following, we will consider the isospin 0 and 1 channels for the np states separately. Each of the two-body channels is represented by a temperature dependent resonance energy ($\tilde{E}_{nn}$, $\tilde{E}_{pp}$, $\tilde{E}_{np0}$, $\tilde{E}_{np1}$) and a corresponding effective degeneracy factor ($\tilde{g}_{nn}$, $\tilde{g}_{pp}$, $\tilde{g}_{np0}$, $\tilde{g}_{np1}$). In general, the resonance energies and degeneracy factors do not necessarily have to be the same as the resonance energies of equation (2.25) or the standard degeneracy factors in equations (2.20) to (2.23). Two-body correlations in the continuum are considered as two-body clusters with mass

$$\tilde{m}_{ij} = N_{ij} m_n + Z_{ij} m_p + \tilde{E}_{ij} \tag{2.89}$$

with a temperature dependent resonance energy $\tilde{E}_{ij}$. We assume that the energy shift of a cluster ΔB_{ij} that appears in the scalar self-energy (2.45) is identical to the binding energy shift of the deuteron ΔB_d for all continuum channels. This is the most simple choice that can be investigated and should be substituted by improved descriptions in the future. The specific functional form of the medium dependent energy shift will affect the form of the transition from very low densities, where the VEoS is applicable, to the high-density regime. However, for the low-density matching of the VEoS and gRMF model it is irrelevant.

The total rest mass of a cluster in the medium is given by

$$\tilde{M}_{ij} = \tilde{m}_{ij} + \Delta B_{ij} \,. \tag{2.90}$$

In case of the virial approach, the appearing masses are given by $m_{ij} = N_{ij}m_n + Z_{ij}m_p + E_{ij}$ and $M_{ij} = m_{ij}$, respectively. We include the effect of the resonance energies in the relativistic correction through the k_2 function and the definition of the thermal wave lengths $\lambda_{ij} = [2\pi/(M_{ij}T)]^{1/2}$ and similarly for $\tilde{\lambda}_{ij}$. With these modifications we can rederive consistency relations between this extended gRMF model and the VEoS.

The virial integrals (2.24) in the virial coefficients are represented by an exponential of the effective resonance energy as defined in (2.25). The two np channels are separated by requiring for the np isospin 1 channel a similar form as for the nn and pp channels. Comparing the fugacity expansion of the gRMF model with two-body correlations with the VEoS at low densities, we finally obtain an extension of the relations (2.84) to (2.86) , where an additional term with temperature dependent resonance energy $\tilde{E}_{ij}(T)$ appears in the right-hand side of the equations (2.91) to (2.92), i.e.

$$\begin{aligned} &-\frac{T}{\lambda_{ij}^3} k_2\left(\frac{M_{ij}}{T}\right) \hat{g}_{ij} \exp\left(-\frac{E_{ij}}{T}\right) \\ &= -\frac{T}{\tilde{\lambda}_{ij}^3} k_2\left(\frac{\tilde{M}_{ij}}{T}\right) g_{ij}^{(\mathrm{eff})} \exp\left(-\frac{\tilde{E}_{ij}}{T}\right) \\ &\quad + \frac{1}{2}\frac{g_i g_j}{\lambda_i^3 \lambda_j^3}\left[\left(C_\omega + C_\rho\right) k_2\left(\frac{m_i}{T}\right) k_2\left(\frac{m_j}{T}\right)\right. \\ &\quad \left. - \left(C_\sigma + C_\delta\right) k_1\left(\frac{m_i}{T}\right) k_1\left(\frac{m_j}{T}\right)\right] \end{aligned} \tag{2.91}$$

for the channels $ij = nn$, pp, $np1$ and

$$\begin{aligned} &-\frac{T}{\lambda_{np0}^3} k_2\left(\frac{M_{np0}}{T}\right) \hat{g}_{np0} \exp\left(-\frac{E_{np0}}{T}\right) \\ &= -\frac{T}{\tilde{\lambda}_{np0}^3} k_2\left(\frac{\tilde{M}_{np0}}{T}\right) g_{np0}^{(\mathrm{eff})} \exp\left(-\frac{\tilde{E}_{np0}}{T}\right) \\ &\quad + \frac{1}{2}\frac{g_n g_p}{\lambda_n^3 \lambda_p^3}\left[\left(C_\omega - 3C_\rho\right) k_2\left(\frac{m_n}{T}\right) k_2\left(\frac{m_p}{T}\right)\right. \\ &\quad \left. - \left(C_\sigma - 3C_\delta\right) k_1\left(\frac{m_n}{T}\right) k_1\left(\frac{m_p}{T}\right)\right] \end{aligned} \tag{2.92}$$

for the channel $np0$. These consistency relations offer sufficient freedom to reproduce the exact VEoS at low densities in the gRMF model. There are different possibilities to achieve this goal depending on the choice of the zero-density couplings and on the choice of the effective resonance energies and degeneracy factors that represent the continuum contributions in the extended gRMF model. The structure on the left-hand side shares some similarities with the generalized Beth-Uhlenbeck approach in Subsection 2.2.4. One part of the effects of the two-body correlations is included in the explicit continuum contributions and the remaining part is

covered by the mean-field terms. There is the freedom to shift the correlation strength between these terms rather arbitrarily. We will discuss several possibilities in the following.

We have described one of the options in Subsection 2.3.5, where the case without introducing explicit continuum channels in the gRMF model, i.e. shifting the full correlation strength into a redefinition of the vacuum couplings, turned out to be impossible. The other extreme is to represent the correlations by the introduction of the effective continuum states described by temperature dependent resonance energies $\tilde{E}_{ij}$ with medium corrections ΔB_{ij} as described above. In this case the contribution of the virial integral in the left-hand side of the equations (2.91) and (2.92) is fully represented by the the resonance energies $\tilde{E}_{ij}$ in the first term in the right-hand side of these equations. Therefore the mean-field part has to vanish in the non-relativistic limit, leading to $C_\omega - C_\sigma = 0$ and $C_\rho - C_\delta = 0$. The coupling coefficients C_m in relations (2.87) to (2.88) were expressed through the virial integral taken in the effective range approximation. In the new relations, given above, the virial integral and thus the scattering lengths are implemented in the definition of the resonance energies $\tilde{E}_{ij}(T)$. Therefore, neglecting the term proportional to $g_{ij}^{(\mathrm{eff})} \exp\left(-\tilde{E}_{ij}/T\right)$ in the relations (2.91) and (2.92), we recover equations (2.84) to (2.86), leading to the consistency conditions (2.87) to (2.88). Then one can try to fix the four couplings C_m unambiguously. We again tried to describe low-energy nucleon-nucleon scattering, by solving the Schrödinger equation with one-boson exchange potentials as described in Subsection 2.3.5 simultaneously with the two conditions on the couplings $C_\omega - C_\sigma = 0$, $C_\rho - C_\delta = 0$. We observed that the required coupling constants at zero density are drastically different in comparison with the previous values of the parametrization DD2 or DD-MEδ leading to problems such as a rather unphysical behavior of the EoS at low densities by similar reasons as in the first attempt discussed at the end of Subsection 2.3.5. Consequently, this approach was discarded. Within the framework of the relativistic mean-field model it turned out to be impossible to describe both the NN scattering data and the VEoS simultaneously with this second choice for representing the continuum correlations.

Therefore the most straightforward way to fulfill the consistency relations (2.91) and (2.92) is to leave the density dependence of meson-nucleon couplings untouched as given by the gRMF model parametrization and to turn down the idea of an additional fit to NN scattering data, thus concentrating only on the reproduction of the VEoS. The effective resonance energies are chosen as identical to those of the VEoS, i.e. $\tilde{E}_{ij} = E_{ij}$, thus including two-body correlations. Then, the consistency relations (2.91) and (2.92) serve as the defining equations for the effective degeneracy factors $g_{ij}^{(\mathrm{eff})}$ that now depend on temperature. In the non-relativistic limit, these equations simplify to

$$g_{nn}^{(\mathrm{eff})}(T) = \hat{g}_{nn} + \frac{g_n^2}{2T}\frac{\lambda_{nn}^3}{\lambda_n^6} C_1 \exp\left[\frac{E_{nn}(T)}{T}\right], \tag{2.93}$$

$$g_{pp}^{(\mathrm{eff})}(T) = \hat{g}_{pp} + \frac{g_p^2}{2T}\frac{\lambda_{pp}^3}{\lambda_p^6} C_1 \exp\left[\frac{E_{pp}(T)}{T}\right], \tag{2.94}$$

$$g_{np1}^{(\mathrm{eff})}(T) = \hat{g}_{np1} + \frac{g_n g_p}{2T}\frac{\lambda_{np1}^3}{\lambda_n^3\lambda_p^3} C_1 \exp\left[\frac{E_{np1}(T)}{T}\right], \tag{2.95}$$

$$g_{np0}^{(\mathrm{eff})}(T) = \hat{g}_{np0} + \frac{g_n g_p}{2T}\frac{\lambda_{np0}^3}{\lambda_n^3\lambda_p^3} C_0 \exp\left[\frac{E_{np0}(T)}{T}\right], \tag{2.96}$$

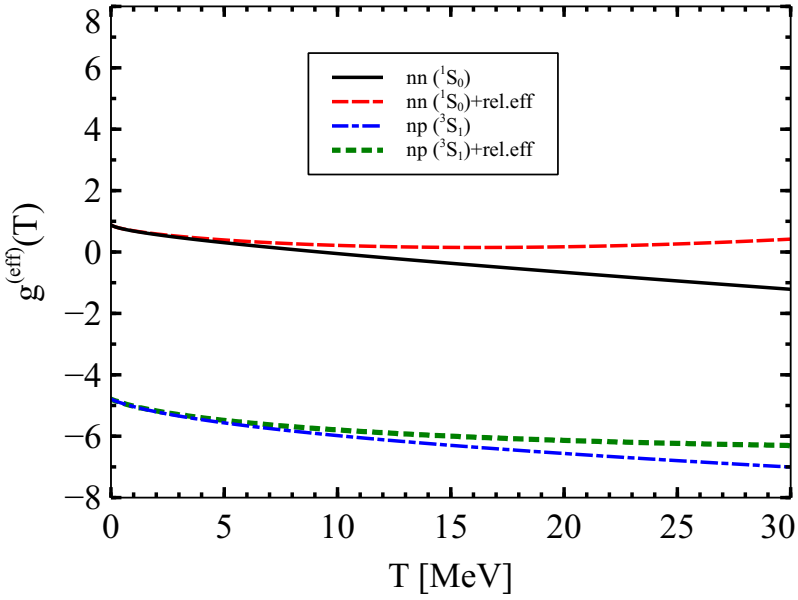

Figure 2.4.: Temperature dependence of the effective degeneracy factors $g_{nn}^{(\mathrm{eff})}$ and $g_{np0}^{(\mathrm{eff})}$ with and without relativistic corrections.

where

$$C_1 = C_\omega - C_\sigma + C_\rho - C_\delta\,, \tag{2.97}$$

$$C_0 = C_\omega - C_\sigma - 3\left(C_\rho - C_\delta\right) \tag{2.98}$$

are the relevant couplings in the two isospin channels. If $C_1 = C_0 = 0$ as was discussed before as a possible condition, we recover the standard degeneracy factors $\hat{g}_{ij}$ in the s-wave. The degeneracy factors on the right-hand side are $\hat{g}_{nn} = \hat{g}_{pp} = \hat{g}_{np1} = 1$ and $\hat{g}_{np0} = -3$, respectively. The negative sign for $\hat{g}_{np0}$ is related to the positive s-wave scattering length in this channel. Note that in the NSE description, c.f. Subsection 2.2.3, the temperature dependence of the degeneracy factors follows from the inclusion of excited states of the nuclei. In our approach, it represents the contribution of the continuum states and thus is very similar.

The temperature dependence of the effective degeneracy factors is depicted in Fig. 2.4. Scattering correlations in the nn and $np0$ channels are considered. Because the curves for the pp and $np1$ channels are practically identical to the nn scattering case, they are not shown. The fully relativistic results from equations (2.91) and (2.92) are compared with their nonrelativistic limits (2.93) and (2.96), respectively. We see that the relativistic corrections caused by the k_1 and k_2 functions are of minor size at low temperatures but grow with the increase of temperature as expected, being larger for the case of nn scattering. The large relativistic correction in the effective degeneracy factors is caused by an accidental change of sign in the factor containing the coupling coefficients in equation (2.91).

In the zero-temperature limit, the effective degeneracy factors are given by

$$g_{ij}^{(\mathrm{eff})}(0) = \hat{g}_{ij} - \frac{\hat{g}_{ij}}{g_{ij}}\frac{C_1}{2\pi a_{ij}}\frac{2m_i m_j}{m_i + m_j}\,, \tag{2.99}$$

$$g_{np0}^{(\mathrm{eff})}(0) = \hat{g}_{np0} - \frac{\hat{g}_{np0}}{g_{np0}}\frac{C_0}{2\pi a_{np0}}\frac{2m_n m_p}{m_n + m_p} \tag{2.100}$$

for the channels $ij = nn, pp, np1$ and $np0$, respectively, when the approximation (2.33) with the scattering length is used. Thus, there is still a difference as compared to $\hat{g}_{ij} = 1$ and $\hat{g}_{np0} = -3$, respectively, when the correction due to the meson couplings is not taken into account. This is a clear indication that the mean field effectively takes over a part of the correlations.

2.5 Neutron matter

For the case of nuclear matter with arbitrary neutron to proton ratio, the two-body correlations appear in all nucleon-nucleon channels. Therefore, they should be all considered in the calculation of thermodynamic properties. The deuteron contribution, in particular, dominates at low temperatures. In pure neutron matter only the the *nn* channel without a bound state is relevant. Thus, neutron matter is ideally suited to demonstrate the effects of the continuum correlations in the extension of the gRMF model. First we consider the case of $T = 0$ in the limit of small densities, proceeding with the general case of finite temperatures.

2.5.1 Zero temperature limit

The Fermi momentum k_{F_n} defined through the neutron density $n_n = k_{F_n}^3/(3\pi^2)$, sets the scale for all results at zero temperature. Instead of an expansion in powers of the neutron fugacity at finite temperature, a series expansion in powers of k_{F_n} is the relevant method to study the low-density behavior of the EoS. In Ref. [LY57] it was shown that the energy per neutron E/N (without rest mass) at very small k_{F_n} can be expanded as

$$\frac{E}{N} = E_{\text{free}}\xi, \tag{2.101}$$

with the power series

$$\xi = 1 + \frac{10}{9\pi}\zeta + \frac{4}{21\pi^2}(11 - 2\ln 2)\,\zeta^2 + \ldots \tag{2.102}$$

in the dimensionless parameter $\zeta = a_{^1S_0}^{(nn)} k_{F_n}$. Here $E_{\text{free}} = 3k_{F_n}^2/(10m_n)$ is the energy per neutron of a non-interacting Fermi gas that defines the relevant energy scale. Because of the unnaturally large negative nn scattering length $a_{^1S_0}^{(nn)} \approx -18.8$ fm [WSS95], the radius of convergence is unfortunately very small, i.e. $n_n \ll 243\pi/|10a_{^1S_0}^{(nn)}|^3 \approx 1.1 \cdot 10^{-4}$ fm^{-3}.

In the gRMF model without effective contributions of two-body correlations the energy per nucleon is given as

$$\frac{E}{N} = \frac{3}{4}E_{F_i} + \frac{1}{4}(m_i - S_i)\frac{n_i^s}{n_i} + \frac{1}{2}(C_\sigma + C_\delta)\frac{n_i^{s\,2}}{n_i} + \frac{1}{2}(C_\omega + C_\rho)n_i, \tag{2.103}$$

with the Fermi energy $E_{F_i} = \sqrt{k_{F_i}^2 + (m_i - S_i)^2}$ and Fermi momenta k_F. Then we can expand this function in terms of $k_F/(m_i - S_i)$. An expansion of the energy per neutron (see Appendix B) leads to

$$\frac{E}{N} = E_{\text{free}}\xi_{\text{RMF}}, \tag{2.104}$$

with

$$\xi_{\mathrm{RMF}} = 1 + \frac{5}{9\pi^2}\left(C_\omega - C_\sigma + C_\rho - C_\delta\right) m_n k_{F_n} + \dots . \tag{2.105}$$

A comparison with Eq. (2.102) gives the relation

$$C_\omega - C_\sigma + C_\rho - C_\delta = \frac{2\pi}{m_n} a_{^1S_0}^{(nn)}. \tag{2.106}$$

This condition coincides with condition (2.84) for neutron matter, although it is derived in the low k_{F_n}/m_n limit for $T = 0$ whereas condition (2.84) in the $T \to 0$ limit of the finite temperature virial expansion with vanishing convergence radius in density. From a physical point of view, this coincidence is not surprising since both approaches only use two-body scattering information. However, it is gratifying to find the coincidence from the two very different approaches. We find the values of -2.91 fm^2 and -2.35 fm^2 for $C_\omega - C_\sigma + C_\rho - C_\delta$ in the DD2 and DD-MEδ parametrizations, respectively. However, these are much smaller in modulus as compared to the required value of $2\pi a_{^1S_0}^{(nn)}/m_n = -24.83$ fm^2.

A particular situation arises in the unitary limit [DLWM12], i.e. if $a_{^1S_0}^{(nn)}$ approaches $-\infty$. Then the series expansion (2.102) can no longer be applied since the radius of convergence shrinks to zero. In fact, the energy per nucleon should scale as the energy per neutron of a noninteracting Fermi gas E_{free} with a universal constant ξ independent of k_{F_n}. The parameter ξ_{RMF} is independent of k_{F_n} in first order only if the combination $C_\omega - C_\sigma + C_\rho - C_\delta$ diverges as $k_{F_n}^{-1}$. Hence a particular density dependence of at least one meson-nucleon coupling is required in this case.

In the nonlinear RMF model of Ref. [SHT10] with nonlinear self-interactions of the scalar meson, a density dependence of the σ meson coupling was introduced for densities lower than a particularly chosen transition density with the aim to reproduce the energy per neutron for unitary neutron matter assuming $\xi = 0.44$ [CCPS03]. This condition required a divergence of $\Gamma_\sigma(n) \propto n^{-1/6}$ that is consistent with the expectation from Eq. (2.105). However, mixing the nonlinear RMF approach and the RMF model with density dependent and divergent couplings does not seem to be very natural. In our approach, we do not aim to describe the neutron matter EoS at zero temperature and low densities as a unitary Fermi gas (FG) but require consistency with the VEoS for $T > 0$.

2.5.2 Finite temperatures

We will demonstrate the main effects due to interactions and correlations for fixed $T = 4$ MeV and $T = 10$ MeV. The description of thermodynamic properties will be shown and compared for different approximations, ranging from the ideal Fermi gas via the virial approach to the gRMF model. Nucleons are treated as Fermions and clusters as Maxwell-Boltzmann particles because they appear at high temperatures with low abundancies when deviations from the correct Bose-Einstein statistics are negligible.

There are two quantities that exhibit finite low-density limits and hence are very advantageous for a comparison of the models: the ratio of the pressure over total particle number density p/n and the internal energy per baryon $E/N = \varepsilon/n - m_n$ (without the rest mass of the neutron). The energy density

$$\varepsilon = \frac{1}{V}(\Omega + TS) + \sum_{i=n,nn} \tilde{\mu}_i n_i \tag{2.107}$$

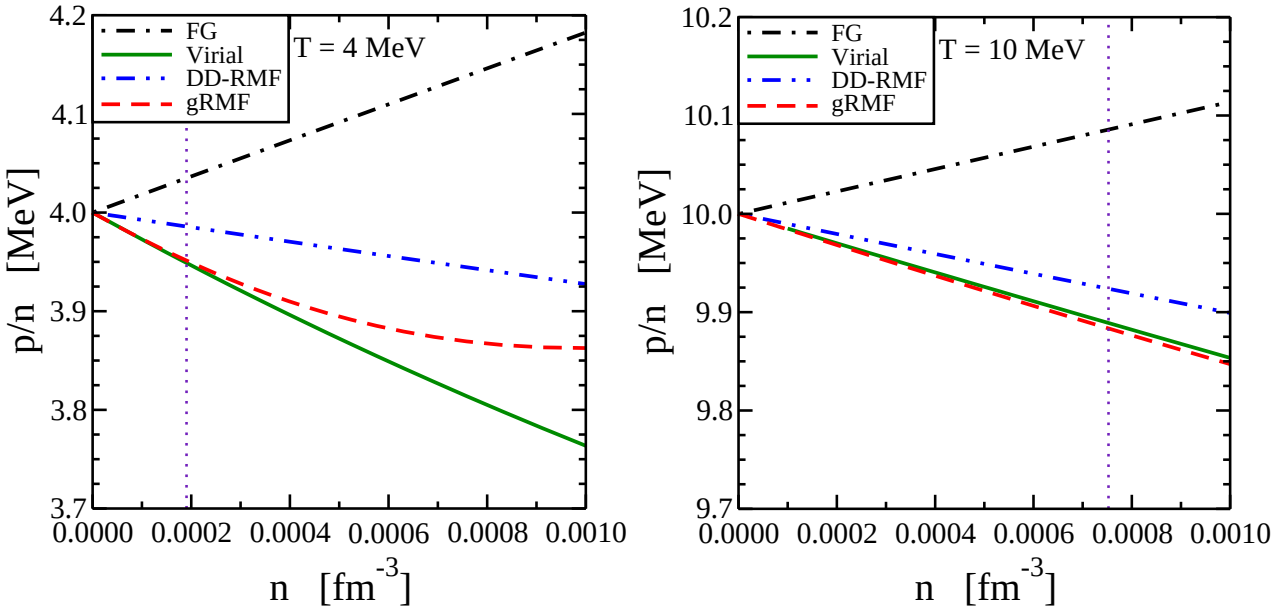

Figure 2.5.: Ratio of pressure over total particle number density, p/n, of neutron matter as a function of the total density n for temperatures of $T = 4$ MeV (left) and $T = 10$ MeV (right). Vertical dotted lines indicate the density where $n\lambda_n^3 = 1/10$.

can be calculated from the grand canonical potential Ω, the entropy S and the relativistic chemical potentials $\tilde{\mu}_i$. The sum contains the contribution of the neutrons and that of the correlated two-neutron continuum. Correspondingly, the total particle number density n is the sum

$$n = n_n + 2n_{nn} \tag{2.108}$$

and the mass fraction of correlated two-neutron states is defined by

$$X_{nn} = \frac{2n_{nn}}{n_n + 2n_{nn}}\,. \tag{2.109}$$

For an ideal gas with Maxwell-Boltzmann statistics and nonrelativistic kinematics, we have the simple result that $p/n = T$ and $E/N = 3T/2$ are independent of the density of the system and trivially $X_{nn} = 0$. Deviations from these values indicate the effects of correlations and interactions.

Low densities

In Figures 2.5 and 2.6 the two quantities p/n and E/N, respectively, are depicted for the two selected temperatures as a function of the total particle number density n in different theoretical approaches. In case of the relativistic Fermi gas (see FG-curve), effects of the Pauli principle are taken into account leading to an increase of the pressure and of the energy per neutron as compared to the ideal Boltzmann gas. The limit $\lim_{n\to 0}(p/n) = T$ is not affected by statistical corrections or relativistic kinematics since the k_2 factors cancel in the lowest order of the fugacity expansion. This is easily seen considering the ratio $p/n = -\Omega/(Vn)$ using Eqs. (2.63)

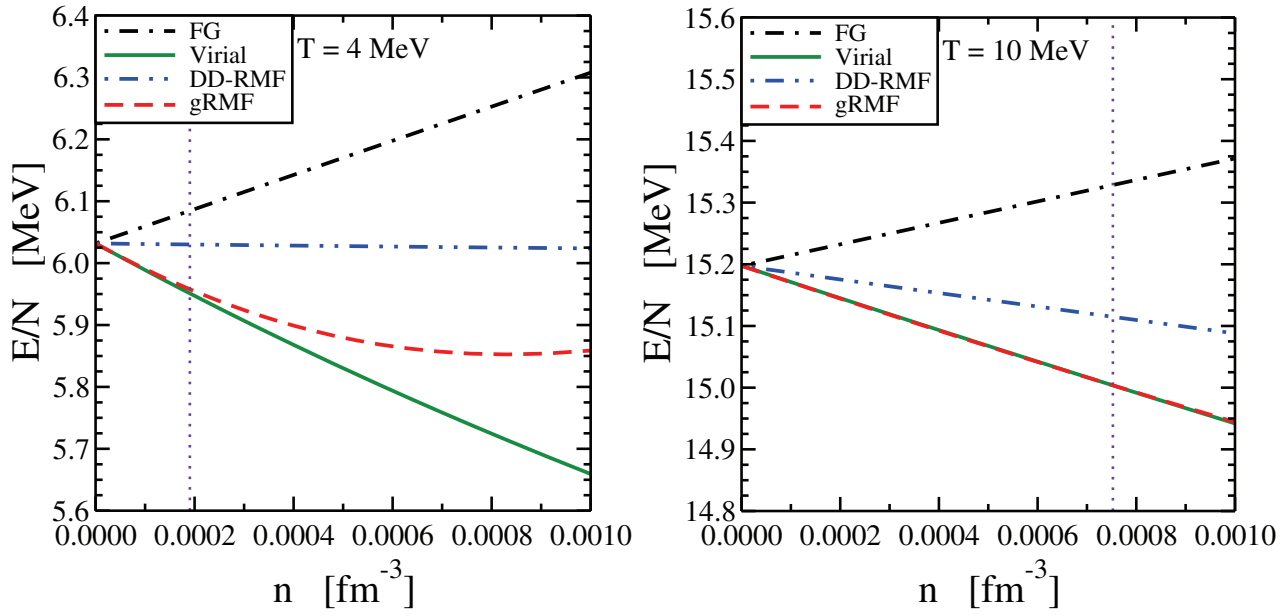

Figure 2.6.: Internal energy per baryon (without contribution of the neutron rest mass) in neutron matter as a function of the total particle number density n for temperatures of $T = 4$ MeV (left) and $T = 10$ MeV (right). Vertical dotted lines indicate the density where $n\lambda_n^3 = 1/10$.

and (2.65). In contrast, the relativistic correction factor k_2 in Eq. (2.65) modifies the relation between the neutron density and neutron chemical potential appearing in Eq. (2.107) and thus $\lim_{n\to 0}(E/N) > 3T/2$ in Fig. 2.6. The relativistic corrections become larger with increasing temperature. The shift of E/N at zero density can be estimated as $2T^2/m_n$.

The VEoS predicts a dependence of p/n and E/N on the density with a negative slope. This is the effect of the correlations induced by the nn interaction. The vertical lines in Figures 2.5 and 2.6 denote the density n where $n\lambda_n^3 = 1/10$. At densities above this value, higher-order contributions to the VEoS, which are not considered in the fugacity expansion up to second order, can be expected to contribute significantly. Fig. 2.6 also demonstrates that the virial corrections at low densities are smaller than the relativistic correction, which leads to an overall shift.

The curves of the DD-RMF model with DD2 parametrization without correlations lie between the VEoS and the FG results. They do not show the correct dependence given by the VEoS at low densities. When the nn correlations are taken into account in the gRMF model with the quadratic form of the energy shift (see next subsection) the low-density behavior of the VEoS is nicely reproduced. Only at higher densities, medium effects, which are not incorporated in the VEoS, lead to a deviation. The precise density dependence of the deviation will depend on the choice of the functional form of the energy shift, but the agreement in the low-density limit is not affected. Obviously, deviations of the gRMF EoS from the VEoS start to become more important with increasing density at lower temperatures.

It is also worthwhile to compare the predictions of the VEoS, the original DD-RMF and gRMF models in the DD2 parametrization with the results of other approaches used in astrophysical applications. We examine two other RMF models that employ nonlinear selfinteractions of the mesons: the model of G. Shen et al. (SHO) [SHO11] with the FSUGold parametrization and

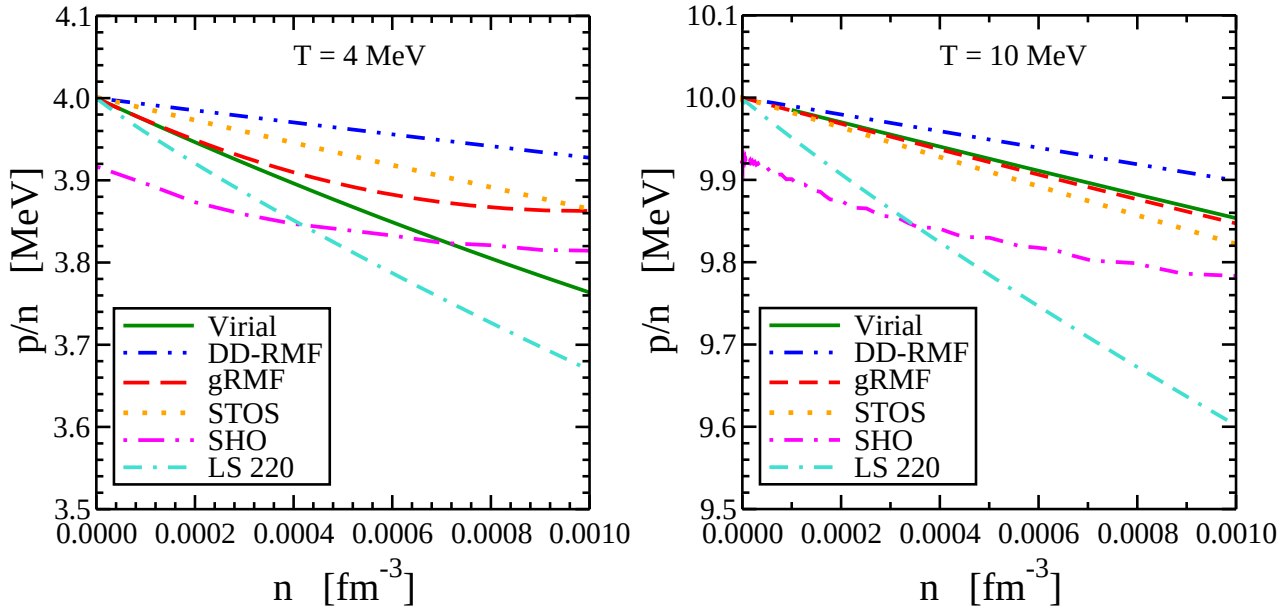

Figure 2.7.: Ratio of pressure over total particle number density, p/n, of neutron matter as a function of the density n for temperatures of $T = 4$ MeV (left) and $T = 10$ MeV (right) in different models. See text for details.

the model of H. Shen et al. (STOS) [STOS11] with the parameter set TM1. In addition, the non-relativistic Lattimer-Swesty EoS [LS91] with incompressibility $K = 220$ MeV (LS 220) is considered.

In Fig. 2.7 the density dependence of the quantity p/n at $T = 4$ MeV and $T = 10$ MeV is depicted for all models below 0.001 fm^{-3}. The curves of the STOS model, which does not include two-body nn correlations, are surprisingly close to the exact VEoS line for $T = 10$ MeV, but do not reproduce it exactly. The deviations are larger at $T = 4$ MeV and the close agreement seems to be accidental for $T = 10$ MeV. The SHO approach with the FSUGold parametrization claims to be constructed such that the case of unitary neutron matter is reproduced at low densities by introducing a particular density dependent coupling of the σ meson, see the discussion at the end of Subsection 2.5.1. A large deviation from the VEoS result can be seen in Fig. 2.7 and the correct low-density limit for p/n is not reproduced. Furthermore, the tabulated data exhibit some oscillations that are probably related to the choice of the interpolation procedure [She11]. The LS EoS shows a much larger negative slope of p/n as a function of n as compared to the other models but reproduces the correct ideal gas limit.

2.6 Symmetric nuclear matter

In case of symmetric matter, all correlations of neutrons and protons in scattering and bound states should be taken into account for the calculation of thermodynamic quantities. At low densities, two-body correlations will be most important, but with increasing density also many-body correlations, in particular the appearance of clusters, i.e. many-body bound states, are relevant. Presently we include contributions from $nn(^1S_0)$, $np(^1S_0)$, $pp(^1S_0)$ and $np(^3S_1)$ scattering channels and clusters with $A \leq 4$ in our calculations. In the gRMF model light clusters (deuteron, triton, helion and α particle) are introduced as additional degrees of freedom with

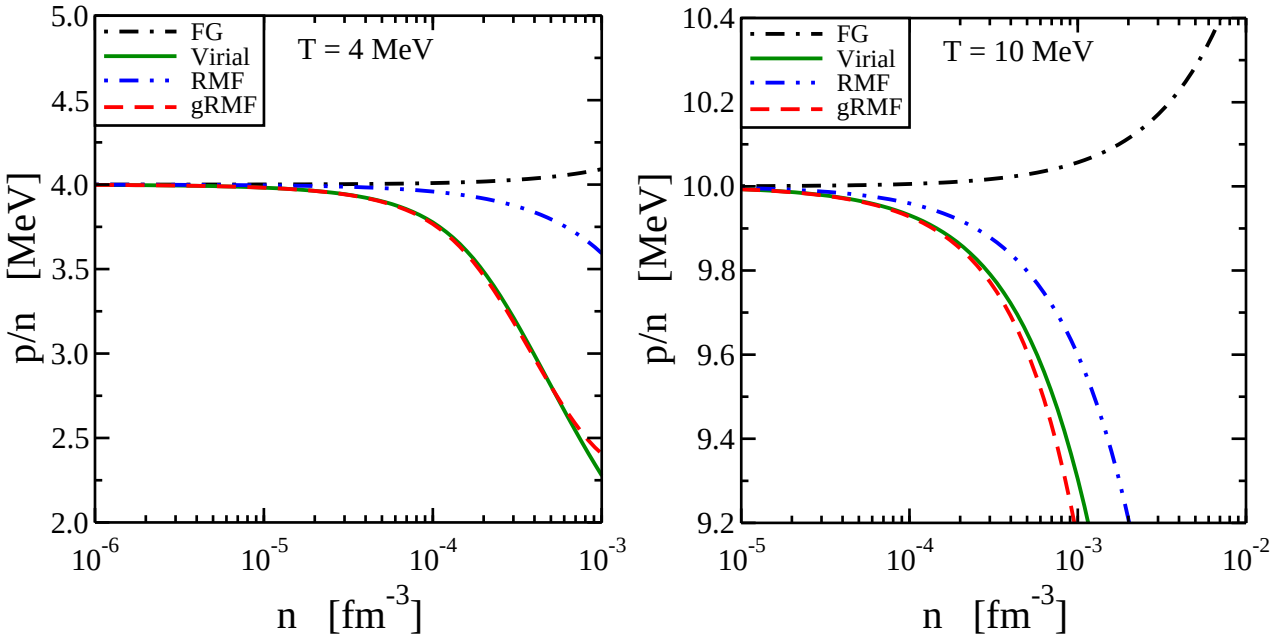

Figure 2.8.: Ratio of pressure over total particle number density, p/n, of symmetric nuclear matter as a function of the total density n for temperatures of $T = 4$ MeV (left) and $T = 10$ MeV (right).

temperature and density dependent binding energy shifts given in Ref. [TRK+10]. Because we do not consider the formation of nuclei with mass numbers $A > 4$ the present model can only be applied to rather low densities where the fraction of heavier clusters can be neglected.

2.6.1 Low densities

We show the quantities p/n and E/N for different approaches, similar as in case of neutron matter, in Figures 2.8 and 2.9 for $T = 4$ MeV and $T = 10$ MeV as a function of the total particle number density n. The extended gRMF model very well reproduces the VEoS at low densities, deviating from it with increasing density and lower temperature due to medium effects. Note that in the depicted results of the VEoS calculation the same nuclei are considered as in the gRMF model. It is also worth noticing that the standard RMF calculation without clusters and the extended gRMF model differ substantially. Again, we see the effect of the relativistic corrections on the internal energy per baryon E/N in comparison with the ideal gas limit. In contrast to the neutron matter case, where scattering correlations are essential for reproducing the VEoS, in symmetric matter the main contribution is caused by the appearance of bound states with positive binding energy.

2.6.2 Composition

By comparing the fractions of various particles we can study the detailed composition of symmetric nuclear matter. In Fig. 2.10 particle fractions $X_i = A_i n_i / n$ of nucleons and light clusters are shown for $T = 4$ MeV and $T = 10$ MeV for the gRMF (dotted lines) and VEoS (solid lines) models. The deuteron fraction X_d contains the contribution of the bound state and the isospin

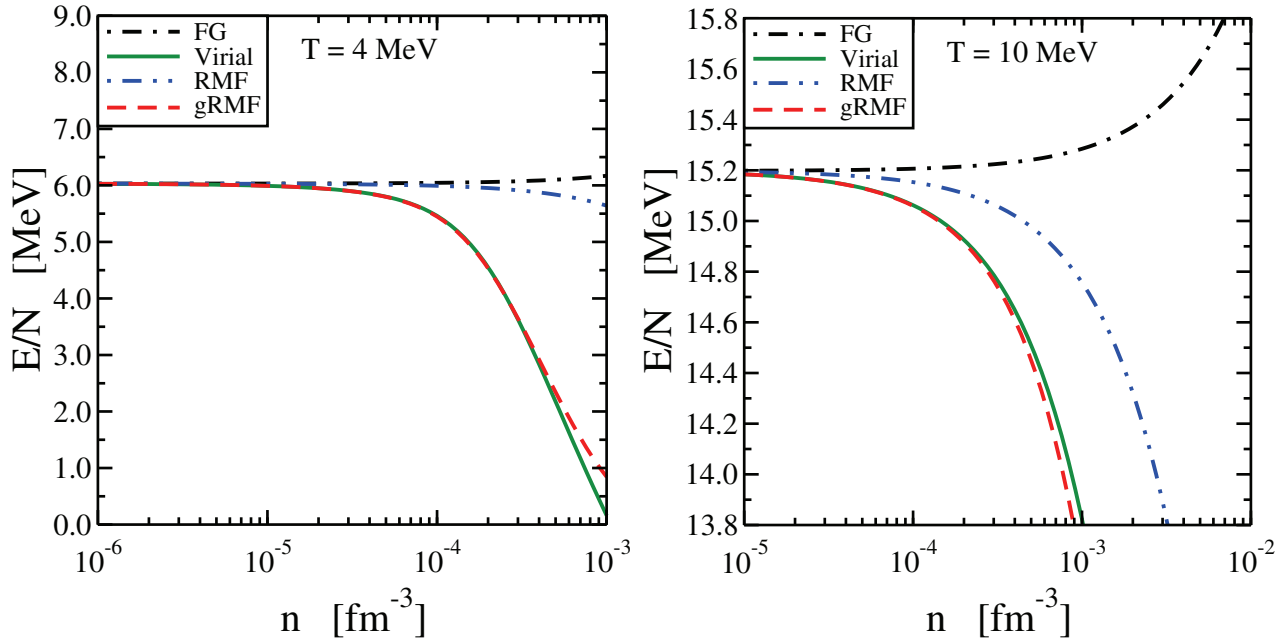

Figure 2.9.: Internal energy per baryon (without contribution of the neutron rest mass) in symmetric nuclear matter as a function of the total particle number density n for temperatures of $T = 4$ MeV (left) and $T = 10$ MeV (right).

singlet np scattering channel. As is seen from the figures, in symmetric matter higher mass clusters become more important with increasing densities. One notes that the particle fraction for deuterons in the VEoS and gRMF models are substantially different, especially in case for $T = 10$ MeV. This behavior is caused by the fact that in the gRMF model part of the two-body correlation strength is shifted to the mean-field, thus reducing the contribution of the original two-body correlations. The same effect will be observed in case of neutron matter for the particular case of nn correlations, see Subsection 2.6.3. We also notice different slopes of the curves for light clusters, with the α particle having the steepest inclination. The reason is that at low total densities cluster densities are proportional to fugacities in a certain power, e.g. $n_d \sim z^2$, $n_t \sim z^3$ and $n_\alpha \sim z^4$ with $z = z_n \approx z_p$ in symmetric nuclear matter. The overall scaling of the cluster fractions at low densities is determined by the cluster binding energies. At densities n above 10^{-4} fm^{-3} and 10^{-3} fm^{-3} for $T = 4$ MeV and $T = 10$ MeV, respectively, heavier nuclei will contribute significantly to the composition in symmetric nuclear matter and they have to be incorporated in the model calculations. Hence, it is not reasonable to discuss the transition to higher densities in the present description of symmetric nuclear matter.

2.6.3 Higher densities

We have shown in Subsection 2.5.2, that the inclusion of effective nn scattering correlations in the gRMF model allowed to reproduce the low-density limit of the VEoS for thermodynamical quantities such as p/n and E/N. With increasing density, the VEoS approach is no longer applicable and a smooth transition of the gRMF predictions to the DD-RMF results with neutrons as quasiparticles is expected. The details of this transition are affected by several ingredients of the gRMF model that are not constrained by the low-density expansion: the strength of the

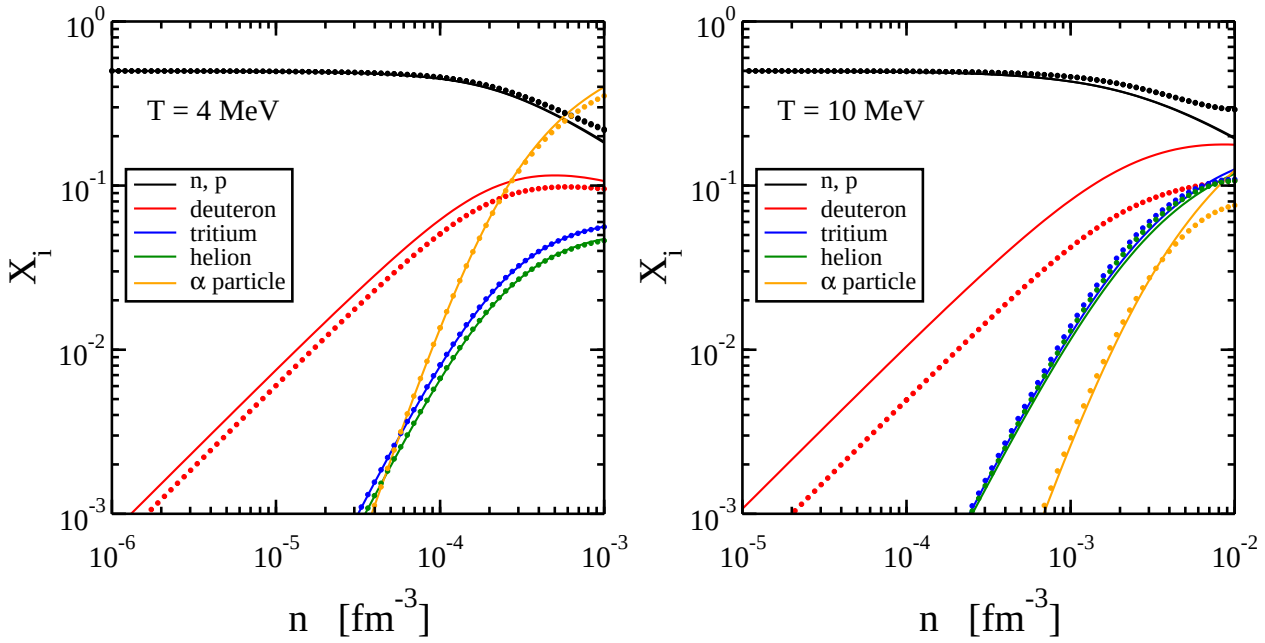

Figure 2.10.: Particle fractions X_i of nucleons and light clusters in symmetric nuclear matter as a function of the density n for temperatures of $T = 4$ MeV (left) and $T = 10$ MeV (right). Solid lines correspond to the VEoS and dotted lines to the gRMF model.

cluster-meson couplings (2.46), the shift ΔB_{nn} of the effective resonance energy E_{nn} and possible contributions from three, four, ...and many-neutron correlations. In the following, only the variation of the transition with different choices of ΔB_{nn} will be discussed. The strength of the cluster-meson couplings is kept as given in the original gRMF model and described in Section 2.3.

When the total density of neutron matter increases, the contribution of the nn cluster in the gRMF model will be affected by the applied shift to the resonance energy that represents the continuum correlations. The functional dependence of the energy shift ΔB_i of a cluster i in (2.45) with temperature T and the meson fields ω and σ is not determined by the low-density considerations. Here, we explore three different choices. Similar as in Ref. [TRK+10], we write

$$\Delta B_i = f\,[n_i^{(\mathrm{eff})}]\,\delta B_i(T), \tag{2.110}$$

with a function f that depends on the effective density

$$n_i^{(\mathrm{eff})} = \frac{m_\omega^2}{\Gamma_\omega(0)}\omega + \frac{N_i - Z_i}{A_i}\frac{m_\rho^2}{\Gamma_\rho(0)}\rho \tag{2.111}$$

and a temperature dependent factor $\delta B_i(T)$. At low effective densities, ΔB_i should be linear in $n_i^{(\mathrm{eff})}$ and an obvious choice is $f = n_i^{(\mathrm{eff})}$. In Ref. [TRK+10] the quadratic form

$$f = n_i^{(\mathrm{eff})}\left[1 + \frac{1}{2}\frac{n_i^{(\mathrm{eff})}}{n_i^{(0)}}\right] \tag{2.112}$$

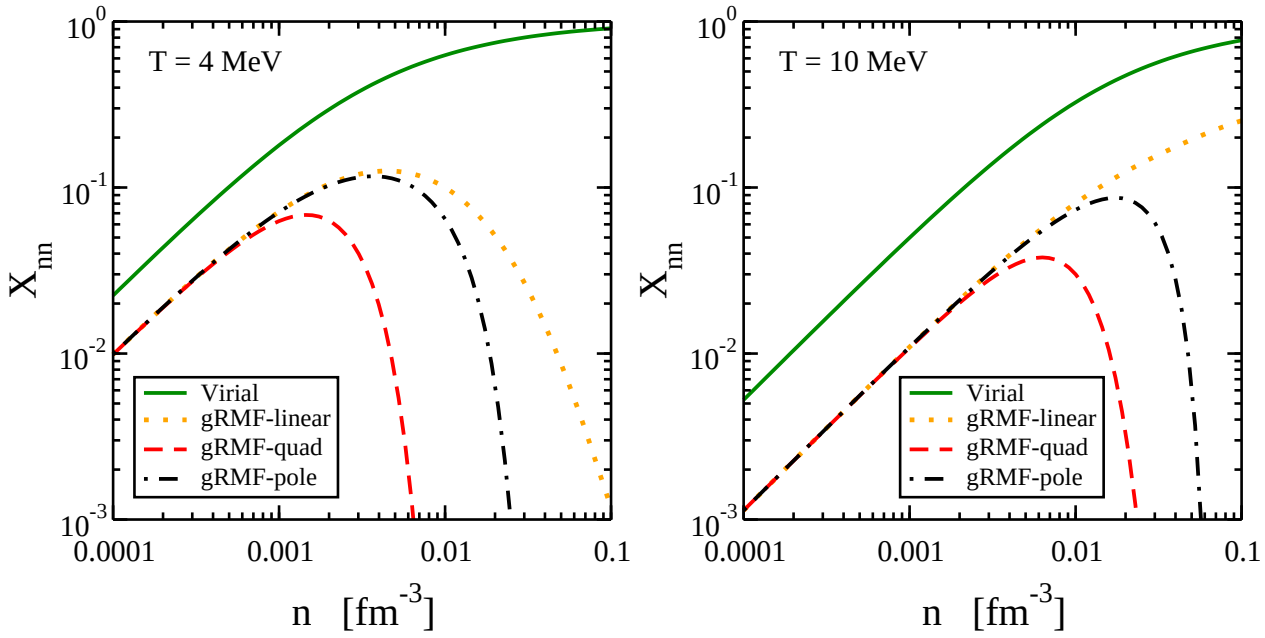

Figure 2.11.: Mass fraction X_{nn} of the two-neutron correlation state in neutron matter as a function of the density n for temperatures of $T = 4$ MeV (left) and $T = 10$ MeV (right).

was used for the light clusters in order to obtain a stronger suppression of the cluster abundancies with increasing density. The density scale $n_i^{(0)} = B_i^{(\mathrm{vac})}/\delta B_i(T)$ is set by the vacuum binding energy $B_i^{(\mathrm{vac})}$. Another possible choice is the pole form

$$f = \frac{n_i^{(\mathrm{eff})} n_{\mathrm{sat}}}{n_{\mathrm{sat}} - n_i^{(\mathrm{eff})}} \tag{2.113}$$

for $n_i^{(\mathrm{eff})}$ smaller than the saturation density n_{sat} of the gRMF model resulting in a complete dissolution of the cluster when n_{sat} is approached from below because $\lim_{n_i^{(eff)} \to n_{\mathrm{sat}}} f = \infty$.

The evolution of the two-neutron mass fraction

$$X_{nn} = 2n_{nn}/(n_n + 2n_{nn}) \tag{2.114}$$

with increasing total density is depicted in Fig. 2.11 for the VEoS and the gRMF model with the linear, quadratic and pole form of the energy shift ΔB_{nn}, respectively. We assume $\delta B_{nn}(T) = \delta B_d(T)$ and set the density scale $n_{nn}^{(0)} = n_d^{(0)} = B_d^{(\mathrm{vac})}/\delta B_d(T)$ with the deuteron values for the quadratic dependence. The *nn* fraction in the VEoS model rises monotonously with the total density reaching unrealistically high values much beyond the range of applicability of the approach. At low densities, the *nn* fractions for the different choices of the energy shift in the gRMF model agree perfectly with each other. They exhibit the same slope as the VEoS result. In general, the *nn* mass fraction at low densities is larger for the lower temperature but the two-neutron cluster dissolves earlier with increasing total density. The maximum mass fraction and range of cluster dissolution depends sensitively on the form of the energy shift ΔB_{nn}. There are substantial variations that need to be constrained in future investigations. On an absolute

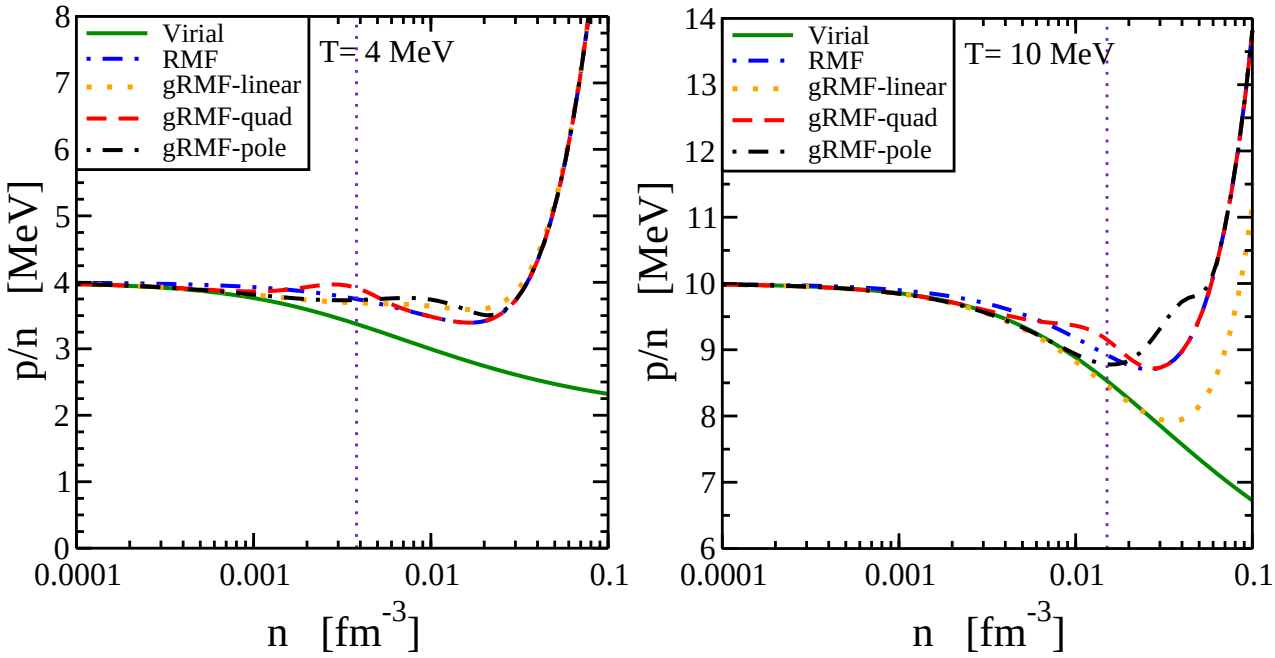

Figure 2.12.: Ratio of pressure over total particle number density, p/n, of neutron matter as a function of the density n for temperatures of $T = 4$ MeV (left) and $T = 10$ MeV (right). Vertical dotted lines indicate the density where $n\lambda_n^3 = 1$.

scale, the gRMF predictions for X_{nn} are substantially smaller than those of the VEoS at low densities. This difference is caused by the fact that in the gRMF approach the correlations of quasiparticles are considered and part of the correlation strength is contained in the self-energies, cf. the generalized Beth-Uhlenbeck approach in Subsection 2.2.4. The distribution of correlations between the explicit contribution from the cluster state and the implicit contribution via the self-energies depends on the nucleon-meson couplings at zero density of the particular gRMF parametrization.

The dependence of the quantities p/n and E/N in neutron matter on the total density is shown in Figures 2.12 and 2.13 for temperatures $T = 4$ MeV and $T = 10$ MeV and a wider range of densities compared to that shown in Figures 2.5 and 2.6. The vertical lines in Figures 2.12 and 2.13 denote the density n where $n\lambda_n^3 = 1$. In the low-density limit, all gRMF calculations reproduce the VEoS predictions by construction but deviate from the DD-RMF model that does not take cluster formation into account. At higher densities, the VEoS fails to predict the strong increase of the pressure and energy per neutron caused by the short-range repulsive nn interaction. The transition of the gRMF results at low densities to the DD-RMF curve at higher densities substantially depends on the choice of the energy shift ΔB_{nn} for the effective resonance energy E_{nn}. A distinctive bump in p/n and E/N appears, which is correlated with the sudden dissolution of the two-body clusters as depicted in Fig. 2.11. This feature was already observed in Ref. [TRK+10] for symmetric nuclear matter including only the bound states of light clusters. The origin of this structure is related to the contribution with the derivatives of the energy shifts in the ω and ρ-meson field equations (2.56) and (2.57). The functional form of the density dependence and absolute scale of the meson-cluster coupling strengths Γ_{im} from (2.46) and (2.47) will also have an impact on the detailed form of the transition from the low-density limit to higher-densities. In this work, only the most simple choice of the factor g_{im},

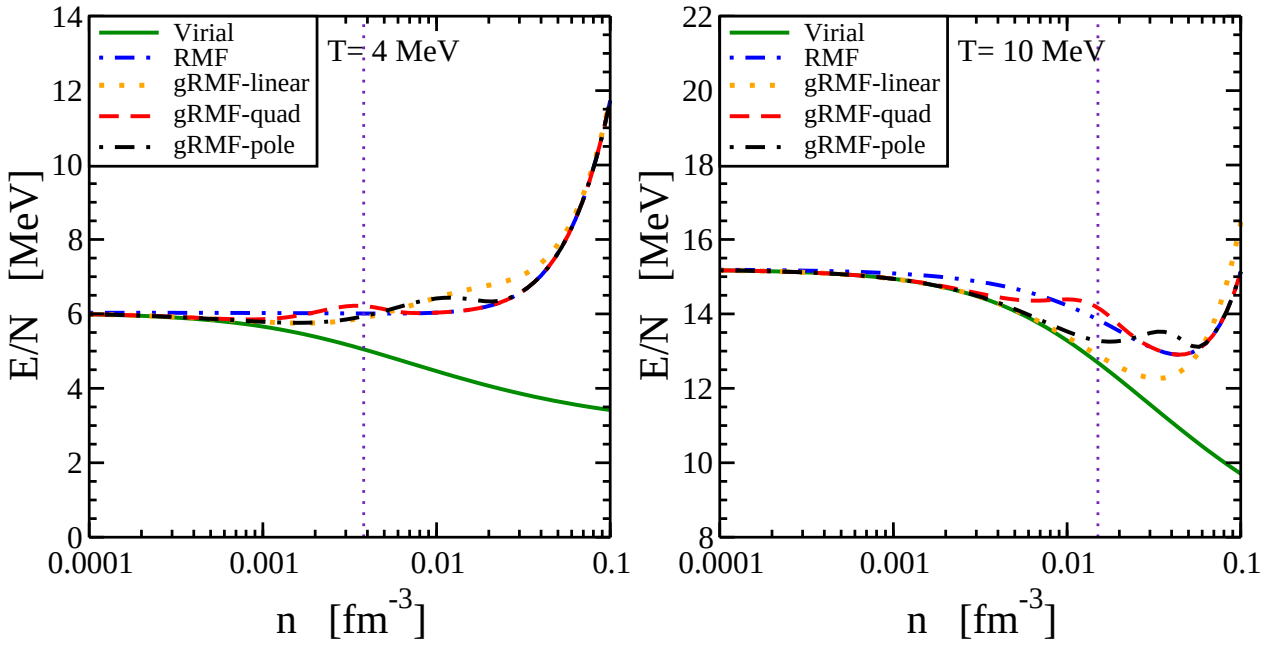

Figure 2.13.: Internal energy per baryon (without contribution of the nucleon rest masses) in neutron matter as a function of the total particle number density n for temperatures $T = 4$ MeV (left) and $T = 10$ MeV (right). Vertical dotted lines indicate the density where $n\lambda_n^3 = 1$.

proportional to the number of nucleons in the cluster, was examined. Further investigations are needed to fix the cluster-meson couplings and the energy shifts less ambiguously. Correlations beyond two-neutron states, that are not considered for neutron matter in the present approach, could also modify the features in the quantities p/n and E/N.

2.7 Conclusions

In this chapter we have described an extension of the generalized relativistic mean-field model with density dependent couplings that would include two-body scattering correlations. The consistency of the finite-temperature equation of state at low densities with the virial equation of state was required. New degrees of freedom were introduced in the generalized RMF approach that represent two-nucleon correlations in the continuum. These clusters are characterized by medium dependent effective resonance energies. From the comparison of the fugacity expansions of both the relativistic mean-field and virial equation of state models, consistency relations were derived that contain the nucleon-nucleon scattering phase shifts, the relativistic mean-field nucleon-meson coupling constants, the resonance energies and effective degeneracy factors of the clusters. Various choices of the relevant parameter functions were investigated. The successful application of the approach required the introduction of the temperature dependent degeneracy factors. Resonance energies were assumed to be equal to those in the VEoS. First results for pure neutron matter were shown, where the effect of scattering correlations can be easily observed. A comparison with well-known models used in astrophysical applications was demonstrated, which shows the failure of these models to describe the virial limit. For the symmetric matter case, where also bound states appear, the effect of two-body scattering

correlations is less pronounced. We observe a smooth interpolation of the extended generalized relativistic mean-field model between the correct low and high density limits describing the dissolution of the clusters. However, the precise form of the transition depends on the coupling strength of the clusters to the meson fields and the energy shift of the resonance energies. These quantities are not fixed by the low-density constraints and the consequences of different choices were investigated. This point deserves more studies in the future. In the case of symmetric nuclear matter the formation of many-body bound states is crucial for a realistic description of correlations. The proposed model can be extended by including heavier clusters. For astrophysical applications, further contributions to the EoS than those considered in this work have to be included in the model. E.g. electrons, muons, photons, mesons etc. need to be considered which also change the behavior of various thermodynamical quantities in the low-density limit. The proposed extension of the generalized relativistic mean field model is rather general and can also be applied to other mean-field approaches

3 Pairing correlations

3.1 Motivation

In this chapter we continue to study the effect of two-body correlations on the thermodynamic properties of low-density nuclear matter. The particular case of pairing in pure neutron matter is considered for various temperatures up to the critical temperature T_c, where the gap vanishes and the system returns to the unpaired phase. We have performed the calculation of the gap and thermodynamic properties by using the extended gRMF model with density dependent couplings. In our investigation we use the separable Yamaguchi potential, with parameters fitted to the ${}^1S_0$ scattering length and effective range. We compare the standard relativistic Fermi gas with pairing and the RMF model. We consider the case of zero and finite temperatures separately. For zero temperature, the results of the pairing gap are compared with calculations performed with realistic microscopic potentials. We also compare our RMF results with other methods from many-body calculations. The EoS of low-density matter is compared with other neutron matter equation of states. The effect of pairing correlations on thermodynamic quantities is studied for different temperatures and the results are compared with other well-known EoS models for astrophysical applications as done in Section 2.5.

3.1.1 History

The phenomenon of superfluidity in neutron matter has proven to be an interesting and important subject in many-body nuclear physics and astrophysics. It has been supported by many experimental facts like the binding energy difference between even-even and odd-even nuclei and the origin of pulsar glitches. Superfluidity in neutron matter is often connected to cooling observations of neutron stars.

A general understanding of the electron superconductivity (superfluidity of charged particles) was achieved by J. Bardeen, L.N. Cooper and J.R. Schrieffer in [BCS57]. This effect is explained by the formation of Cooper pairs under a weak attraction of electrons generated by the electron-phonon interaction. It leads to the appearance of an energy gap Δ in the electron energy spectrum near the Fermi level. This theory was later successfully applied to nuclei by Bohr, Mottelson and Pines [BMP58] and Belyaev [Bel59]. Other methods, explaining this interesting phenomenon have also been developed which include the Green's function formalism [Gor58] developed by Gorkov for superconducting fermion systems with an electron-phonon interaction. Nambu introduced a matrix formalism to the theory of superconducting metals [Nam60] (Green's functions formulated in the Nambu-Gorkov space). Eliashberg extended the Migdal theory of the strong electron-phonon interaction in normal metals [Mig60] to include Cooper pairs in [Eli60] .

In 1960 Migdal suggested a possibility of the existence of superfluid neutrons and superconducting protons in neutron stars [Mig60]. This theory was then generalized by Larkin and Migdal for the description of fermion superfluids at zero temperature [LM63]. Superfluidity

was further studied by Ginzburg and Kirzhnits in 1964 [GK64, GK65]. They have estimated the size of the singlet-state pairing gap. In 1966 Wolf has shown that the singlet-state neutron pairing occurs at densities associated with the inner neutron star crust. He predicted that the pairing effect would disappear in the core where the $^1S_0$ nn interaction becomes repulsive. The possibility of the triplet-state nn pairing in the core of the neutron star was understood later in the works of Hoffberg et al. [HGRR70]. In the following decades this theory was supported by observations of glitches in the timing data of Vela pulsar [RM69, RD69] in 1969. Pulsar glitches are believed to be related to the dynamics of the neutron superfluid in the inner layers of the solid neutron star crust [AI75, CC06, GA09]. Theoretical calculations of cooling rates also seem to favor the presence of superfluidity [Tsu98, HHJ00, YKGH01, YP04]. A detailed description of the neutron star cooling was given in Subsection 1.4.2. All these observational data suggest the importance of pairing correlations in the study of the neutron stars and nuclear matter.

3.1.2 Superfluidity in nuclear matter

In neutron star matter an attractive component of nn interaction favors the formation of Cooper pairs, leading to the appearance of the superfluid state. The theory predicts superfluidity of neutrons in the inner crust of a neutron star and of nucleons in atomic nuclei. Kucharek and Ring have performed the first relativistic study of superfluidity in infinite nuclear matter [KR91]. The relativistic Hartree-Bogoliubov (RHB) method with a one-boson-exchange (OBE) potential was used in the application to symmetric nuclear matter. In order to have a correct description of the pairing gap, potentials fitted to NN scattering data have been applied.

Two different kinds of superfluid are predicted to exist in neutron star interiors [LS01, DHJ03, BST05, SC06]. At densities below nuclear saturation density the S-wave pairing occurs due to the long-range attraction of the $^1S_0$ nn potential. This channel is characterized by a large and negative scattering length $a_s^{nn} \approx -18.5$ fm. With increasing density the short range repulsion becomes more effective leading to the reduction of the pairing gap. It vanishes near the boundary between the neutron star core and crust. At higher densities $n \geq n_{sat}$ neutrons may also pair in the $^3P_2 - {}^3F_2$ partial waves. The $^3P_2 - {}^3F_2$ neutron pairing is affected by non central, tensor and spin-orbit components of the interaction.

Many modern many-body theories based on NN potentials are expected to provide a realistic description of the superfluid phase. These models include the method of correlated basis functions (CBF) [Fee69], the Bethe-Brueckner-Goldstone expansion (BBG) [Bal99], the self-consistent Green's functions theory (SCGF) [VDPR93], and lately quantum Monte Carlo Calculations (QMC) [WPCP00]. The neutron matter EoS [FP81, APR98, CMPR03, SP05, MvDF07, BM08, EKLM09, EHM09, HS10, RPV09, MD05, FFIS05, CLS06, MSH08, GIF$^+$08, AS09b, GIP$^+$09] has been the subject of many studies over the years. The obtained results differ in the size of the pairing gap depending on the model for the nucleon-nucleon interaction and the calculation scheme. In our work pairing correlations will be studied in the RMF theory, in particular with respect to thermodynamic properties for the neutron matter EoS at low densities. Equations of state of neutron matter for the particular case of the low-density regime, have been developed in the past [GIF$^+$08, FP81, APR98, CMPR03, SP05, BEK$^+$08, Lee09, EKLM09, GC08, AS09b, AS09a]. Most of the models give essentially similar results for thermodynamical quantities and nuclear properties at saturation density as described in Chapter 1. However there are significant differences in the $^1S_0$ pairing gaps depending on the method used. We concentrate on the RMF model with density dependent couplings and extend it by including S-wave neutron-neutron pairing

correlations. Our approach with the simple separable interaction shows the main features of pairing in low-density neutron matter. It allows to estimate the size of the effects on the equation of state. So far global equations of state tables for astrophysical applications do not include neutron pairing effects.

3.2 Pairing correlations with a separable interaction

There are different ways how one can treat pairing and derive the corresponding equations. Examples are the BCS theory or the Green's function method to derive the Hartree-Fock-Bogoliubov (HFB) equations. In this chapter we concentrate on the thermodynamic aspects of pairing. We show only main results avoiding complicated derivations of the formulas. We introduce the separable Yamaguchi interaction and derive the gap equation.

3.2.1 The separable Yamaguchi nucleon-nucleon interaction

In general one can use realistic potentials fitted to the NN scattering phase shifts up to 250 MeV, like Nijmegen or Paris [SKRdS93]. We will, however, perform our calculations with the separable Yamaguchi potential, that is fitted to the scattering parameters, e.g scattering length and effective range. With the following potential in momentum space representation depending on the relative momentum of the incoming k and outgoing k' particle respectively

$$v_{k,k'} =< k|v|k' >= -\frac{\lambda}{V}\omega(k)\omega(k') \tag{3.1}$$

one solves the two-particle Schrödinger equation,where λ defines the strength of the interaction and V is the volume. The form-factor

$$\omega(k) = \frac{1}{\frac{k^2}{\gamma^2}+1}. \tag{3.2}$$

depends on the parameter γ. An example of such a potential is the Yamaguchi interaction [Yam54]. In the following we will consider only the $l = 0$ channel with particles of equal mass $m_1 = m_2 = m_n$. We solve the two-particle Schrödinger equation with such an interaction. The phase shifts $\delta(E)$ can be calculated analytically using the effective range expansion

$$k\cot\delta = -\frac{1}{a} + \frac{r_0 k^2}{2} - \dots. \tag{3.3}$$

One obtains relations between the parameters γ and λ of the potential and the scattering parameters

$$a = \left(1 - \frac{8\pi}{\lambda\mu\gamma}\right)^{-1}\frac{2}{\gamma}, \tag{3.4}$$

$$r_0 = \left(1 + 2\frac{8\pi}{\lambda\mu\gamma}\right)\frac{1}{\gamma}, \tag{3.5}$$

where $\mu = \frac{m_1 m_2}{m_1+m_2} = \frac{m}{2}$ is the effective mass, a is the ${}^1S_0$ scattering length and r_0 is the corresponding effective range. The detailed derivation of these relations is given in Appendix C. Having defined the parameters of the potential we can now calculate the pairing gap and thermodynamic quantities. We will show that using this potential one obtains values of the gap function, which can be compared with the predictions of other models.

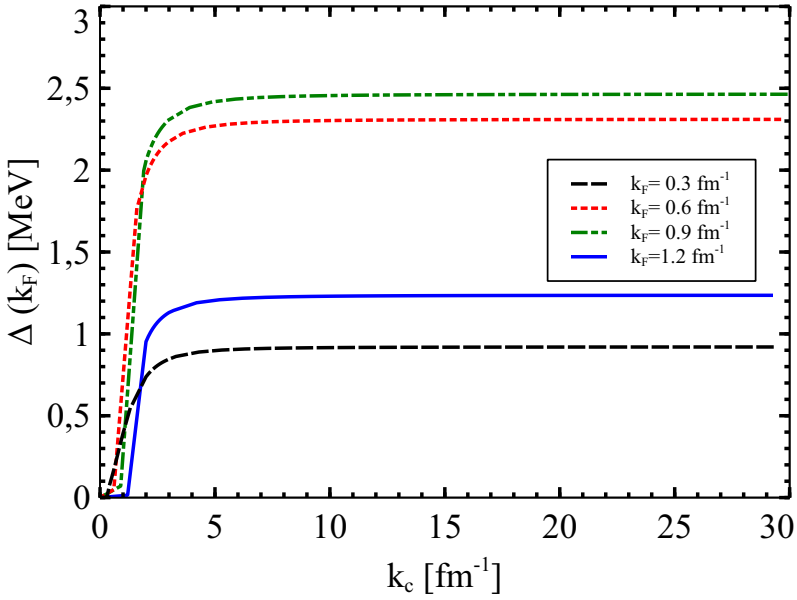

Figure 3.1.: Pairing gap $\Delta(k_F)$ at the Fermi surface as a function of the cutoff momentum k_c for different values of Fermi momentum

3.3 Zero temperature case

We will start with the zero temperature case. We will derive the pairing gap equation and the corresponding the equation of state. The results of the pairing gap will be compared with other calculations.

3.3.1 Relativistic Fermi gas with pairing

We use the relativistic Fermi gas with pairing as a reference for comparison with the RMF calculation. In this case we don't have the contribution of a mean-field part. In the following we will denote Fermi gas quantities with the prime. The single-particle energy and quasiparticle energy assume the form

$$e'_k = \sqrt{k^2 + m_n^2} \qquad E'_k = \sqrt{(e'_k - \mu')^2 + \Delta_k^2}. \tag{3.6}$$

The pressure is given by

$$p(k_F) = \frac{1}{3\pi^2}\int_0^{k_F} \frac{k^4}{e'_k}\frac{e'_k - \mu'}{\sqrt{(e'_k - \mu')^2 + \Delta_k^2}}dk + \frac{1}{4\pi^2}\int_0^{k_F} k^2 \frac{\Delta_k^2}{2E'_k}dk, \tag{3.7}$$

where the fermi momentum $k_F = (3\pi^2 n)^{1/3}$ is a function of the density n and the chemical potential μ' is defined as

$$\mu' = \sqrt{k_F^2 + m_n^2}. \tag{3.8}$$

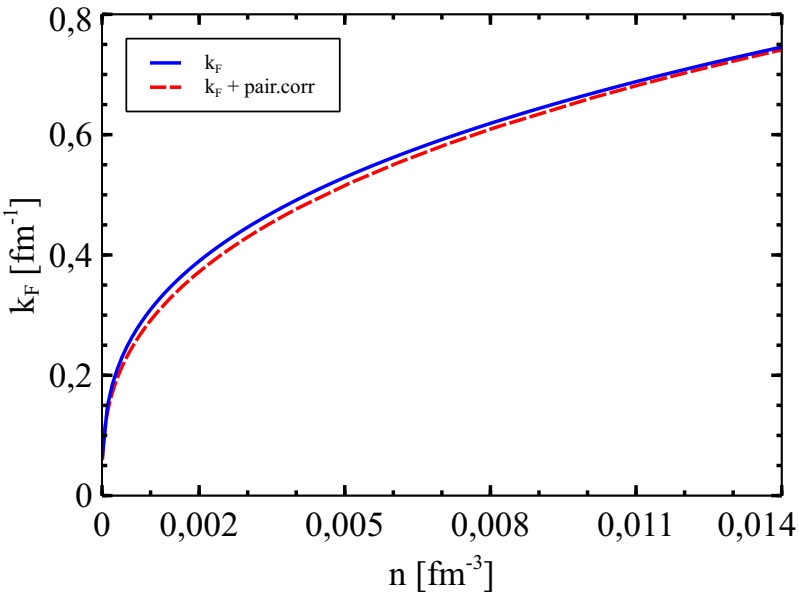

Figure 3.2.: Comparison of the Fermi momentum of neutron matter as a function of density n for the case without pairing and with pairing correlations at $T = 0$ as a function of the density n.

3.3.2 RMF model with pairing

With the given pairing Hamiltonian $\hat{H}$ and particle number operator $\hat{N}$ we have for T=0

$$\langle \hat{H} - \mu \hat{N} \rangle = 2V \sum_k (e_k - \mu) n_k + V^2 \sum_{k,k'} \nu_k \upsilon_{k,k'} \nu_{k'}, \tag{3.9}$$

where $\upsilon_{k,k'}$ is the matrix element of the pairing interaction 3.1. The chemical potential

$$\mu = e(k_F) = \sqrt{k_F^2 + M^2} \tag{3.10}$$

appears in eq.(3.9) with $\hat{N}$ in order to fix the particle number, M is the effective mass given by eq.(1.8). The quantity

$$n_k = \frac{1}{2}\left(1 - \frac{e_k - \mu}{E_k}\right) \tag{3.11}$$

is the occupation number distribution. The pairing occupation number distribution

$$\nu_k = \frac{\Delta_k}{2E_k} \tag{3.12}$$

depends on the pairing gap Δ_k. Single particle energy $e(k)$ and quasiparticle energy $E(k)$ have the form

$$e_k = V + \sqrt{k^2 + M^2} \qquad E_k = \sqrt{(e_k - \mu)^2 + \Delta_k^2}. \tag{3.13}$$

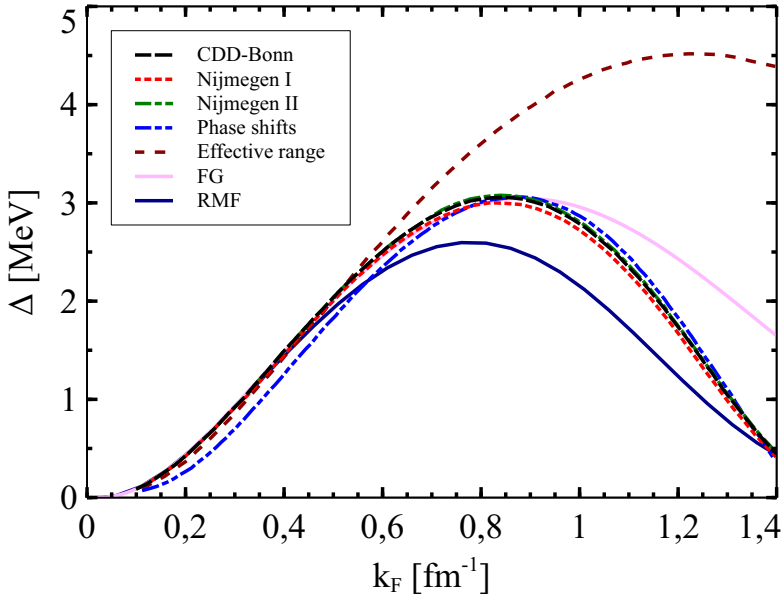

Figure 3.3.: $^1S_0$ pairing gap of neutron matter as a function of the Fermi momentum k_F calculated with different potentials. All the results are compared with the relativistic Fermi gas and RMF calculations.

Thus the relation (3.9) transforms to

$$\langle H-\mu N\rangle = V\sum_k \left[(e_k-\mu)\left(1-\frac{e_k-\mu}{E_k}\right)+V\sum_k \frac{\Delta_k}{2E_k}v_{k,k'}\frac{\Delta_{k'}}{2E_{k'}}\right]. \tag{3.14}$$

Then we find

$$\frac{d}{d\Delta_p}\langle H-\mu N\rangle = \frac{(e_p-\mu)^2}{E_p^3}\left(\Delta_p+V\sum_{k'}\frac{\Delta_k}{2\,E_k}v_{kp}\right)=0.$$

From this relation we obtain the gap equation

$$\Delta_k = -V\sum_{k'} v_{kk'}\frac{\Delta_{k'}}{2E_{k'}}. \tag{3.15}$$

Transforming the sum to the integral $\sum_k \to \int \frac{d^3k}{(2\pi)^3}$ one obtains the relation for the gap function at zero temperature

$$\Delta_k = -\frac{V}{2}\int \frac{d^3k'}{(2\pi)^3}v_{kk'}\frac{\Delta_{k'}}{\sqrt{(e_{k'}-\mu)^2+\Delta_{k'}^2}}. \tag{3.16}$$

Due to the separable form of the potential one can make a substitution $\Delta(k)=\Delta_F\frac{\omega(k)}{\omega(k_F)}$, where Δ_F is the energy gap at the Fermi surface. Inserting this form in relation 3.16 one gets

$$1=\frac{1}{2}\int \frac{d^3k'}{(2\pi)^3}\frac{\lambda\omega(k')^2}{\sqrt{(e_{k'}-\mu)^2+(\Delta_F\frac{\omega(k')}{\omega(k_F)})^2}}. \tag{3.17}$$

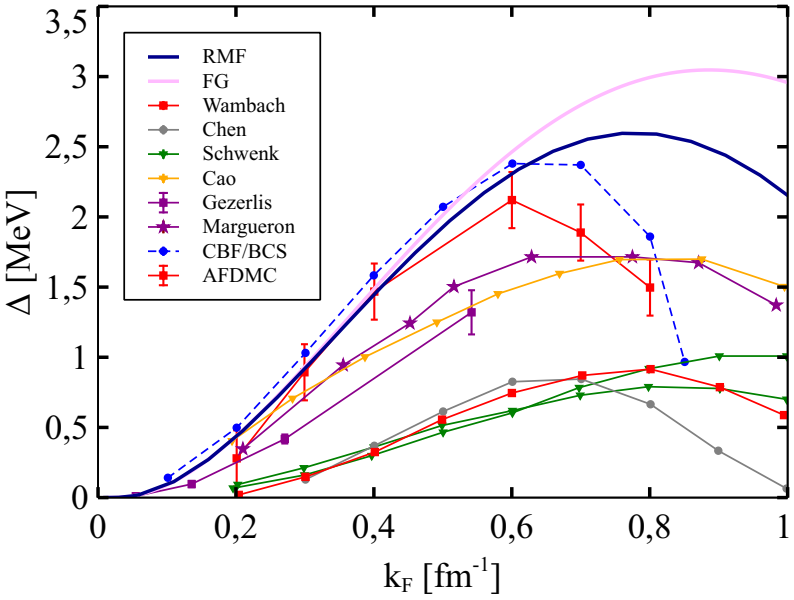

Figure 3.4.: The comparison of the ${}^1S_0$ pairing gap of neutron matter as a function of the Fermi momentum k_F for different methods. All the results are compared with the Fermi gas and RMF calculations. The curves are taken from [GIP+09].

The momentum integration in the gap equation goes to infinity, however for the simplification of the calculation we introduce a cutoff momentum k_c. The dependence of the pairing gap on the cutoff for different Fermi momenta is shown in Fig. 3.1. We can see the numerical convergence for the cutoff moment above $k_c > 20$ fm^{-1} , therefore in the following we will use $k_c = 20$ fm^{-1} in our calculations. With the corresponding occupation numbers given by (3.11) one can rederive the equations of motion and define the scalar and vector densities respectively:

$$\begin{aligned} n_s &= \frac{2}{\pi^2}\int_0^\infty n_k \frac{M}{\sqrt{k^2+M^2}} k^2 dk, \\ n &= \frac{2}{\pi^2}\int_0^\infty n_k k^2 dk. \end{aligned} \tag{3.18}$$

We can already see the effect of the pairing correlations on the Fermi momentum k_F in Fig. 3.2. In case of the Fermi gas without pairing the Fermi momentum is given by $k_F = (3\pi^2 n)^{1/3}$. With pairing correlations we see the reduction of the Fermi momentum at constant density.

Then for the pressure $p = -\Omega/V$ one has

$$p = -\sum_k (e_k - \mu)\left(1 - \frac{e_k - \mu}{E_k}\right) - \sum_k \frac{\Delta_k^2}{2E_k}. \tag{3.19}$$

3.3.3 Comparison of various models

In Fig. 3.3 we show the comparison of the pairing gap between RMF and FG models, calculated using the Yamaguchi separable potential and other potentials calculated in the BCS approximation [EHJ97]. These include the CD-Bonn potential, Nijmegen I and Nijmegen II calculations all

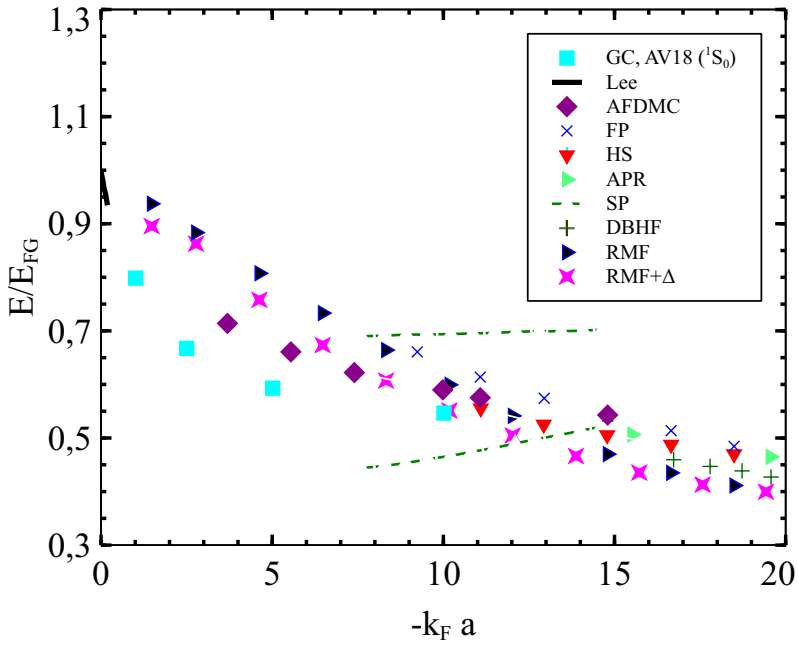

Figure 3.5.: The equation of state of neutron matter as a function of Fermi momentum k_F multiplied with the scattering length a calculated for various models. All the results are compared with the Fermi gas and RMF calculations. The curves are taken from [GC10].

fitted to NN scattering data. The figures show the insensitivity to the choice of NN interaction, resulting in the approximately the same maximum value of 3 MeV of the pairing gap at ≈ 0.85 fm^{-1}. We can also see the agreement between the calculation with the effective range approximation [EHJ97] and the realistic potentials up to momentum of 0.6 fm^{-1}. The calculation with the exact phase shifts [EHJ97] for all momenta follows the results of the realistic potentials for all Fermi momenta. The parameters of the Yamaguchi interaction were fitted to the following values of $a_0 = -18.8$ fm and $r_0 = 2.75$ fm of the singlet neutron-neutron scattering length and effective range, respectively. The results for the pairing gap are in close agreement with other potentials results up to 1 fm^{-1} for relativistic Fermi gas and up to 0.6 fm^{-1} for RMF calculations. The RMF calculation shows the reduction of the gap due to the mean-field potentials.

The comparison with other methods is shown in Fig. 3.4. The RMF and FG results approach maximum gap values of $\approx$ 2.5 and 3 MeV. Other models that include the polarization effect given by the medium demonstrate a stronger reduction as compared to our results. These models originate either from the many-body calculation using effective interactions based on Brueckner theory, Hartree-Fock calculations, or the microscopic calculations (Monte Carlo methods or correlated basis function theory). On the plot we show the results of the many-body effective-interaction calculations of Wambach et al. [WAP93], Chen et al. [CCDK93], Schulze et al. [SCL$^+$96] and Schwenk et al. [SFB03]. These calculations result in a maximum value for the pairing gap of $\approx$ 1 MeV. Microscopic calculations of Gezerlis and Carlson [GC08] using the quantum Monte Carlo technique neglect several contributions from some channels of the interaction and thus are limited to the lower density range.

Other microscopic calculations based on the correlated basis function and the auxiliary field diffusion Monte Carlo method (which is an extension of the diffusion Monte Carlo method

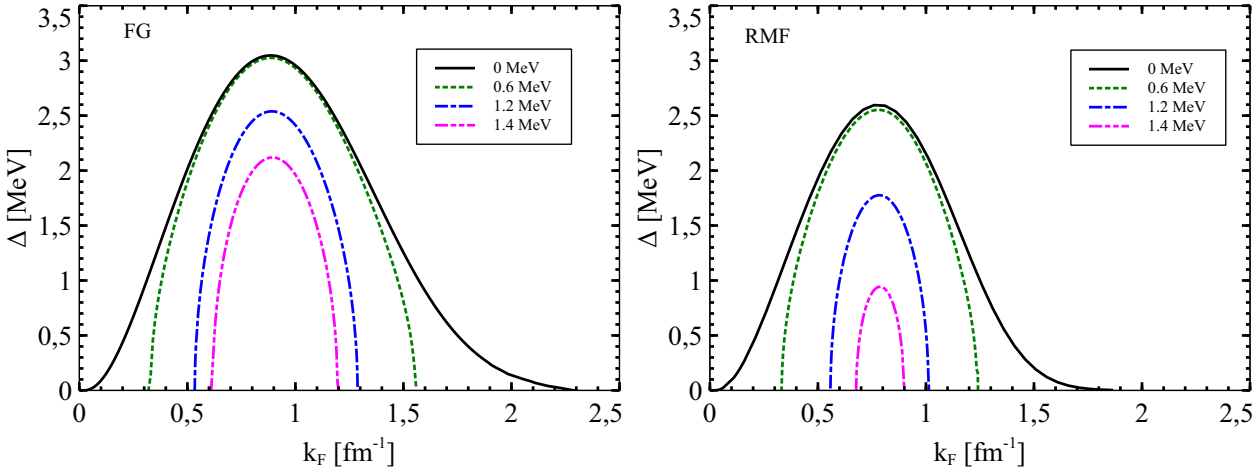

Figure 3.6.: Pairing gaps at the Fermi surface in neutron matter in FG and RMF models versus Fermi moment k_F.

[And75] and Green's function Monte Carlo method [Car87]) give a maximum value of 2.4 MeV. Other many-body techniques using Bruckner Hartree-Fock and new effective interactions by Cao et al. [CLS06] and Margueron et al. [MSH08] predict a superfluid gap closer to the AFDMC result. One can also see that all of the models predict different densities where the gap reaches its maximum value.

With the corresponding pairing gap, we can now calculate thermodynamic quantities and compare them with other models. In Fig. 3.5, taken from [GC10], the equation of state of low-density neutron matter is shown. The energy has been divided by the energy of the noninteracting Fermi gas $E_{FG} = \frac{3}{5}\frac{k_F^2}{2m_n}$. Our results are compared with the variational hypernetted-chain calculations by Friedman and Pandharipande (FP) [FP81] and the well-known calculation by Akmal, Pandharipande, and Ravenhall (APR) [APR98]. We also include the Dirac-Brueckner-Hartree-Fock (DBHF) calculation [MvDF07] and the latest auxiliary field diffusion Monte Carlo (AFDMC) result, the diffusion Monte Carlo results of Gezerlis and Carlson with only the 1S0 channel interaction of the Argonne AV18 potential (GC, AV18 $^1S_0$) [GC08], a difermion EFT result (shown as the error bands) (SP) [SP05] and an approach based on chiral N2LO effective interactions with three-nucleon forces (HS) [HS10]. The results are also compared with the analytic calculation by Lee and Yang, described in Chapter 1. All the results seem to agree at intermediate and higher momenta, where they show the same trend. There are larger deviations at lower momenta.

3.4 Finite temperatures

We will start with the derivation of the gap equation for finite temperatures similarly as for zero temperature case. The occupation numbers

$$n_k = \frac{1}{2}\left(1 - \frac{e_k - \mu}{E_k}\left[1 - 2f(E_k)\right]\right) \tag{3.20}$$

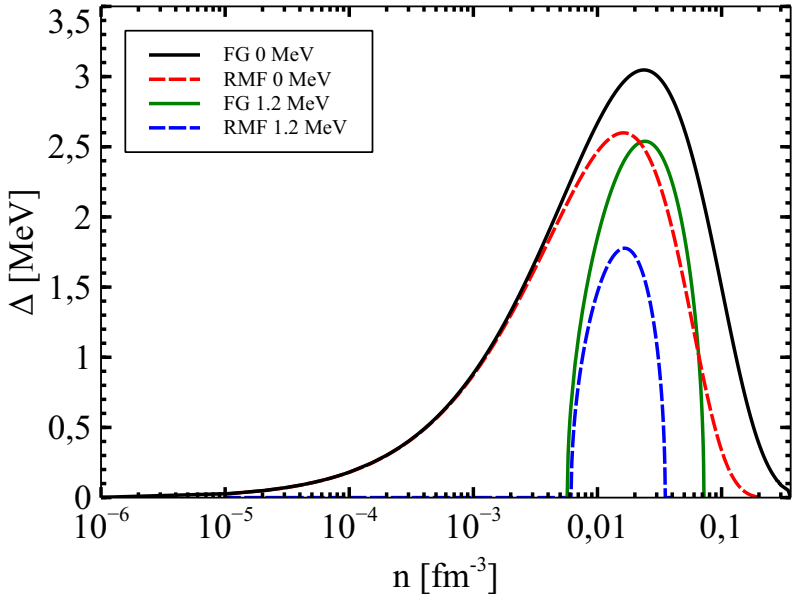

Figure 3.7.: Pairing gaps at the Fermi surface in neutron matter in FG and RMF models versus density n.

are expressed through the Fermi distribution function

$$f(E_k) = \left[\exp\left(\frac{E_k}{T}\right) + 1\right]^{-1}. \tag{3.21}$$

We get a similar modification for the pairing density distribution

$$\nu_k = \frac{\Delta_k}{2E_k}\left[1 - 2f(E_k)\right] \tag{3.22}$$

expressed through the pairing gap Δ.

Then we can define the thermodynamic quantities and in particular the thermodynamical potential

$$\begin{aligned}\Omega &= \langle H - \mu N - TS\rangle = V\sum_k (e_k - \mu)\left\{1 - \frac{e_k - \mu}{E_k}[1 - 2f(E_k)]\right\} \\ &+ V^2\sum_{k,k'}\frac{\Delta_k}{2E_k}[1 - 2f(E_k)]\nu_{k,k'}\frac{\Delta_{k'}}{2E_{k'}}[1 - 2f(E_{k'})] \\ &+ 2TV\sum_k\{f(E_k)\ln f(E_k) + [1 - f(E_k)]\ln[1 - f(E_k)]\}\end{aligned} \tag{3.23}$$

that includes the contribution of the entropy. Using the relation of the energy derivative of the distribution function

$$\frac{\partial}{\partial E}f(E) = -\frac{1}{T}\frac{1}{[\exp\left(\frac{E}{T}\right)+1]}\frac{1}{[\exp\left(\frac{-E}{T}\right)+1]} = -\frac{1}{T}f(E)[1 - f(E)], \tag{3.24}$$

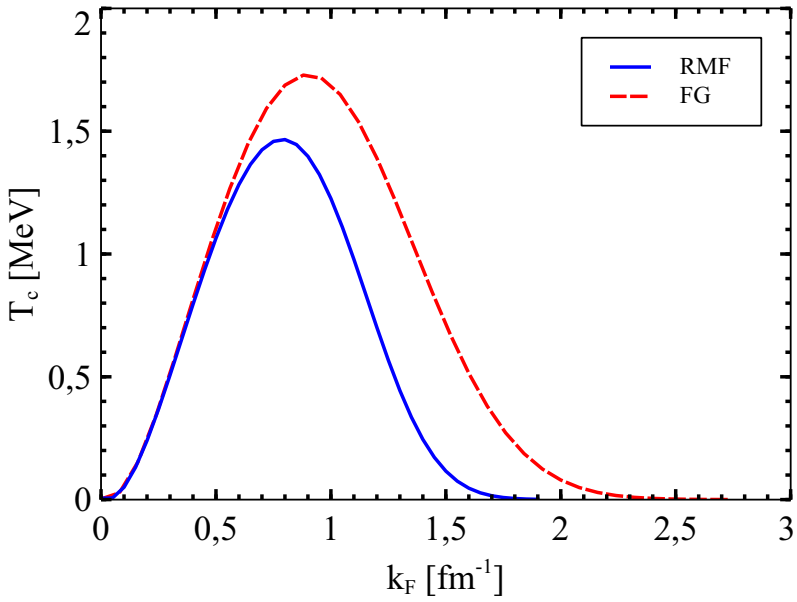

Figure 3.8.: Critical temperature versus Fermi momenta k_F in the $^1S_0$ channel in the RMF and Fermi gas models.

we can now derive the gap equation

$$\frac{d\Omega}{d\Delta_p} = \left(\Delta_p + V \sum_k \frac{\Delta_k}{2E_k} [1 - 2f(E_k)] v_{kp} \right) = 0.$$

Since

$$[1 - 2f(E_{k'})] = \tanh \frac{E_{k'}}{2T}, \tag{3.25}$$

we obtain the final result for the gap equation

$$\Delta_k = -V \sum_{k'} v_{kk'} \frac{\Delta_{k'}}{2E_{k'}} [1 - 2f(E_{k'})] = -V \sum_{k'} v_{kk'} \frac{\Delta_{k'}}{2E_{k'}} \tanh \frac{E_{k'}}{2T}. \tag{3.26}$$

Again, we can transform the sum to the integral and use k_F =20 fm^{-1} as the upper boundary of integration to achieve convergence.

Since $E_{k'} > 0$ and the limit

$$\lim_{T \to 0} \tanh \frac{E_{k'}}{2T} = 1, \tag{3.27}$$

we can now write the thermodynamic potential and thus the pressure as

$$\begin{aligned} -p = \Omega(T, \mu)/V = \sum_k (e_k - \mu) \left(1 - \frac{e_k - \mu}{E_k} [1 - 2f(E_k)] \right) - \sum_k \frac{\Delta_k^2}{2E_k} [1 - 2f(E_k)] \\ + 2T \sum_k (f(E_k) \ln f(E_k) + [1 - f(E_k)] \ln [1 - f(E_k)]). \end{aligned} \tag{3.28}$$

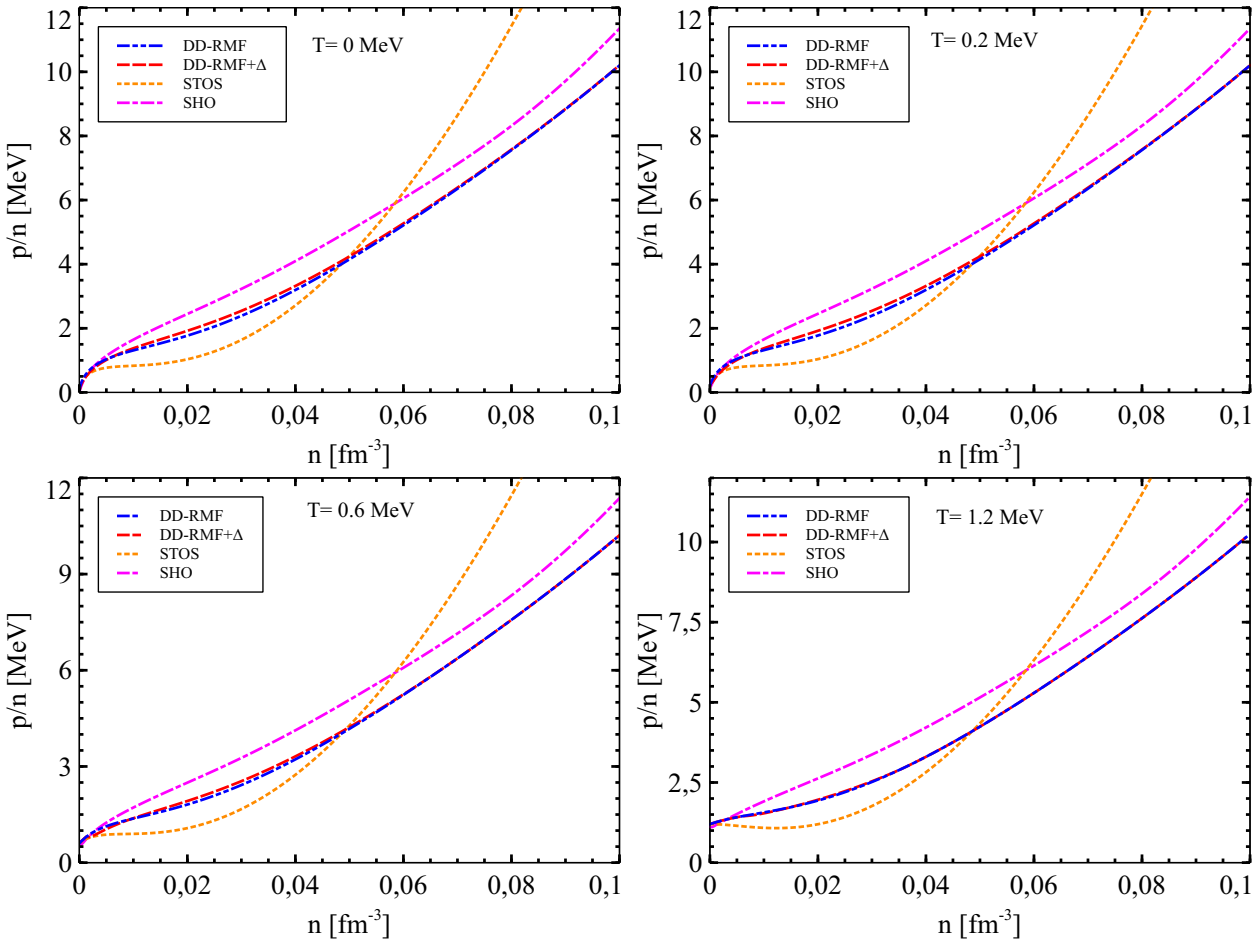

Figure 3.9.: Comparison of pressure p over density n in neutron matter for various models.

The entropy is found using

$$\frac{\partial}{\partial T} f(E) = f(E)[1 - f(E)] \frac{E}{T^2}. \tag{3.29}$$

Then it has the form

$$\begin{aligned} S &= -\left(\frac{\partial \Omega}{\partial T}\right)|_\mu = \sum_k \frac{\Delta_k^2}{T^2} f(E_k)[1 - f(E_k)] - 2\sum_k (f(E_k) \ln f(E_k) \\ &+ [1 - f(E_k)] \ln[1 - f(E_k)]). \end{aligned} \tag{3.30}$$

with an additional contribution from the pairing gap.

3.4.1 Comparison of pairing gaps

It is interesting to compare the pairing gaps calculated in the RMF and FG models. In Fig. 3.6 we present the results for $\Delta(k_F)$ for various temperatures. We can clearly see the effect of the mean-field resulting in the reduction of the gap as compared to the FG calculation. One can also notice the shift of the gap towards lower k_F in case of the RMF calculation. In the RMF model the maximum gap of $\approx$ 2.6 MeV corresponds to k_F =0.8 fm^{-1}, while in case of the FG calculation

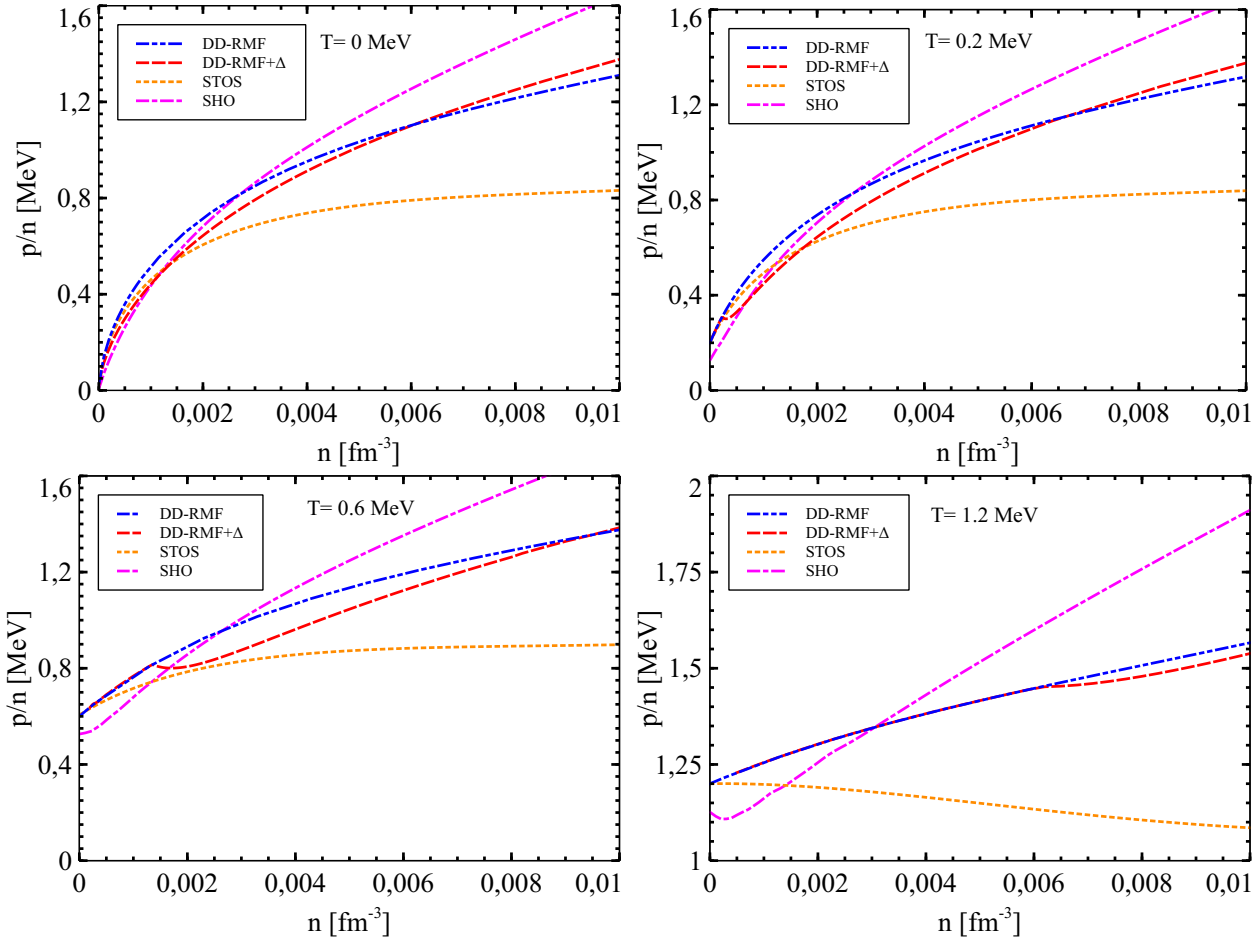

Figure 3.10.: Comparison of pressure p over density n in neutron matter for various models.

we get $\approx$ 3 MeV for k_F =0.9 fm^{-1}. This trend can also be easily seen in Fig. 3.7 where for the FG and RMF models $\Delta(k_F)$ versus density n is shown for two selected temperatures. We see that the biggest effect is in the region above $\approx$ 0.01 fm^{-3}.

Another interesting value is the critical temperature T_c, where the gap vanishes. We calculate this value from the gap equation by requiring $\Delta = 0$:

$$1 = -\frac{1}{4\pi^2}\sum_{k'}\int \lambda \frac{k^2\omega(k)^2}{|e_k-\mu|}\tanh\left(\frac{|e_k-\mu|}{2T}\right)dk. \tag{3.31}$$

The results are presented in Fig. 3.8. We get the value of $\approx$ 1.45 MeV for RMF calculation and $\approx$ 1.72 MeV for FG.

3.4.2 Thermodynamic quantities. High densities

We want to estimate the size of the pairing effects on the pressure in the RMF model and compare it to the variation of the EoS in different models, widely used in astrophysical applications. Similar as in Subsection 2.5.2, we choose the model of Shen, Horowitz and O'Connor (SHO) [SHO11] with the FSUGold parametrization and the model of Shen, Toki, Oyamatsu and

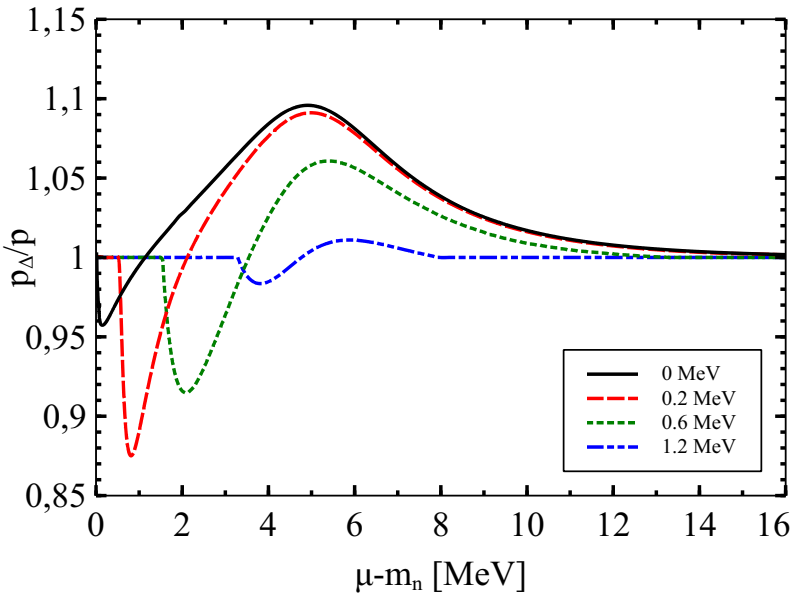

Figure 3.11.: Ratio of pressure for various temperatures in RMF model with and without pairing versus chemical potential in neutron matter.

Sumiyoshi (STOS) [STOS11] with the parameter set TM1. From the comparison in Fig. 3.9 we see that the pairing contributions are a minor effect.

We show the results for the RMF model with pairing correlations and without and see that the effect is quite small in a broad range of densities. The difference in the pressure for the RMF calculation without and with pairing is much smaller than the difference between the various EoS model calculations. We can also notice that the effect of pairing correlation reduces with increasing temperature as expected from the pairing gap behavior. At $T = 1.45$ MeV the two curves of the RMF calculations coincide.

3.4.3 Thermodynamic quantities. Lower densities

In order to study the effect of pairing correlations in detail, we show a similar comparison of different models on a smaller density scale in Fig. 3.10. We see that the biggest effect is given for the zero temperature case. Here the tail of the Δ function is long and smooth, while for finite temperatures one has a strong drop, see Fig. 3.6 and Fig. 3.7. This results in a kink in the pressure as a function of the density for finite temperatures.

Additionally, we can estimate how large the pairing correlation effect is for the given model. In Fig. 3.11 the ratio of pressure with pairing p_Δ to the standard RMF pressure p without pairing versus chemical potential μ is shown. We see that the ratio starts with unity at low chemical potentials. This corresponds to the unpaired phase. With the increase of the chemical potential the ratio p_Δ/p first shows a strong decrease transitioning to a smooth increase at higher μ. The ratio becomes unity again at high chemical potentials. When the ratio p_Δ/p crosses unity from below, a phase transition from the unpaired to the paired phase will occur because the state with the higher pressure will be realized in Nature. This also indicates a formation of a mixed phase appearing in the transition from the unpaired to the paired state, an effect that should be studied in detail in the future. The transition point is shifted to higher chemical potentials and

the pairing effect on the pressure becomes smaller with an increase of the temperature. Overall the change of the pressure due to pairing is in the order of 10 %. It can be a sizable correction for the specific equation of state.

3.5 Conclusions

The main goal of this chapter was to study the effect of pairing correlations on thermodynamic properties of the neutron matter equation of state. For this purpose the Yamaguchi separable interaction was assumed and the corresponding $^1S_0$ pairing gap was calculated for various temperatures. Two cases of a relativistic Fermi gas and a RMF model were investigated. The pairing gap at zero temperature was compared to calculations with other nucleon-nucleon potentials. We notice the good agreement of the relativistic FG calculation with the separable Yamaguchi interaction with other results. A reduction of the pairing gap in the RMF model is observed, which is caused by the mean-field effects. In order to investigate thermodynamic properties, we calculate the energy density versus Fermi momenta. The corresponding curves were depicted in the plot with other calculations showing similar trends. We investigated the temperature dependence of the pairing gap up to the critical temperature. Finally, a comparison of the pressure in different models was shown, including well-known equations of state for astrophysical applications. Although the pairing correlations represent a sizable correction at low densities for a single EoS in the order of 10 %, the variation of the pressure comparing different models is much larger than the pairing effect. For the astrophysical application, e.g in describing the crust of neutron stars, pairing effects need to be included in global EoS tables. This might improve the description of the cooling history of stars within a self-consistent theory.

4 Conclusions

In this thesis we have studied the role of correlations on the nuclear matter EoS. We investigated the effect of two-body correlations on thermodynamic properties of the system. Two different types of correlations were considered. The first are the scattering correlations described model-independently in the VEoS, which helps to constrain the low-density behavior of the EoS in other models. The second type of correlations is pairing in the $^1S_0$ nn channel. All the calculations were performed within the framework of the relativistic mean-field model with density dependent couplings.

In the first chapter we proposed an extension of the generalized relativistic mean-field model that includes scattering correlations as additional degrees of freedom. The virial equation of state is used as a model-independent benchmark in the low-density limit. Consistency is required between these two equations of state. For this purpose, new quasiparticles were introduced in the generalized RMF approach that represent two-nucleon correlations in the continuum. Such clusters are characterized by medium dependent effective resonance energies with temperature dependent effective degeneracy factors. Consistency relations were derived from the comparison of the fugacity expansions of both the relativistic mean-field and virial equation of state models. These relations include the contributions of nucleon-nucleon scattering phase shifts, the relativistic mean field nucleon-meson coupling, the resonance energies and effective degeneracy factors of the clusters. We have investigated various possibilities of the relevant parameter functions to satisfy these relations. In order to obtain a successful inclusion of two-body correlations and the description of the virial limit the following assumptions were made. The density dependence of the original relativistic mean-field model was kept and not modified at low densities. The effective resonance energies were taken as given by the calculation with the scattering phase shifts and the effective degeneracy factors were assumed to be temperature dependent similar as in the case of the nuclear statistical equilibrium model with thermally excited nuclei.

We have studied the cases of pure neutron matter and symmetric nuclear matter separately. In pure neutron matter only the *nn* scattering channel contributes to the thermodynamic properties, no bound states are present. Therefore it serves as a wonderful ground to estimate its influence on quantities like pressure or energy per nucleon. We show that relativistic effects become important with increasing temperature even at very low densities. In the case of symmetric nuclear matter the formation of many-body bound states is important for a realistic description of correlations. We have also observed that the extended generalized relativistic mean-field model smoothly interpolates between the correct low-density limit given by the VEoS and the high density limit where clusters dissolve. However, the precise form of the transition depends on the coupling strength of the clusters to the meson fields and the energy shift of the bound state and resonance energies. These quantities are not fixed by the low-density constraints and the consequences of different choices were investigated. This point deserves more studies in the future.

We note that the proposed inclusion of the two-body scattering correlations is rather general and can be applied to other mean-field approaches that aim at describing the equation of state of

nuclear matter. Bound states of light clusters with mass numbers $A \leq 4$ can be readily included as in Ref. [TRK$^+$10]. A further extension to heavier nuclei with medium-dependent binding energies and finite-temperature excitations is also possible.

We continue to consider two-body correlations in the second chapter, where an extended RMF model is proposed, which includes pairing. We want to self-consistently include pairing in the RMF model and investigate the effect that it has on the EoS. As a comparison to test our results we also show the calculation for the relativistic Fermi gas. The particular case of neutron matter is considered and the corresponding $^1S_0$ pairing gap appears for densities below saturation. A simple separable Yamaguchi interaction is considered for the calculation of the pairing gap for various temperatures. First we consider the zero temperature case. We show that there is a good agreement of the obtained results with the calculations with other nucleon-nucleon potentials. The reduction of the pairing gap in the RMF model in comparison with the Fermi gas is observed which is caused by the mean-field effects. The results for the energy per nucleon are compared with other calculations showing similar trends. The temperature dependence of the pairing gap is investigated up to the critical temperature where the gap vanishes. A comparison of the pressure in different models is shown, including well-known equations of state used in astrophysical applications. We see that pairing correlations do not substantially affect the EoS in comparison to other approaches. However for a given EoS a 10 % correction is obtained when pairing is considered.

In this work, two-body correlations were self-consistently included in the RMF model. They affect the composition and thermodynamic properties of the EoS. These corrections might be relevant for astrophysical applications e.g in describing the crust of neutron stars and affecting the neutrino transport properties. Finally, equation of state tables with the thermodynamic properties and the composition of nuclear matter for a broad range in temperature, density and proton-neutron asymmetry can be generated for astrophysical simulations of, e.g., core-collapse supernovae.

A Virial equation in our model and in Ref. [HS06a]

The authors of Ref. [HS06a] use a slightly different definition of some quantities in their approach to the nonrelativistic VEoS compared to the ones we use in section 2.2. In order to facilitate the comparison, we indicate the correspondence of the two formulations. Quantities of Ref. [HS06a] are indicated by a $\check{}$ in the following.

The single-particle partitions functions are defined in the same way, i.e. $Q_i = \check{Q}_i$ for nucleons and α-particles, however, there is a small difference in the thermal wavelengths because the neutron and proton mass are assumed to be equal $\check{m} = \check{m}_n = \check{m}_p$ in Ref. [HS06a] and the α-particle mass is set to $\check{m}_\alpha = 4\check{m}$ without considering the binding energy as in Eq. (2.41). Similarly, for the nonrelativistic chemical potentials the relation $\check{\mu}_\alpha = 2\check{\mu}_n + 2\check{\mu}_p$ is used instead of $\mu_\alpha = 2\mu_n + 2\mu_p - B_\alpha$ in our case. Nevertheless, the fugacities are identical. The main differences stem from the definition of the many-body partition functions. In Eq. (2.1) we place factors $1/n!$ in front of the n-body terms. Consequently $\check{Q}_{ij} = Q_{ij}/2$. Comparing Eq. (2.5) with Eq. (11) in [HS06a], we identify

$$\check{b}_n = b_{nn}/2 = b_{pp}/2, \qquad \check{b}_{pn} = b_{pn}/2 \tag{A.1}$$

and

$$\check{b}_\alpha = b_{\alpha\alpha}, \qquad \check{b}_{\alpha n} = b_{\alpha n}/\sqrt{8} = b_{\alpha p}/\sqrt{8}\,. \tag{A.2}$$

In Eq. (2.17) we use the c.m. energy E as the integration variable. In contrast, in Ref. [HS06a] the laboratory energies $\check{E} = 2E$ are used in Eqs. (19), (22) and (24) and the integrals are transformed with the help of a partial integration with respect to $\check{E}$. Noting that $\check{b}_{pn} = \check{b}_{\mathrm{nuc}} - \check{b}_n$ in Ref. [HS06a], the formulas given there for $\check{b}_n$, $\check{b}_{pn}$ and $\check{b}_\alpha$ are consistent with the relations (A.1) and (A.2). For the virial coefficient $\check{b}_{\alpha n}$, the authors of Ref. [HS06a] use the nucleon laboratory energy $\check{E} = 5E/4$ as integration variable. The expression (26) in Ref. [HS06a], however, is a factor two too large to be consistent with the relation given in (A.2). This discrepancy was already noted in Ref. [MDSS08].

B Zero temperature low-density limit in the gRMF model

In the case of pure neutron matter at zero temperature, all relevant thermodynamical quantities can be represented analytically as a function of the Fermi momentum k_{F_n}. The energy density ε of pure neutron matter without contributions of the rest mass reads, cf., e.g., Ref. [TW99],

$$\begin{aligned} \varepsilon &= \frac{3}{4}\sqrt{k_{F_n}^2+(m_n-S_n)^2}\,n_n+\frac{1}{4}(m_n-S_n)\,n_n^{(s)} \\ &\quad +\frac{1}{2}\left[\frac{\Gamma_\omega^2(n_n)}{m_\omega^2}+\frac{\Gamma_\rho^2(n_n)}{m_\rho^2}\right]n_n^2+\frac{1}{2}\left[\frac{\Gamma_\sigma^2(n_n)}{m_\sigma^2}+\frac{\Gamma_\delta^2(n_n)}{m_\delta^2}\right][n_n^{(s)}]^2, \end{aligned} \tag{B.1}$$

where the scalar neutron density is given by

$$n_n^{(s)}=\frac{3}{2x^3}f(x)\,n_n, \tag{B.2}$$

with the function

$$f(x)=x\sqrt{1+x^2}-\ln\left(x+\sqrt{1+x^2}\right), \tag{B.3}$$

that depends on the dimensionless parameter $x=k_{F_n}/(m_n-S_n)$. We define the derivative of the function (B.3), $f'=2x^2/\sqrt{1+x^2}$, and use the expansion

$$(1+z)^\alpha = \sum_{k=0}^{\infty}\frac{\Gamma(\alpha+1)}{k!\Gamma(\alpha+1-k)}z^{2k} \tag{B.4}$$

to rewrite equation (B.2) after integration as

$$\frac{n_n^{(s)}}{n_n} = 1-\frac{3}{10}\left[\frac{k_{F_n}}{m_n-S_n}\right]^2+\frac{9}{56}\left[\frac{k_{F_n}}{m_n-S_n}\right]^4+\ldots \tag{B.5}$$

Substituting $n_n^{(s)}$ in (B.1) by (B.5) and doing subsequent expansions in powers of k_{F_n} we arrive at expression (2.104-2.105) for the energy per neutron.

C Parameters of the separable potential

In order to define the parameters λ and γ in eq.3.1, one has to solve the Bethe-Salpeter equation in ladder approximation

$$T(12,1'2',z) = V(12,1'2') + \sum_{1'',2''} V(12,1''2'')G_2^0(1''2'',z)T(1''2'',1'2',z), \tag{C.1}$$

with the two-particle propagator

$$G_2^0(1''2'',z) = \frac{1-f(1'')-f(2'')}{z-\epsilon_{1''}-\epsilon(2'')}. \tag{C.2}$$

Using a separable ansatz for the T-matrix [RM09]

$$T(12,1'2',z) = \omega(12)\omega(1'2')t(P,z) \tag{C.3}$$

with the relative and total center-of-mass momenta

$$p = \frac{p_{1''}-p_{2''}}{2} \quad P = p_{1''}+p_{2''} = p_1+p_2 \tag{C.4}$$

we find

$$t(P,z) = -\frac{\lambda}{\Omega}\left[1+\frac{\lambda}{\Omega}\sum_p \omega^2(p)\frac{1-f(p+P/2)-f(p-P/2)}{z-\epsilon_{p+P/2}-\epsilon_{p-P/2}}\right]^{-1}, \tag{C.5}$$

with the Fermi distribution functions f.

For low densities, one has $f \ll 1$ and after transformation to the center-of-mass system $P = 0$, we find

$$t(0,z) = -\frac{\lambda}{\Omega}\left[1+\frac{\lambda}{\Omega}\sum_p \frac{\omega^2(p)}{z-2\epsilon_p}\right]^{-1} \tag{C.6}$$

and

$$T(12,1'2',z) = -\frac{\lambda}{\Omega}\omega(12)\omega(1'2')\frac{1}{1+\frac{\lambda}{\Omega}\int\frac{\Omega d^3p\omega^2(p)}{(2\pi^3 z-2\epsilon_p)}}. \tag{C.7}$$

The integral in the denominator can be simplified in spherical coordinates:

$$I(z) = \lambda\int\frac{d^3p}{(2\pi^3)}\frac{\omega^2(p)}{z-2\epsilon_p} = \frac{\lambda}{2\pi^2}\int_0^\infty dp\frac{p^2\omega^2(p)}{z-\frac{p^2}{\mu}}. \tag{C.8}$$

In the scattering case $z = E$ and assuming a Yamaguchi type potential, we have:

$$I(E) = \frac{\lambda}{2\pi^2} \int_0^\infty dp \frac{p^2}{(p^2/\gamma^2)} \frac{1}{E - \frac{p^2}{\mu}}. \tag{C.9}$$

Substitution of $x = p/\gamma$ and insertion of the reduced energy $\tilde{E} = \frac{\mu}{\gamma^2} E$ leads to the integral:

$$I(E) = -\frac{\lambda}{2\pi^2} \mu\gamma \int_0^\infty dx \frac{x^2}{(x^2+1)^2(x^2+(-\tilde{E}))} = -\frac{\lambda}{8\pi} \mu\gamma \frac{1}{4(1+i\sqrt{\tilde{E}})^2}. \tag{C.10}$$

Insertion of the real and imaginary part of the integral into the expression for the T-matrix leads to:

$$T(12, 1'2', \tilde{E}) = -\frac{\lambda}{\Omega} \omega(12)\omega(1'2') \frac{1}{1 + Re[I(\tilde{E})] + i\, Im[I(\tilde{E})]}. \tag{C.11}$$

We can now calculate the scattering phase shift:

$$\tan\delta_0(E) = \frac{Im[T(12, 1'2', \tilde{E})]}{Re[T(12, 1'2', \tilde{E})]} = \frac{-Im[\tilde{E}]}{1 + Re[I(\tilde{E})]} = \frac{2\sqrt{\tilde{E}}}{\frac{8\pi}{\lambda}\frac{1}{\mu\gamma}(1+\tilde{E})^2 - (1-\tilde{E})}. \tag{C.12}$$

According to the relation

$$k \cot\delta = -\frac{1}{a} + \frac{r_0 k^2}{2} - ..., \tag{C.13}$$

we find with $\tilde{E} = \frac{k^2}{2\gamma^2}$

$$k \cot\delta(k^2) = k \frac{\frac{8\pi}{\lambda}\frac{1}{\mu\gamma}(1 + \frac{k^2}{2\gamma^2})^2 - (1 - \frac{k^2}{2\gamma^2})}{\sqrt{2}\frac{k}{\gamma}} = \tag{C.14}$$

$$= -\frac{\gamma}{2}(1 - \frac{8\pi}{\lambda\mu\gamma}) + \frac{1}{\gamma}(1 + 2\frac{8\pi}{\lambda\mu\gamma})\frac{k^2}{2}. \tag{C.15}$$

Then we can extract the parameters of Yamaguchi potential from

$$a = \left(1 - \frac{8\pi}{\lambda\mu\gamma}\right)^{-1} \frac{2}{\gamma}, \tag{C.16}$$

$$r_0 = \left(1 + 2\frac{8\pi}{\lambda\mu\gamma}\right) \frac{1}{\gamma}. \tag{C.17}$$

D Derivation of the pairing gap equation

In this section we show the detailed derivation of the gap equation. We will start with the zero temperature case.

$$
\begin{aligned}
\frac{d}{d\Delta_p}\langle H-\mu N\rangle &= \frac{d}{d\Delta_p}\sum_k\left[(e_k-\mu)\left(1-\frac{e_k-\mu}{E_k}\right)+\sum_k\frac{\Delta_k}{2E_k}v_{k,k'}\frac{\Delta_{k'}}{2E_{k'}}\right]= \\
&= \sum_k\left\{\frac{(e_k-\mu)^2}{E_k^2}\frac{\Delta_k}{E_k}\delta_{kp}+\sum_{k'}\left[\left(\frac{1}{2E_k}-\frac{\Delta_k}{2E_k^2}\frac{\Delta_k}{E_k}\right)\delta_{kp}v_{kk'}\frac{\Delta_{k'}}{2E_{k'}}\right.\right. \\
&+ \left.\left.\frac{\Delta_k}{2E_k}v_{kk'}\left(\frac{1}{2E_k}-\frac{\Delta_k}{2E_k^2}\frac{\Delta_k}{E_k}\right)\delta_{k'p}\right]\right\}= \\
&= \sum_k\left\{\frac{(e_k-\mu)^2}{E_k^2}\frac{\Delta_k}{E_k}\delta_{kp}+\sum_{k'}\left[\frac{(e_k-\mu)^2}{2E_k^3}\delta_{kp}v_{kk'}\frac{\Delta_{k'}}{2E_{k'}}\delta_{kp}v_{kk'}\frac{\Delta_{k'}}{2E_{k'}}\right.\right. \\
&+ \left.\left.\frac{\Delta_k}{2E_k}v_{kk'}\frac{(e_{k'}-\mu)^2}{2E_{k'}^3}\delta_{k'p}\right]\right\}= \\
&= \frac{(e_p-\mu)^2}{E_p^2}\frac{\Delta_p}{E_p}+\sum_{k'}\frac{(e_p-\mu)^2}{2E_p^3}v_{pk'}\frac{\Delta_{k'}}{2E_{k'}}+\sum_{k'}\frac{\Delta_k}{2E_k}v_{kp}\frac{(e_p-\mu)^2}{2E_p^3}= \\
&= \frac{(e_p-\mu)^2}{E_p^3}\left(\Delta_p+\sum_k\frac{\Delta_k}{2E_k}v_{kp}\right)=0.
\end{aligned}
\tag{D.1}
$$

Then we obtain the gap equation

$$
\Delta_k=-\sum_{k'}v_{kk'}\frac{\Delta_{k'}}{2E_{k'}}. \tag{D.2}
$$

We can do a similar derivation for finite temperatures

$$
\begin{aligned}
\frac{d\Omega}{d\Delta_p} &= \sum_k \left(\frac{(e_k-\mu)^2}{E_k^2}\frac{\Delta_k}{E_k}[1-2f(E_k)] - \frac{2}{T}\frac{(e_k-\mu)^2}{E_k} f(E_k)[1-f(E_k)]\frac{\Delta_k}{E_k} \right) \delta_{kp} \\
&+ \sum_{k,k'} \left(\frac{1}{2E_k} - \frac{\Delta_k}{2E_k^2}\frac{\Delta_k}{E_k} \right) \delta_{kp}[1-2f(E_k)]v_{k,k'}\frac{\Delta'_k}{E'_k}[1-2f(E'_k)] \\
&+ \sum_{k,k'} \frac{\Delta_k}{2E_k}[1-2f(E_k)]v_{k,k'} \left(\frac{1}{2E'_k} - \frac{\Delta'_k}{2E'^2_k}\frac{\Delta'_k}{E'_k} \right) \delta k', p[1-2f(E'_k)] \\
&+ \sum_{k,k'} \frac{\Delta_k}{2E_k}\frac{2}{T} f(E_k)[1-f(E_k)]\frac{\Delta_k}{E_k}\delta_{kp}v_{kk'}\frac{\Delta'_k}{2E'_k}[1-2f(E'_k)] \\
&+ \sum_{k,k'} \frac{\Delta_k}{2E_k}[1-2f(E_k)]v_{k,k'}\frac{\Delta'_k}{2E'_k}\frac{2}{T} f(E'_k)[1-f(E'_k)]\frac{\Delta'_k}{E'_k}\delta_{k'p} \\
&+ 2T\sum_k \left(-\frac{1}{T} f(E_k)[1-f(E_k)]\ln f(E_k) + \frac{1}{T} f(E_k)[1-f(E_k)]\ln[1-f(E_k)] \right) \frac{\Delta_k}{E_k}\delta_{kp} \\
&+ 2T\sum_k \left(-\frac{1}{T} f(E_k)[1-f(E_k)] + \frac{1}{T} f(E_k)[1-f(E_k)] \right) \frac{\Delta_k}{E_k}\delta_{kp} = \\
&= \left(\frac{(e_p-\mu)^2}{E_p^3}[1-2f(E_p)] + \frac{2}{T} f(E_p)[1-f(E_p)]\frac{\Delta_p^2}{E_p^2} \right) \times \\
&\left(\Delta_p + \sum_k \frac{\Delta_k}{2E_k}[1-2f(E_k)]v_{kp} \right) = 0
\end{aligned}
\tag{D.3}
$$

leading to

$$
\Delta_k = -\sum_{k'} v_{kk'}\frac{\Delta_{k'}}{2E_{k'}}[1-2f(E_{k'})] = -\sum_{k'} v_{kk'}\frac{\Delta_{k'}}{2E_{k'}}\tanh\frac{E_{k'}}{2T}. \tag{D.4}
$$

Bibliography

[ABPR05] Mark Alford, Matt Braby, Mark Paris, and Sanjay Reddy. Hybrid stars that masquerade as neutron stars. *Astrophys. J.*, 629:969–978, 2005.

[aHSY84] Masa aki Hashimoto, Hironori Seki, and Masami Yamada. Shape of nuclei in the crust of neutron star. *Progress of Theoretical Physics*, 71(2):320–326, 1984.

[AI75] P. W. Anderson and N. Itoh. Pulsar glitches and restlessness as a hard superfluidity phenomenon. *Nature*, 256:25–27, 1975.

[AMPO$^+$08] A. Arcones, G. Martinez-Pinedo, E. O'Connor, A. Schwenk, H.-Th. Janka, et al. Influence of light nuclei on neutrino-driven supernova outflows. *Phys.Rev.*, C78:015806, 2008.

[And75] James B. Anderson. A random-walk simulation of the schrödinger equation: h_3^+. *The Journal of Chemical Physics*, 63(4):1499–1503, 1975.

[AP97] A. Akmal and V. R. Pandharipande. Spin-isospin structure and pion condensation in nucleon matter. *Phys. Rev.*, C56:2261–2279, 1997.

[APR98] A. Akmal, V. R. Pandharipande, and D. G. Ravenhall. The Equation of state of nucleon matter and neutron star structure. *Phys. Rev.*, C58:1804–1828, 1998.

[AS65] M. Abramowitz and I. A. Stegun. *Handbook of mathematical functions*. Dover, New York, 1965.

[AS09a] T. Abe and R. Seki. From low-density neutron matter to the unitary limit. *Phys. Rev.*, C79:054003, 2009.

[AS09b] T. Abe and R. Seki. Lattice calculation of thermal properties of low-density neutron matter with NN effective field theory. *Phys. Rev.*, C79:054002, 2009.

[AWT02] G. Audi, A. H. Wapstra, and C. Thibault. The Ame2003 atomic mass evaluation (II). Tables, graphs and references. *Nucl. Phys.*, A729:337–676, 2002.

[Bal99] M. Baldo. *Nuclear methods and the nuclear equation of state*. International Review of Nuclear Physics. World Scientific, 1999.

[BB77] J. Boguta and A. R. Bodmer. Relativistic calculation of nuclear matter and the nuclear surface. *Nucl. Phys.*, A292:413–428, 1977.

[BBB97] M. Baldo, I. Bombaci, and G. F. Burgio. Microscopic nuclear equation of state with three-body forces and neutron star structure. *Astron. Astrophys.*, 328:274–282, 1997.

[BCS57] John Bardeen, L. N. Cooper, and J. R. Schrieffer. Theory of superconductivity. *Phys. Rev.*, 108:1175–1204, 1957.

[BDM+06] S. W. Bruenn, C. J. Dirk, A. Mezzacappa, J. C. Hayes, J. M. Blondin, et al. Modeling core collapse supernovae in 2 and 3 dimensions with spectral neutrino transport. *J. Phys. Conf. Ser.*, 46:393–402, 2006.

[BEK+08] Bugra Borasoy, Evgeny Epelbaum, Hermann Krebs, Dean Lee, and Ulf-G. Meissner. Dilute neutron matter on the lattice at next-to-leading order in chiral effective field theory. *Eur. Phys. J.*, A35:357–367, 2008.

[Bel59] S. T. Belyaev. *Effect of pairing correlations on nuclear properties*. Matematisk-fysiske meddelelser. Kong. Dan. Vid. Selskab, 1959.

[Bet53] Hans A. Bethe. What holds the nucleus together? *J. Chem. Phys*, 189(3):56–63, September 1953.

[Bet71] H. A. Bethe. Theory of nuclear matter. *Annual review of nuclear and particle science*, 21:93–244, 1971.

[BHR03] Michael Bender, Paul-Henri Heenen, and Paul-Gerhard Reinhard. Self-consistent mean-field models for nuclear structure. *Rev. Mod. Phys.*, 75:121–180, 2003.

[Bis98] R. F. Bishop. *Microscopic quantum many-body theories and their applications proceedings*. Springer Berlin Heidelberg, Berlin, Heidelberg, 1998.

[BKPP88] G.E. Brown, K. Kubodera, D. Page, and P. Pizzochero. Strangeness condensation and cooling of neutron stars. *Phys.Rev.*, D37:2042–2046, 1988.

[BM08] M. Baldo and C. Maieron. Neutron matter at low density and the unitary limit. *Phys. Rev.*, C77:015801, 2008.

[BM10] A.S. Botvina and I.N. Mishustin. Statistical approach for supernova matter. *Nucl.Phys.*, A843:98–132, 2010.

[BMP58] A. Bohr, B. R. Mottelson, and D. Pines. Possible analogy between the excitation spectra of nuclei and those of the superconducting metallic state. *Phys. Rev.*, 110:936–938, 1958.

[Bod91] A. R. Bodmer. Relativistic mean field theory of nuclei with a vector meson selfinteraction. *Nucl. Phys.*, A526:703–721, 1991.

[Bog81] J. Boguta. Density dependence of the single particle potential in nuclear matter. *Phys. Lett.*, B106:250–254, 1981.

[BPS71] Gordon Baym, Christopher Pethick, and Peter Sutherland. The Ground state of matter at high densities: Equation of state and stellar models. *Astrophys. J.*, 170:299–317, 1971.

[Bro00] B. Alex Brown. Neutron radii in nuclei and the neutron equation of state. *Phys. Rev. Lett.*, 85:5296–5299, 2000.

[Bru55] K. A. Brueckner. Two-body forces and nuclear saturation. III. Details of the structure of the nucleus. *Phys. Rev.*, 97:1353–1366, 1955.

[Bru96] C. R Brune. A comparison of K- and R-matrix parameterizations of s-wave ^{16}O+p elastic scattering. *Nuclear Physics A*, 596(1):122 – 136, 1996.

[BS69] R. Bryan and B. L. Scott. Nucleon-nucleon scattering from one-boson-exchange potentials. III. S waves included. *Phys. Rev.*, 177:1435–1442, 1969.

[BST05] M. Baldo, E. E. Sapershtein, and S. V. Tolokonnikov. Superfluidity in nuclear and neutron matter. *Nucl. Phys.*, A749:42–52, 2005.

[BT92] R. Brockmann and H. Toki. Relativistic density-dependent hartree approach for finite nuclei. *Phys. Rev. Lett.*, 68:3408–3411, Jun 1992.

[BU36] G. E. Beth and E. Uhlenbeck. The quantum theory of the non-ideal gas I. Deviations from the classical theory. *Physica*, 3:729, (1936).

[BU37] E. Beth and G. Uhlenbeck. The quantum theory of the non-ideal gas. II. Behaviour at low temperatures. *Physica*, 4:915–924, 1937.

[Car87] J. Carlson. Green's function Monte Carlo study of light nuclei. *Phys. Rev.*, C36:2026–2033, 1987.

[CC06] Nicolas Chamel and Brandon Carter. Effect of entrainment on stress and pulsar glitches in neutron star crust. *Mon.Not.Roy.Astron.Soc.*, 368:796–808, 2006.

[CCDK93] J. M. C. Chen, J. W. Clark, R. D. Davé, and V. V. Khodel. Pairing gaps in nucleonic superfluids. *Nuclear Physics A*, 555(1):59 – 89, 1993.

[CCPS03] J. Carlson, S.-Y. Chang, V. R. Pandharipande, and K. E. Schmidt. Superfluid Fermi gases with large scattering length. *Phys. Rev. Lett.*, 91:050401, 2003.

[Cep95] D. M. Ceperley. Path integrals in the theory of condensed helium. *Rev. Mod. Phys.*, 67:279–355, 1995.

[CH08] N. Chamel and P. Haensel. Physics of neutron star crusts. *Living Rev. Rel.*, 11:10, 2008.

[CLS06] L. G. Cao, U. Lombardo, and P. Schuck. Screening effects in superfluid nuclear and neutron matter within Brueckner theory. *Phys. Rev.*, C74:064301, 2006.

[CMPR03] J. Carlson, Jr. Morales, J., V. R. Pandharipande, and D.G. Ravenhall. Quantum Monte Carlo calculations of neutron matter. *Phys. Rev.*, C68:025802, 2003.

[DBLO06] L. Dessart, A. Burrows, E. Livne, and C. D. Ott. Multi-dimensional radiation/hydrodynamic simulations of protoneutron star convection. *Astrophys. J.*, 645:534–550, 2006.

[DECVP01] M. Del Estal, M. Centelles, X. Vinas, and S. K. Patra. Effects of new nonlinear couplings in relativistic effective field theory. *Phys. Rev.*, C63:024314, 2001.

[DG80] J. Decharge and D. Gogny. Hartree-Fock-Bogolyubov calculations with the D1 effective interactions on spherical nuclei. *Phys.Rev.*, C21:1568–1593, 1980.

[DG90] R. M. Dreizler and E. K. U. Gross. Density functional theory: an approach to the quantum many-body problem. *Springer, Berlin*, 1990.

[DHJ03] D. J. Dean and M. Hjorth-Jensen. Pairing in nuclear systems: From neutron stars to finite nuclei. *Rev. Mod. Phys.*, 75:607–656, 2003.

[dJL98] F. de Jong and H. Lenske. Relativistic Bruckner-Hartree-Fock calculations with explicit intermediate negative energy states. *Phys. Rev.*, C58:890–899, 1998.

[DLL02] Pawel Danielewicz, Roy Lacey, and William G. Lynch. Determination of the equation of state of dense matter. *Science*, 298:1592–1596, 2002.

[DLWM12] Joaquin E. Drut, Timo A. Lahde, Gabriel Wlazlowski, and Piotr Magierski. The equation of state of the unitary fermi gas: An update on lattice calculations. *Phys. Rev.*, A85:051601, 2012.

[DM92] W. H. Dickhoff and H. Muther. Nucleon properties in the nuclear medium. *Rept. Prog. Phys.*, 55:1947–2023, 1992.

[DMB69] Roger Dashen, Shang-Keng Ma, and Herbert J. Bernstein. S-matrix formulation of statistical mechanics. *Phys. Rev.*, 187:345–370, 1969.

[DPR$^+$10] Paul Demorest, Tim Pennucci, Scott Ransom, Mallory Roberts, and Jason Hessels. Shapiro delay measurement of a two solar mass neutron star. *Nature*, 467:1081–1083, 2010.

[EHJ97] O. Elgaroy and M. Hjorth-Jensen. Properties of pairing correlations in infinite nuclear matter. *Condensed Matter theories*, 21, 1997.

[EHM09] Evgeny Epelbaum, Hans-Werner Hammer, and Ulf-G. Meissner. Modern Theory of Nuclear Forces. *Rev. Mod. Phys.*, 81:1773–1825, 2009.

[EKLM09] Evgeny Epelbaum, Hermann Krebs, Dean Lee, and Ulf-G. Meissner. Ground state energy of dilute neutron matter at next-to-leading order in lattice chiral effective field theory. *Eur. Phys. J.*, A40:199–213, 2009.

[Eli60] G. M. Eliashberg. Interactions between electrons and lattice vibrations in a superconductor. *Sov. Phys. JETP*, 11:696, 1960.

[EW88] T. E. O. Ericson and W. Weise. Pions and nuclei. *Oxford University Press, Clarendon, Oxford*, (1988).

[Fee69] Eugene Feenberg. *Theory of quantum fluids*. Academic Press, New York, 1969.

[FF98] S. Fantoni and A. Fabrocini. *Microscopic quantum many-body theories and their applications*. Springer, Berlin, Heidelberg, 1998.

[FFIS05] Adelchi Fabrocini, Stefano Fantoni, Alexey Yu. Illarionov, and Kevin E. Schmidt. $^1S_0$ superfluid phase-transition in neutron matter with realistic nuclear potentials and modern many-body theories. *Phys.Rev.Lett.*, 95:192501, 2005.

[FKL$^+$04] Andrew J. Faulkner, M. Kramer, A. G. Lyne, R. N. Manchester, M. A. McLaughlin, et al. PSR J1756-2251: A New relativistic double neutron star system. *Astrophys. J.*, 618:L119–L122, 2004.

[FLW95] C. Fuchs, H. Lenske, and H. H. Wolter. Density dependent hadron field theory. *Phys. Rev.*, C52:3043–3060, 1995.

[FP81] B. Friedman and V. R. Pandharipande. Hot and cold, nuclear and neutron matter. *Nucl. Phys.*, A361:502–520, 1981.

[FST97] R. J. Furnstahl, Brian D. Serot, and Hua-Bin Tang. A chiral effective Lagrangian for nuclei. *Nucl. Phys.*, A615:441–482, 1997.

[Fuc04] Christian Fuchs. The Relativistic Dirac-Brueckner approach to nuclear matter. *Lect. Notes Phys.*, 641:119–146, 2004.

[Fuc06] Christian Fuchs. Kaon production in heavy ion reactions at intermediate energies. *Prog. Part. Nucl. Phys.*, 56:1–103, 2006.

[Fur02] R. J. Furnstahl. Neutron radii in mean field models. *Nucl. Phys.*, A706:85–110, 2002.

[GA09] Kostas Glampedakis and Nils Andersson. A hydrodynamical trigger mechanism for pulsar glitches. *Phys. Rev. Lett.*, 102:141101, 2009.

[GB04] S. Gmuca and J. K. Bunta. Nuclear symmetry energy constraints for RMF calculations of superheavy nuclei. *Nucl. Phys.*, A734:172, 2004.

[GBFF99] T. Gross-Boelting, C. Fuchs, and Amand Faessler. Covariant representations of the relativistic Bruckner T matrix and the nuclear matter problem. *Nucl. Phys.*, A648:105–137, 1999.

[GC08] Alexandros Gezerlis and J. Carlson. Strongly paired fermions: cold atoms and neutron matter. *Phys. Rev.*, C77:032801, 2008.

[GC10] Alexandros Gezerlis and J. Carlson. Low-density neutron matter. *Phys. Rev.*, C81:025803, 2010.

[GIF+08] S. Gandolfi, A. Yu. Illarionov, S. Fantoni, F. Pederiva, and K. E. Schmidt. Equation of state of superfluid neutron matter and the calculation of $^1S_0$ pairing gap. *Phys. Rev. Lett.*, 101:132501, 2008.

[GIP+09] S. Gandolfi, A. Yu. Illarionov, F. Pederiva, K.E. Schmidt, and S. Fantoni. Equation of state of low-density neutron matter and the $^1S_0$ pairing gap. *Phys. Rev.*, C80:045802, 2009.

[GK64] V. L. Ginzburg and D. A. Kirzhnits. On superfluidity of neutron stars. *Zh. Eksp. Teor. Fiz.*, 47:2006, 1964.

[GK65] V. L. Ginzburg and D. A. Kirzhnits. On superfluidity of neutron stars. *Sov. Phys. JETP.*, 20:1346, 1965.

[Gle92] Norman K. Glendenning. First order phase transitions with more than one conserved charge: Consequences for neutron stars. *Phys.Rev.*, D46:1274–1287, 1992.

[Gle96] N. K. Glendenning. Compact stars: Nuclear Physics, Particle Physics, and General Relativity. *Springer*, 1996.

[Gle00] N. K. Glendenning. Compact stars: Nuclear physics, particle physics, and general relativity. *Springer, New York*, 2000.

[Gmu91] Stefan Gmuca. Relativistic mean-field fit to microscopic results in nuclear matter. *J. Phys. G*, 17:115, 1991.

[Gmu92a] Stefan Gmuca. Finite-nuclei calculations based on relativistic mean-field effective interactions . *Nucl. Phys*, A526:703, 1992.

[Gmu92b] Stefan Gmuca. Relativistic mean-field parametrization of effective interaction in nuclear matter. *Zeitschrift für Physik A Hadrons and Nuclei*, 342:387–392, 1992.

[Gor58] L. P Gorkov. On the energy spectrum of superconductors. *Soviet Physics JETP-USSR*, 7:505, 1958.

[GRT90] Y. K. Gambhir, P. Ring, and A. Thimet. Relativistic mean field theory for finite nuclei. *Annals of Physics*, 198:132–179, 1990.

[GSB99] Norman K. Glendenning and Jurgen Schaffner-Bielich. First order kaon condensate. *Phys.Rev.*, C60:025803, 1999.

[HAJ+12] C. J. Horowitz, Z. Ahmed, C. M. Jen, A. Rakhman, P. A. Souder, et al. Weak charge form factor and radius of ^{208}Pb through parity violation in electron scattering. *Phys. Rev.*, C85:032501, 2012.

[HCC+98] C. R. Howell, Q. Chen, T. S. Carman, A. Hussein, W. R. Gibbs, et al. Toward a resolution of the neutron-neutron scattering-length issue. *Phys. Lett.*, B444:252–259, 1998.

[HGRR70] M. Hoffberg, A. E. Glassgold, R. W. Richardson, and M. Ruderman. Anisotropic superfluidity in neutron star matter. *Phys. Rev. Lett.*, 24:775–777, Apr 1970.

[HH10] Craig O. Heinke and Wynn C. G. Ho. Direct observation of the cooling of the Cassiopeia A neutron star. *Astrophys. J.*, 719:L167–L171, 2010.

[HHJ00] Henning Heiselberg and Morten Hjorth-Jensen. Phases of dense matter in neutron stars. *Phys.Rept.*, 328:237–327, 2000.

[HKL01] F. Hofmann, C. M. Keil, and H. Lenske. Density dependent hadron field theory for asymmetric nuclear matter and exotic nuclei. *Phys. Rev.*, C64:034314, 2001.

[HLPS10] K. Hebeler, J. M. Lattimer, C. J. Pethick, and A. Schwenk. Constraints on neutron star radii based on chiral effective field theory interactions. *Phys. Rev. Lett.*, 105:161102, 2010.

[HP00] Henning Heiselberg and Vijay Pandharipande. Recent progress in neutron star theory. *Ann. Rev. Nucl. Part. Sci.*, 50:481–524, 2000.

[HP01a] C. J. Horowitz and J. Piekarewicz. Neutron star structure and the neutron radius of ^{208}Pb. *Phys. Rev. Lett.*, 86:5647, 2001.

[HP01b] Charles J. Horowitz and Jorge Piekarewicz. The neutron radii of ^{208}Pb and neutron stars. *Phys. Rev.*, C64:062802, 2001.

[HPS93] H. Heiselberg, C.J. Pethick, and E.F. Staubo. Quark matter droplets in neutron stars. *Phys.Rev.Lett.*, 70:1355–1359, 1993.

[HPSM01] C. J. Horowitz, S. J. Pollock, P. A. Souder, and R. Michaels. Parity violating measurements of neutron densities. *Phys. Rev.*, C63:025501, 2001.

[HPY10] P. Haensel, A.Y. Potekhin, and D.G. Yakovlev. *Neutron Stars 1: Equation of State and Structure*. Astrophysics and Space Science Library. Springer, 2010.

[HS06a] C. J. Horowitz and A. Schwenk. Cluster formation and the virial equation of state of low-density nuclear matter. *Nucl. Phys.*, A776:55–79, 2006.

[HS06b] C. J. Horowitz and A. Schwenk. The neutrino response of low-density neutron matter from the virial expansion. *Phys. Lett.*, B642:326–332, 2006.

[HS06c] C. J. Horowitz and A. Schwenk. The virial equation of state of low-density neutron matter. *Phys. Lett.*, B638:153–159, 2006.

[HS10] K. Hebeler and A. Schwenk. Chiral three-nucleon forces and neutron matter. *Phys.Rev.*, C82:014314, 2010.

[HSB10] Matthias Hempel and Jurgen Schaffner-Bielich. Statistical model for a complete supernova equation of state. *Nucl. Phys.*, A837:210–254, 2010.

[JEL96] S. M. Johns, P. J. Ellis, and J. M. Lattimer. Numerical approximation to the thermodynamic integrals. *Astrophys. J.*, 473:1020–1028, 1996.

[JLM76] J. P. Jeukenne, A. Lejeune, and C. Mahaux. Many body theory of nuclear matter. *Phys. Rept.*, 25:83–174, 1976.

[JLM$^+$07] Hans-Thomas Janka, K. Langanke, A. Marek, G. Martinez-Pinedo, and B. Mueller. Theory of Core-Collapse Supernovae. *Phys. Rept.*, 442:38–74, 2007.

[JMMS08] H.-Th. Janka, A. Marek, B. Mueller, and L. Scheck. Supernova explosions and the birth of neutron stars. *AIP Conf. Proc.*, 983:369–378, 2008.

[JR05] Buras R. Kifonidis K. Marek A. Janka, H.-Th. and Rampp. Cosmic Explosions, On the 10th Anniversary of SN1993J. *IAU Colloq*, 192:253, 2005.

[KBT$^+$06] T. Klaehn, D. Blaschke, S. Typel, E. N. E. van Dalen, A. Faessler, et al. Constraints on the high-density nuclear equation of state from the phenomenology of compact stars and heavy-ion collisions. *Phys. Rev.*, C74:035802, 2006.

[KLZ78] H. Kummel, K. H. Luhrmann, and J. G. Zabolitzky. Many-fermion theory in expS- (or coupled cluster) form. *Phys. Rept.*, 36:1–36, 1978.

[KR91] H. Kucharek and P. Ring. Relativistic field theory of superfluidity in nuclei. *Zeitschrift für Physik A Hadrons and Nuclei*, 339:23–35, 1991.

[KS65] W. Kohn and L. J. Sham. Quantum density oscillations in an inhomogeneous electron gas. *Phys. Rev.*, 137:A1697–A1705, 1965.

[KS06] Plamen G. Krastev and Francesca Sammarruca. Neutron star properties and the equation of state of neutron-rich matter. *Phys. Rev.*, C74:025808, 2006.

[KST06] Kei Kotake, Katsuhiko Sato, and Keitaro Takahashi. Explosion mechanism, neutrino burst, and gravitational wave in core-collapse supernovae. *Rept. Prog. Phys.*, 69:971–1144, 2006.

[KV05] E. E. Kolomeitsev and D. N. Voskresensky. Relativistic mean-field models with effective hadron masses and coupling constants, and rho- condensation. *Nucl. Phys.*, A759:373–413, 2005.

[Lan06] K. Langanke. Neutrino nucleus reactions in core-collapse supernovae. *Prog. Part. Nucl. Phys.*, 57:324–333, 2006.

[LCK08] Bao-An Li, Lie-Wen Chen, and Che Ming Ko. Recent progress and new challenges in isospin physics with heavy-ion reactions. *Phys. Rept.*, 464:113–281, 2008.

[Lee09] Dean Lee. Lattice simulations for few- and many-body systems. *Prog. Part. Nucl. Phys.*, 63:117–154, 2009.

[LKR97] G. A. Lalazissis, J. Konig, and P. Ring. A new parametrization for the Lagrangian density of relativistic mean field theory. *Phys. Rev.*, C55:540–543, 1997.

[LL09] Birbrair B. L. and Kryshen E. L. Nuclear matter within the relativistic-mean-field model involving free-space nucleon nucleon forces. *Phys. Atom. Nucl.*, 72:1154–1164, 2009.

[LL12] James M. Lattimer and Yeunhwan Lim. Constraining the symmetry parameters of the nuclear interaction. *arXiv:1203.4286*, 2012.

[LLPR78] D. Q. Lamb, J. M. Lattimer, C. J. Pethick, and D. G. Ravenhall. Hot dense matter and stellar collapse. *Phys. Rev. Lett.*, 41:1623–1626, 1978.

[LLR$^+$80] M. Lacombe, B. Loiseau, J. M. Richard, R. Vinh Mau, J. Cote, et al. Parametrization of the Paris NN potential. *Phys. Rev.*, C21:861–873, 1980.

[LM63] A. I. Larkin and A. B Migdal. Theory of superfluid fermi liquid - application to the nucleus. *Sov. Phys. JETP*, 17:1146, 1963.

[LMB92] G. Q. Li, R. Machleidt, and R. Brockmann. Properties of dense nuclear and neutron matter with relativistic nucleon-nucleon interactions. *Phys. Rev.*, C45:2782–2794, 1992.

[LMVGZ04] Wen-hui Long, Jie Meng, Nguyen Van Giai, and Shan-Gui Zhou. New effective interactions in RMF theory with nonlinear terms and density dependent meson nucleon coupling. *Phys. Rev.*, C69:034319, 2004.

[LNVR05] G. A. Lalazissis, T. Niksic, D. Vretenar, and P. Ring. New relativistic mean-field interaction with density-dependent meson-nucleon couplings. *Phys. Rev.*, C71:024312, 2005.

[LP01] J. M. Lattimer and M. Prakash. Neutron star structure and the equation of state. *Astrophys. J.*, 550:426, 2001.

[LP04] J. M. Lattimer and M. Prakash. The physics of neutron stars. *Science*, 304:536–542, 2004.

[LS91] James M. Lattimer and F. Douglas Swesty. A generalized equation of state for hot, dense matter. *Nucl. Phys.*, A535:331–376, 1991.

[LS01] U. Lombardo and H. J. Schulze. Superfluidity in neutron star matter. *Lect. Notes Phys.*, 578:30–53, 2001.

[LS06] Bao-An Li and Andrew W. Steiner. Constraining the radii of neutron stars with terrestrial nuclear laboratory data. *Phys. Lett.*, B642:436–440, 2006.

[LY57] T. D. Lee and C. N. Yang. Many-body problem in quantum mechanics and quantum statistical mechanics. *Phys. Rev.*, 105:1119–1120, 1957.

[Mac89] R. Machleidt. The meson theory of nuclear forces and nuclear structure. *Adv. Nucl. Phys.*, 19:189–376, 1989.

[MD05] H. Muther and W. H. Dickhoff. Pairing properties of nucleonic matter employing dressed nucleons. *Phys. Rev.*, C72:054313, 2005.

[MDSS08] S. Mallik, J. N. De, S. K. Samaddar, and Sourav Sarkar. S-matrix approach to equation of state of nuclear matter. *Phys. Rev.*, C77:032201, 2008.

[Mig60] A. B. Migdal. Superfluidity and the moments of inertia of nuclei. *Soviet Physics JETP 10,*, pages 176–185, 1960.

[Mig78] Arkady B. Migdal. Pion fields in nuclear matter. *Rev. Mod. Phys.*, 50:107–172, 1978.

[MJ09] A. Marek and H.-Th. Janka. Delayed neutrino-driven supernova explosions aided by the standing accretion-shock instability. *Astrophys. J.*, 694:664–696, 2009.

[MSH08] Jerome Margueron, Hiroyuki Sagawa, and Kouichi Hagino. Effective pairing interactions with isospin density dependence. *Phys.Rev.*, C77:054309, 2008.

[MSS96] R. Machleidt, F. Sammarruca, and Y. Song. The nonlocal nature of the nuclear force and its impact on nuclear structure. *Phys. Rev.*, C53:1483–1487, 1996.

[MSTV90] Arkady B. Migdal, E. E. Saperstein, M. A. Troitsky, and D. N. Voskresensky. Pion degrees of freedom in nuclear matter. *Phys. Rept.*, 192:179–437, 1990.

[MvDF07] Jerome Margueron, Eric van Dalen, and Christian Fuchs. Low densities in asymmetric nuclear matter. *Phys. Rev.*, C76:034309, 2007.

[Nam60] Yoichiro Nambu. Quasiparticles and Gauge Invariance in the Theory of Superconductivity. *Phys.Rev.*, 117:648–663, 1960.

[NRT+10] J.B. Natowitz, G. Roepke, S. Typel, D. Blaschke, A. Bonasera, et al. Symmetry energy of dilute warm nuclear matter. *Phys. Rev. Lett.*, 104:202501, 2010.

[NVFR02] T. Niksic, D. Vretenar, P. Finelli, and P. Ring. Relativistic Hartree-Bogolyubov model with density dependent meson nucleon couplings. *Phys. Rev.*, C66:024306, 2002.

[OaHY84] Kazuhiro Oyamatsu, Masa aki Hashimoto, and Masami Yamada. Further study of the nuclear shape in high-density matter. *Progress of Theoretical Physics*, 72(2):373–375, 1984.

[OGH+07] E. O'Connor, D. Gazit, C. J. Horowitz, A. Schwenk, and N. Barnea. Neutrino breakup of A=3 nuclei in supernovae. *Phys. Rev.*, C75:055803, 2007.

[OV39] J. R. Oppenheimer and G. M. Volkoff. On massive neutron cores. *Phys. Rev.*, 55:374–381, 1939.

[PR06] Dany Page and Sanjay Reddy. Dense matter in compact stars: Theoretical developments and observational constraints. *Ann. Rev. Nucl. Part. Sci.*, 56:327–374, 2006.

[PRB87] W. Pannert, P. Ring, and J. Boguta. Relativistic mean-field theory and nuclear deformation. *Phys. Rev. Lett.*, 59:2420–2422, Nov 1987.

[PU59] A. Pais and G. E. Uhlenbeck. On the quantum theory of the third virial coefficient. *Phys. Rev.*, 116:250–269, 1959.

[QCD] *http://theor.jinr.ru/twiki-cgi/view/NICA/WebHome*.

[RD69] P. E. Reichley and G. S. Downs. Observed decrease in the periods of pulsar PSR 0833-45. *Nature*, 222:229, 1969.

[Rei88] P. G. Reinhard. The nonlinearity of the scalar field in a relativistic mean-field theory of the nucleus. *Zeitschrift für Physik A Hadrons and Nuclei*, 329:257–266, 1988.

[RHSB06] Stefan B. Ruester, Matthias Hempel, and Jurgen Schaffner-Bielich. The outer crust of non-accreting cold neutron stars. *Phys. Rev.*, C73:035804, 2006.

[RM69] V. Radhakrishnan and R. N. Manchester. Detection of a change of state in the pulsar PSR 0833-45. *Nature*, 222:228, 1969.

[RM09] G. Roepke and Winkel M. Green's functions technique for statistical ensembles. *Lecture note, Institute fuer Physik Rostock Universitys*, 2009.

[RMS82a] G. Roepke, L. Muenchow, and H. Schulz. On the phase stability of hot nuclear matter and the applicability of detailed balance equations. *Physics Letters B*, 110(1):21 – 24, 1982.

[RMS82b] G. Roepke, L. Muenchow, and H. Schulz. Particle clustering and mott transitions in nuclear matter at finite temperature: (i). method and general aspects. *Nuclear Physics A*, 379(3):536 – 552, 1982.

[RMVC+11] X. Roca-Maza, X. Vinas, M. Centelles, P. Ring, and P. Schuck. Relativistic mean field interaction with density dependent meson-nucleon vertices based on microscopical calculations. *Phys. Rev.*, C84:054309, 2011.

[RPV09] Arnau Rios, Artur Polls, and Isaac Vidana. Hot neutron matter from a Self-Consistent Green's Functions approach. *Phys.Rev.*, C79:025802, 2009.

[RPW83] D. G. Ravenhall, C. J. Pethick, and J. R. Wilson. Structure of matter below nuclear saturation density. *Phys. Rev. Lett.*, 50:2066–2069, 1983.

[RRM+86] P. G. Reinhard, M. Rufa, J. Maruhn, W. Greiner, and J. Friedrich. Nuclear ground state properties in a relativistic meson field theory. *Z. Phys.*, A323:13–25, 1986.

[RSBW01] Angels Ramos, Jurgen Schaffner-Bielich, and Jochen Wambach. Kaon condensation in neutron stars. *Lect. Notes Phys.*, 578:175–202, 2001.

[RW00] Krishna Rajagopal and Frank Wilczek. The condensed matter physics of QCD. *At the frontier of particle physics, vol. 3*, 2000.

[SC92] K. E. Schmidt and D. M. Ceperley. *The Monte Carlo method in condensed matter physics*, volume 7. Springer New York, Berlin, Heidelberg, 1992.

[SC06] Armen Sedrakian and John Walter Clark. Nuclear superconductivity in compact stars: BCS theory and beyond. *Pairing in Fermionic Systems: Basic Concepts and Modern Applications*, 2006.

[SCL+96] H. J. Schulze, J. Cugnon, A. Lejeune, M. Baldo, and U. Lombardo. Medium polarization effects on neutron matter superfluidity. *Phys. Lett.*, B375:1–8, 1996.

[SFB03] Achim Schwenk, Bengt Friman, and Gerald E. Brown. Renormalization group approach to neutron matter: Quasiparticle interactions, superfluid gaps and the equation of state. *Nucl. Phys.*, A713:191–216, 2003.

[SFM00] Madan M. Sharma, Ameenah R. Farhan, and S. Mythili. Shell effects in nuclei with vector selfcoupling of omega meson in relativistic Hartree-Bogolyubov theory. *Phys. Rev.*, C61:054306, 2000.

[SGS90] M. Schmidt, Roepke G., and H. Schulz. Many-body problem in quantum mechanics and quantum atatistical mechanics. *Ann. Phys.*, 202:57, 1990.

[She11] G. Shen. private communication. 2011.

[SHO11] G. Shen, C. J. Horowitz, and E. O'Connor. A second relativistic mean field and virial equation of state for astrophysical simulations. *Phys. Rev.*, C83:065808, 2011.

[SHT10] G. Shen, C. J. Horowitz, and S. Teige. Equation of state of dense matter from a density dependent relativistic mean field model. *Phys. Rev.*, C82:015806, 2010.

[SKRdS93] V. G. J. Stoks, R. A. M. Kompl, M. C. M. Rentmeester, and J. J. de Swart. Partial wave analaysis of all nucleon-nucleon scattering data below 350-MeV. *Phys. Rev.*, C48:792–815, 1993.

[SKTdS94] V. G. J. Stoks, R. A. M. Klomp, C. P. F. Terheggen, and J. J. de Swart. Construction of high quality NN potential models. *Phys. Rev.*, C49:2950–2962, 1994.

[Sky59] T. Skyrme. The effective nuclear potential. *Nucl. Phys.*, 9:615–634, 1959.

[SLB12] Andrew W. Steiner, James M. Lattimer, and Edward F. Brown. The neutron star mass-radius relation and the equation of state of dense matter. *arXiv:1205.6871 [nucl-th]*, 2012.

[SLR93] M. M. Sharma, G. A. Lalazissis, and P. Ring. Anomaly in the charge radii of Pb isotopes. *Phys. Lett.*, B317:9–13, 1993.

[SNR93] M. M. Sharma, M. A. Nagarajan, and P. Ring. Rho meson coupling in the relativistic mean field theory and description of exotic nuclei. *Phys. Lett.*, B312:377–381, 1993.

[SP05] A. Schwenk and C. J. Pethick. Resonant Fermi gases with a large effective range. *Phys. Rev. Lett.*, 95:160401, 2005.

[SR08] Kohsuke Sumiyoshi and Gerd Roepke. Appearance of light clusters in post-bounce evolution of core-collapse supernovae. *Phys. Rev.*, C77:055804, 2008.

[ST83] Stuart L. Shapiro and Saul A. Teukolsky. Black Holes, White Dwarfs, and Neutron Stars,The Physics of Compact Objects. *John Wiley and Sons, New York*, 1983.

[ST94] Y. Sugahara and H. Toki. Relativistic mean field theory for unstable nuclei with nonlinear sigma and omega terms. *Nucl. Phys.*, A579:557–572, 1994.

[STOS98a] H. Shen, H. Toki, K. Oyamatsu, and K. Sumiyoshi. Relativistic equation of state of nuclear matter for supernova and neutron star. *Nucl. Phys.*, A637:435–450, 1998.

[STOS98b] H. Shen, H. Toki, K. Oyamatsu, and K. Sumiyoshi. Relativistic equation of state of nuclear matter for supernova explosion. *Prog. Theor. Phys.*, 100:1013, 1998.

[STOS11] H. Shen, H. Toki, K. Oyamatsu, and K. Sumiyoshi. Relativistic equation of state for Core-Collapse Supernova simulations. *Astrophys. J. Suppl.*, 197:20, 2011.

[SW86] Brian D. Serot and John Dirk Walecka. The relativistic nuclear many body problem. *Adv. Nucl. Phys.*, 16:1–327, 1986.

[SW97] Brian D. Serot and John Dirk Walecka. Recent progress in quantum hadrodynamics. *Int. J .Mod. Phys.*, E6:515–631, 1997.

[SW05] Tod E. Strohmayer and Anna L. Watts. Discovery of fast x-ray oscillations during the 1998 giant flare from SGR 1900+14. *Astrophys. J.*, 632:L111–L114, 2005.

[SYS+05] Kohsuke Sumiyoshi, S. Yamada, H. Suzuki, H. Shen, S. Chiba, et al. Postbounce evolution of core-collapse supernovae: Long-term effects of equation of state. *Astrophys. J.*, 629:922–932, 2005.

[TB01] S. Typel and B. Alex Brown. Neutron radii and the neutron equation of state in relativistic models. *Phys. Rev. C*, 64:027302, Jun 2001.

[TC99] S. E. Thorsett and D. Chakrabarty. Neutron star mass measurements. 1. Radio pulsars. *Astrophys. J.*, 512:288, 1999.

[Tol34] Richard C. Tolman. Effect of inhomogenity on cosmological models. *Proc. Nat. Acad. Sci.*, 20:169–176, 1934.

[TRK+10] S. Typel, G. Roepke, T. Klaehn, D. Blaschke, and H. H. Wolter. Composition and thermodynamics of nuclear matter with light clusters. *Phys. Rev.*, C81:015803, 2010.

[Tsu98] Sachiko Tsuruta. Thermal properties and detectability of neutron stars. ii. thermal evolution of rotation-powered neutron stars. *Physics Reports*, 292:1 – 130, 1998.

[TTT93] T. Takatsuka, R. Tamagaki, and T. Tatsumi. Characteristic aspects of pion condensed phases. *Prog. Theor. Phys. Suppl.*, 112:67–106, 1993.

[TvCW03] S. Typel, T. van Chossy, and H. H. Wolter. Relativistic mean field model with generalized derivative nucleon meson couplings. *Phys. Rev.*, C67:034002, 2003.

[TW99] S. Typel and H. H. Wolter. Relativistic mean field calculations with density dependent meson nucleon coupling. *Nucl. Phys.*, A656:331–364, 1999.

[Typ05] S. Typel. Relativistic model for nuclear matter and atomic nuclei with momentum-dependent self-energies. *Phys. Rev.*, C71:064301, 2005.

[TZD+09] M. B. Tsang, Yingxun Zhang, P. Danielewicz, M. Famiano, Zhuxia Li, W. G. Lynch, and A. W. Steiner. Constraints on the density dependence of the symmetry energy. *Phys. Rev. Lett.*, 102:122701, 2009.

[vDFF04] E. N. E. van Dalen, C. Fuchs, and Amand Faessler. The Relativistic Dirac-Brueckner approach to asymmetric nuclear matter. *Nucl. Phys.*, A744:227–248, 2004.

[vDFF05a] E. N. E. van Dalen, C. Fuchs, and Amand Faessler. Effective nucleon masses in symmetric and asymmetric nuclear matter. *Phys. Rev. Lett.*, 95:022302, 2005.

[vDFF05b] E. N. E. van Dalen, C. Fuchs, and Amand Faessler. Momentum, density, and isospin dependence of the symmetric and asymmetric nuclear matter properties. *Phys. Rev.*, C72:065803, 2005.

[vDFF07] E. N. E. van Dalen, C. Fuchs, and Amand Faessler. Dirac-Brueckner-Hartree-Fock calculations for isospin asymmetric nuclear matter based on improved approximation schemes. *Eur. Phys. J.*, A31:29–42, 2007.

[VDPR93] B.E. Vonderfecht, W.H. Dickhoff, A. Polls, and A. Ramos. Influence of tensor and short-range correlations on nucleon properties in the nuclear medium. *Nuclear Physics A*, 555(1):1 – 32, 1993.

[VT12] M. D. Voskresenskaya and S. Typel. Constraining mean-field models of the nuclear matter equation of state at low densities. *Nucl. Phys.*, A887:42–76, 2012.

[Wal74] J. D. Walecka. A theory of highly condensed matter. *Annals of Physics*, 83:491–529, 1974.

[WAP93] J. Wambach, T. L. Ainsworth, and D. Pines. Quasiparticle interactions in neutron matter for applications in neutron stars. *Nucl. Phys.*, A555:128–150, 1993.

[WFF88] Robert B. Wiringa, V. Fiks, and A. Fabrocini. Equation of state for dense nucleon matter. *Phys. Rev.*, C38:1010–1037, 1988.

[WPCP00] R. B. Wiringa, S. C. Pieper, J. Carlson, and V. R. Pandharipande. Quantum Monte Carlo calculations of A = 8 nuclei. *Phys. Rev.*, C62:014001, 2000.

[WS06] Anna L. Watts and Tod E. Strohmayer. Detection with rhessi of high frequency x-ray oscillations in the tail of the 2004 hyperflare from sgr 1806-20. *Astrophys. J.*, 637:L117–L120, 2006.

[WSS95] Robert B. Wiringa, V. G. J. Stoks, and R. Schiavilla. An accurate nucleon-nucleon potential with charge independence breaking. *Phys. Rev.*, C51:38–51, 1995.

[Yam54] Yoshio Yamaguchi. Two nucleon problem when the potential is nonlocal but separable. 1. *Phys. Rev.*, 95:1628–1634, 1954.

[YKGH01] D. G. Yakovlev, A. D. Kaminker, Oleg Y. Gnedin, and P. Haensel. Neutrino emission from neutron stars. *Phys. Rept.*, 354:1, 2001.

[YP04] D. G. Yakovlev and C. J. Pethick. Neutron star cooling. *Ann. Rev. Astron. Astrophys.*, 42:169–210, 2004.

Acknowledgements

My first thanks go to my supervisor Prof. Dr. Karlheinz Langanke who has introduced me to theoretical projects in GSI during the Summer Student Program 2006, when I was a bachelor student. I thank him for giving me the opportunity to do my PhD in the Theory group of GSI and for constantly supporting me throughout my work. I am grateful to him for many fruitful discussions, guidance through my work and wise advices.

I express my sincere gratitude to Dr. Stefan Typel, my caring mentor, who was always supporting and helping me whenever I had questions or difficulties in my work. Many inspiring discussions with him allowed me to learn a lot during these years and encouraged my research. With the help of his valuable advices and continuous assistance we have approached the final results of this thesis.

I am grateful to Prof. Dr. Bengt Friman for his wise and helpful advices during my PhD Committee meetings.

I acknowledge the organization of my scholarship by HGS-HIRe for FAIR.

Also, I would like to thank Prof. Dr. Joern Knoll for the organization of Summer Student Program 2006, which has provided me with an amazing experience and motivation.

Furthermore, I'd like to thank all people in the GSI theory department, whose company I have enjoyed through these years. The names are too many to mention but special thanks go to Dr. Alexander Semke who has helped me a lot during my PhD. Also I want to thank Dr. Elena Litvinova for her amazing company in our office and wonderful talks. Next, I thank Dr. Klaas Vantournhout, Dr. Dennis Weber and Dr. Tobias Fischer for their help and many fruitful discussions.

Additionally, I want to thank all of my friends from school and university times, who have given me a lot of personal support whenever I needed it.

Finally, I thank my family: my parents, who have been my main inspiration and support through the years, my brothers Vanya and Lesha and my husband Igor. This thesis is dedicated to them.

Lebenslauf

Name:	**Maria Voskresenskaya**
Geburtsdatum:	30. September 1986
Geburtsort:	Moskau (Russland)
Familienstand:	verheiratet

Sep. 1993 - Mai 2003	Gymnasium Nr. 1201, Leistungskurs Englisch
Sep. 2003 - Aug. 2009	Studium der Physik am Moscow Engineering Physics Institute (Technische Hochschule)
Aug. 2007	Abschluss: Bachelor of Science in Physics Titel der Bachelorarbeit: "*Neutrino und Antineutrinostreuung an ^{16}O und ^{12}C Kernen*"
Juni 2009	Abschluss: Master of Science in Physics Titel der Masterarbeit: "*Streuung am Kern und wechselwirkendes Nukleonengas und Zustandsgleichung der Kernmaterie*"
seit Aug. 2009	Promotionsstudium an der Technischen Universität Darmstadt Doktorand in der Theorie-Abteilung des GSI Helmholtzzentrums für Schwerionenforschung und Anfertigung der Dissertation